R-08-102

Fracture mineralogy of the Forsmark site

SDM-Site Forsmark

Björn Sandström
Department of Earth Sciences, University of Gothenburg

Eva-Lena Tullborg, Terralogica AB

John Smellie, Conterra AB

Angus B, MacKenzie, SUERC

Juhani Suksi
Department of Chemistry, University of Helsinki

August 2008

Svensk Kärnbränslehantering AB
Swedish Nuclear Fuel
and Waste Management Co
Box 250, SE-101 24 Stockholm
Tel +46 8 459 84 00

ISSN 1402-3091
SKB Rapport R-08-102

Fracture mineralogy of the Forsmark site

SDM-Site Forsmark

Björn Sandström
Department of Earth Sciences, University of Gothenburg

Eva-Lena Tullborg, Terralogica AB

John Smellie, Conterra AB

Angus B, MacKenzie, SUERC

Juhani Suksi
Department of Chemistry, University of Helsinki

August 2008

Keywords: Fracture mineralogy, Geochemistry, Stable isotopes, U-series, Ar-Ar.

Abstract

Detailed investigations of the fracture mineralogy and altered wall rock have been carried out as part of the site characterisation programme between 2003 and 2007 at Forsmark. The results have been published in a number of P-reports and in contributions to scientific journals. This report summarises and evaluates the data obtained during the detailed fracture mineralogical studies.

The report includes descriptions of the identified fracture minerals and their chemical composition. A sequence of fracture mineralisations has been distinguished and provides information of the low to moderate temperature (brittle) geological and hydrogeological evolution at the site. Special focus has been paid to the chemical and stable isotopic composition of calcite to obtain palaeohydrogeological information. Chemical analyses of bulk fracture filling material have been carried out to identify possible sinks for certain elements and also to reveal the presence of minor phases rich in certain elements which have not been possible to detect by X-ray diffraction (XRD).

Statistical analysis of the mineralogy in fractures outside deformation zones (i.e. within fracture domains FFM01, FFM02, FFM03 and FFM06) have been carried out concerning variation of fracture mineral distribution at depth and in different fracture domains.

Uranium contents and uranium-series isotopes have been analysed on fracture coating material from hydraulically conductive fractures. Such analyses are also available from the groundwaters and the results are combined in order to reveal recent (< 1 Ma) removal/deposition of uranium in the fracture system.

The redox conditions in the fracture system have been evaluated based on mineralogical and chemical indicators as well as Mössbauer analyses.

Contents

1 Background, aims and scope

The Swedish Nuclear Fuel and Waste Management Company (SKB) is undertaking site investigations at Forsmark and Oskarshamn in Sweden with the objective of finding a suitable location for a final repository for spent nuclear fuel. A comprehensive study of the fracture mineralogy in the Forsmark area has been carried out as part of the site investigation programme from 2003 to 2007. The results have been published in numerous P- and R-reports, peer-reviewed papers, Licentiate Thesis and in abstract volumes to scientific conferences (Table 1-1). P-reports are SKB site investigation reports with the principally purpose of reporting analytical results and are only published as pdf-files on the SKB website whereas R-reports are technical reports reporting results from modelling printed in english or swedish and are referable by their ISSN number. The objective with this report is to summarise and evaluate the comprehensive data set obtained during these studies.

Mapping of fractures and fracture minerals has been carried out routinely on all drill cores from the site investigation by on-site geologists. The resulting data set served as a basis for further and more detailed fracture mineralogical studies. Data from the drill core mapping have been used to evaluate how fracture mineralogy varies between different Fracture Domains, which were recognized and described in /Olofsson et al. 2007/ and subsequently used in, for example, the geological modeling work in /Fox et al. 2007/ and /Stephens et al. 2007/. The variation of fracture mineralogy versus depth is studied /see also Stephens et al. 2007/ and the orientations of different fracture mineral parageneses outside deformation zones (DZ) have also been evaluated on a fracture domain basis. The occurrence of fracture minerals inside deformation zones has also been adressed in /Stephens et al. 2007/.

One of the aims with the detailed fracture mineralogical studies has been to interpret and describe the low to moderate temperature geological and palaeohydrogeological evolution in the Forsmark area, in order to contribute to a better conceptual geological understanding of the site. Low to moderate temperature here means temperatures below ~ 400°C, corresponding to the post-metamorphic evolution in the area. Most of this evolution has occurred in the brittle regime of the crust although some brittle-ductile deformation also has been identified in the oldest fractures/cataclasites.

Analyses of fracture filling material, preferably selected from hydraulically conductive fractures, have been carried out to provide input to the hydrogeochemical modelling and conceptual hydrogeochemical understanding of the site. Analyses include chemical composition, uranium series disequilibrium (USD), Mössbauer spectroscopy and determination of the stable isotopic composition of fracture minerals.

Mineralogy, geochemistry, porosity and redox capacity of red-stained hydrothermally altered wall rock, a common feature adjacent to many fractures in Forsmark, have also been studied. The altered rock has been compared to fresh, unaltered rock.

Table 1-1. Inventory of published material from detailed investigations of fracture minerals and wall rock alteration at Forsmark.

P- and R-reports

P-04-103	Petersson J, Berglund J, Danielsson P, Wängnerud A, Tullborg E-L, Mattson H, Thunehed H, Isaksson H, 2004. Forsmark site investigation. Petrography, geochemistry, petrophysics and fracture mineralogy of boreholes KFM01A, KFM02A and KFM03A+B.
P-04-149	Sandström B, Savolainen M, Tullborg E-L, 2004. Forsmark site investigation. Fracture mineralogy. Results from fracture minerals and wall rock alteration in boreholes KFM01A, KFM02A, KFM03A and KFM03B.
P-05-197	Sandström B, Tullborg E-L, 2005. Forsmark site investigation. Fracture mineralogy. Results from fracture minerals and wall rock alteration in boreholes KFM01B, KFM04A, KFM05A and KFM06A.
P-05-199	Sandström B, Tullborg E-L, 2005. Appendix D: Description of thin sections and surface samples from near-surface fractures at drill site 5 – samples from short drill cores. *In* B Leijon (ed). Forsmark site investigation. Investigations of superficial fracturing and block displacements at drill site 5.
R-06-109	Drake H, Sandström B, Tullborg E-L, 2006. Mineralogy and geochemistry of rocks and fracture fillings from Forsmark and Oskarshamn: Compilation of data for SR-Can.
P-06-213	Sandström B, Page L, Tullborg E-L, 2006. Forsmark site investigation. $^{40}Ar/^{39}Ar$ (adularia) and Rb-Sr (adularia, prehnite, calcite) ages of fracture minerals.
P-06-209	Sandström B, Tullborg E-L, 2006. Forsmark site investigation. Mineralogy, geochemistry, porosity and redox capacity of altered rock adjacent to fractures.
P-06-226	Sandström B, Tullborg E-L. 2006. Forsmark site investigation. Fracture mineralogy. Results from KFM06B, KFM06C, KFM08A, KFM08B.
P-08-14	Sandström B, Page L, Tullborg E-L, 2007. Forsmark site investigation. Fracture mineralogy and $^{40}Ar/^{39}Ar$ ages of fracture filling adularia. Data from drill cores KFM01C, KFM01D, KFM02B, KFM08C, KFM08D, KFM09A, KFM09B, KFM10A and KFM11A.

Peer reviewed papers

Sandström B, Tullborg E-L, de Torres T, Ortiz JE, 2006. The occurrence and potential origin of asphaltite in bedrock fractures, Forsmark, central Sweden. *GFF* 128, 233–242.

Sandström B, Tullborg E-L, 2007. Paleohydrogeological events in Forsmark, central Sweden, recorded by stable isotopes in calcite and pyrite. *In* Bullen & Wang (eds), *Water-Rock Interaction. Proceedings of the 12th international symposium on water-rock interaction. WRI-12, Kunming, China, 31 July–5 August 2007*. Taylor & Francis, London, 773–776.

Tullborg E-L, Drake H, Sandström B, 2008. Palaeohydrogeology: A methodology based on fracture mineral studies. *Applied Geochemistry 23, 1881–1897.*

Sandström B, Annersten H, Tullborg E-L, in press. Fracture-related hydrothermal alteration of metagranitic rock and associated changes in mineralogy, geochemistry and degree of oxidation: A case study at Forsmark, central Sweden. *International Journal of Earth Sciences*. doi: 10.1007/s00531-008-0369-1.

Licentiate Thesis

Sandström B 2006. Low temperature evolution in Forsmark, central Sweden – based on fracture minerals and wall rock alteration. *Earth Sciences Centre, University of Gothenburg, A111.*

Abstracts in conference volumes

Sandström B, Tullborg E-L, de Torres T, Ortiz JE, 2006. The occurrence and potential origin of asphaltite in bedrock fractures, Forsmark, central Sweden. *Bulletin of the Geological Society of Finland, Special Issue 1.* 140.

Drake H, Sandström B, Page L, Tullborg E-L, 2007. $^{40}Ar/^{39}Ar$ ages of fracture fillings in crystalline Precambrian bedrock, Sweden. *Geophysical Research Abstracts* 9, 02289, SRef-ID 1607-7962/gra/EGU2007-A-02289.

Sandström B, Annersten H, Tullborg E-L, 2008. Element mobility, changes in mineralogy and degree of oxidation during hydrothermal alteration of metagranitic rock adjacent to fractures – results from Forsmark, central Sweden. In N.A. Wahl (ed), *28th Nordic Geological Winter Meeting. Jan 7–10, 2008, Aalborg-Denmark. Aalborg University*. p 41.

Sandström B, Tullborg E-L, 2008. Paleohydrogeological events in Forsmark, central Sweden. In N.A. Wahl (ed), *28th Nordic Geological Winter Meeting. Jan 7–10, 2008, Aalborg-Denmark. Aalborg University*. p 104.

Petersson J, Sandström B, Stephens MB, 2008. Hydrothermal alteration in Palaeoproterozoic metagranite, Forsmark, Sweden and its implications for the characterization of a site for the disposal of nuclear waste. 33 IGC International Geological Congress Oslo 2008 August 6–14th

Sandström B, Tullborg E-L, Page L, 2008. Low temperature geological evolution recorded by $^{40}Ar/^{39}Ar$, $^{87}Sr/^{86}Sr$ and stable isotopes in fracture minerals at Forsmark, Fennoscandian Shield, central Sweden. 33 IGC International Geological Congress Oslo 2008 August 8–14th.

2 Available data and methodology

2.1 Opening remarks

During the detailed fracture mineralogical studies, thin sections (30 µm thick rock slices) and fracture surface samples from more than 200 selected fractures have been prepared from 22 drill cores and from the exposed surface after excavation at one drill site (Table 2-1 and Figure 2-1). The samples have, for example, been analysed with hand lens, binocular microscopy, microscopy under polarized light and SEM-EDS (Scanning Electron Microscope equipped with Energy Dispersive Spectrometer). Detailed descriptions of these samples are presented in /Sandström et al. 2004, 2008, Sandström and Tullborg 2005, 2006a/. X-ray diffraction (XRD), Mössbauer spectroscopy, geochemical analyses (including stable isotopes) and radiogenic geochronology have also been carried out on fracture filling material.

Table 2-1. Boreholes sampled during the detailed fracture mineralogical studies. The locations of the boreholes are shown in Figure 2-1. Data extracted from Sicada. Only Boremap data have been used from boreholes KFM07B, KFM07C and KFM12A and no sampling for detailed mineralogical studies were carried out on those drill cores.

Borehole	Borehole length (m)	Length of casing above ground (m)	Top of casing to bedrock surface (m*)	Soil cover (m*)	Elevation (m.a.s.l.) (ToC)	Inclination (°)	Bearing (°)
KFM01A	1,001.49			9.00	3.12	–85	318
KFM01B	500.52			3.80	3.09	–79	268
KFM01C	450.05	0.15	3.36	3.21	2.91	–50	165
KFM01D	800.24	0.23	7.55	7.32	2.95	–55	35
KFM02A	1,002.44			2.30	7.35	–85	276
KFM02B	573.87	0.15			7.62	–80	313
KFM03A	1,001.19				8.29	–86	272
KFM03B	101.54	0.12		0.78	8.47	–85	265
KFM04A	1,001.42			0.80	8.77	–60	45
KFM05A	1,002.71			8.00	5.53	–60	81
KFM06A	1,000.64	0.20	1.70	1.70	4.10	–60	301
KFM06B	100.33	0.00		2.51	4.13	–84	297
KFM06C	1,000.91	0.12	1.90	1.78	4.08	–60	26
KFM07A	1,002.10	0.25	3.80	3.80	3.33	–59	262
KFM07B	298.93	0.15	3.67	3.52	3.36	–55	134
KFM07C	500.34	0.15			3.35	–85	143
KFM08A	1,001.19	0.12	5.60	5.48	2.49	–61	321
KFM08B	200.54	0.15	4.92	4.77	2.25	–59	270
KFM08C	951.08	0.19	3.60	3.41	2.47	–60	36
KFM08D	942.30	0.30			2.61	–55	100
KFM09A	799.67	0.15	7.23	7.08	4.29	–59	200
KFM09B	616.45	0.15	7.47	7.32	4.30	–55	141
KFM10A	500.16	0.23	8.30	8.07	4.51	–50	10
KFM11A	851.21	0.30	7.60	7.30	2.95	–61	40
KFM12A	601.04	0.30			10.74	–61	36

* Length along borehole inclination, ToC = Top of casing.

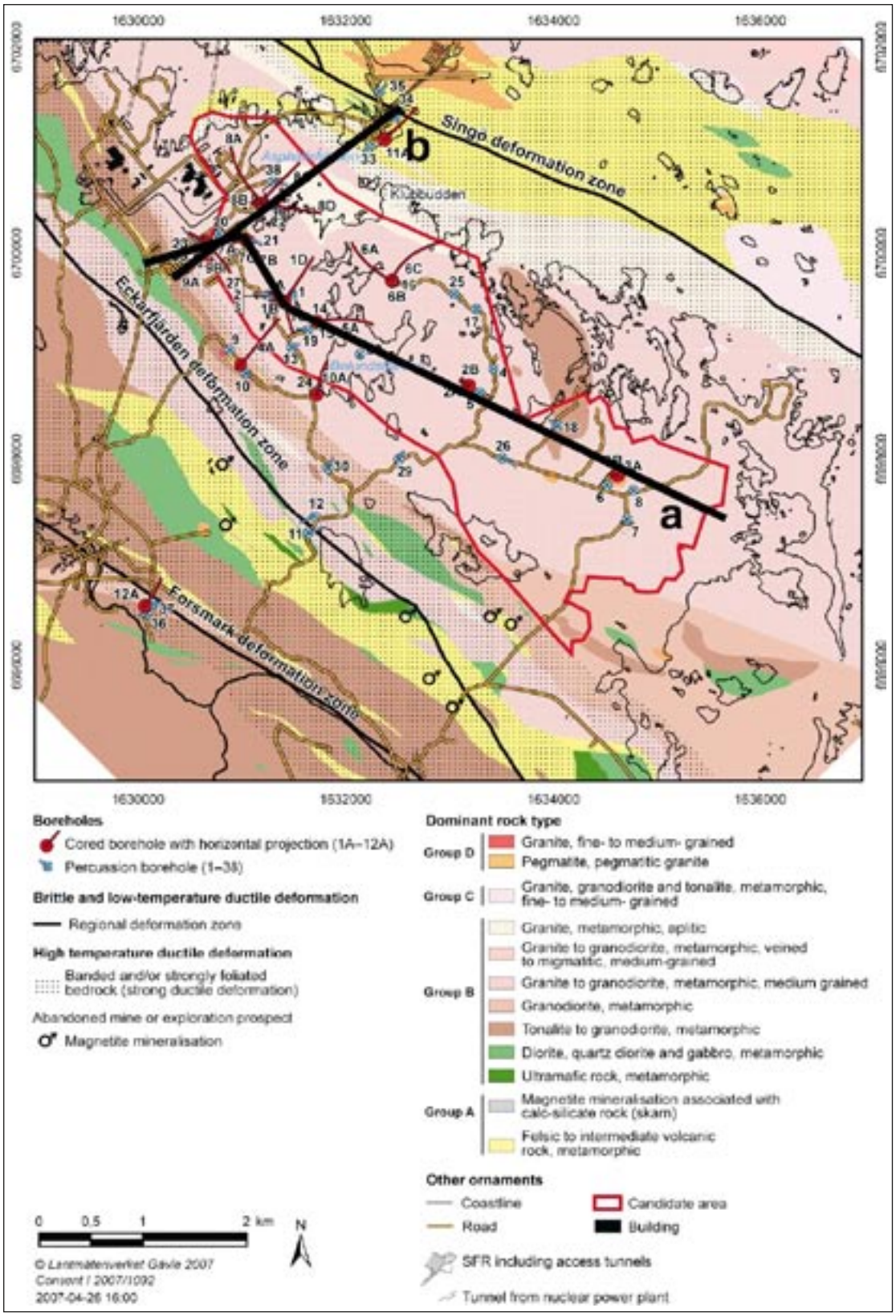

Figure 2-1. *Bedrock geological map (version 2.2) of the candidate area and its surroundings at the Forsmark site. Coordinates are provided using the RT90 (RAK) system. The figure has been adapted from /Stephens et al. 2007/. The approximate positions of the WNW-ESE (a) and WSW-ENE (b) profiles described in Figure 2-3 are indicated.*

Fracture mineralogical studies can never provide a statistical overview due to time and cost constraints. Instead, samples for detailed studies are chosen for their ability to solve specific issues or to provide adequate material to carry out, for example, combined chemical and isotopic analyses from the same fracture filling. For statistical analysis of fracture minerals, quantitative data obtained from the drill core mapping are extracted from SKB's database Sicada and processed. Furthermore, the detailed mineralogical studies have been carried out in close collaboration with the drill core mapping geologists at the site. On this basis there is high confidence that all major fracture mineral phases at Forsmark have been identified.

Communication with the drill core mapping geologists has also been important to evaluate the representativity of the fracture mineral data extracted from Sicada (Boremap data). The Boremap data is well organised and impressive with only a few exceptions:

a) Prehnite is easily mistaken for epidote and can therefore be both underestimated and overestimated in the Boremap data. Communication with the drill core mapping geologists and subsequent analyses of specific fractures suggest that it is more common that epidote has been mistaken for prehnite in the mapping work.

b) Hematite-stained adularia was mapped as hematite in the earliest boreholes (especially KFM01A, KFM02A and KFM03A). Hematite is therefore overestimated in the Boremap data.

c) Different clay minerals are not distinguished during the drill core mapping. It is also probable that clay minerals are partly lost during drilling operations and therefore the frequency of clay minerals in the core mapping can be regarded as an absolute minimum.

A common problem encountered in the fracture mineralogical studies is small sample volumes. The fracture surface intersected by the borehole represents a very small part of the actual fracture surface and its real extension in the rock is often impossible to evaluate. Thus, the representativity of the samples can not be quantified, a fact that needs to be considered in subsequent interpretations.

Since samples for detailed fracture studies have been selected in order to address different tasks in, for example, hydrogeochemical and geological site descriptive modelling work, their selection has been based on different criteria as follows:

- Mineralogical identification; sampling has usually been initiated by the geologists carrying out the drill core logging. Binocular microscopy, XRD and SEM-EDS analyses have been performed on many of these samples, but some have also been selected for thin section preparation and subsequent studies under polarized light.
- Samples selected to study mineral paragenesis (including thin section preparation and fracture surface samples); normally these samples should show a complex mineralogy and preferably contain several generations of fracture minerals (parageneses) representing a relative sequence of mineralisation. Samples exhibiting cross-cutting relations have been of special interest for this purpose.
- Palaeohydrogeological studies; preferably open, and in best case transmissive fractures coated with calcite, pyrite and quartz which can be selected for stable isotopic ($\delta^{13}C$, $\delta^{18}O$, $\delta^{34}S$ and $^{87}Sr/^{86}Sr$) and trace element analyses, etc.
- Currently hydraulically conductive fractures have been sampled based on Posiva Flow Log anomalies (PFL) /cf Forsman et al. 2004/ for geochemical analyses, Mössbauer spectrometry and uranium-series disequilibrium. Priority has been given to fractures corresponding to sections sampled for groundwater chemistry.

In the selected drill core samples, the relative formation sequence of the fracture minerals has been established based on cross-cutting relations and/or overgrowth. This "mapping" of cross-cutting relations is comparable with that used by field geologists during bedrock mapping work, but, in this case it has been carried out on the micro-scale. From this initial data set a more general relative sequence of fracture mineralisations has emerged. The numbers of distinguished fracture

mineral generations (parageneses) was six during the initial phase /Sandström et al. 2004/, the sequence was then adjusted in /Sandström and Tullborg 2005/ as more knowledge was obtained from additional analysed samples. In the latest model, the number of generations is four /Sandström and Tullborg 2006a/. Only small adjustments have been made to the sequence of fracture mineral generations since the geological model 1.2 /SKB 2005/, implying a high degree of stability in the established sequence.

This relative sequence of fracture mineral generations represents a sequence of geological and/or hydrogeological events that succeeded each other in time. This sequence has been used as a basis for radiometric dating of fracture minerals and interpretation of the prevailing conditions during precipitation based on, for example, mineral stabilities, fluid inclusions and stable isotopes.

Within the Forsmark site, the fracture frequency and especially the transmissivity of the fractures show large variation both laterally and vertically. In order to take account of the variability in fracture frequency and to better meet the requirements for hydrogeological modelling, a division of the bedrock inside the the north-western part of the candidate volume, i.e. the target volume /SKB 2005/, was carried out /Olofsson et al. 2007/. This means that the Forsmark site has been divided into a number of fracture domains based on the differences in the frequency of especially open fractures, both laterally along the candidate volume and at depth inside the target volume. Potential differences in fracture frequency related to differences in lithology have also been addressed in the fracture domain modelling. From the view of fracture mineralogy it is of course important to evaluate possible differences in fracture mineral frequency between the different domains, and therefore statistical analyses of fracture mineralogy have been carried out based on the domain concept. Four separate domains are dealt with within the scope of this report (FFM01, FFM02, FFM03 and FFM06). The position of these fracture domains are presented in a 3D model inside the target volume (Figure 2-2) as well as two simplified NW-SE cross-sections along the candidate volume (Figure 2-3). For a more detailed description of fracture domains, the reader is referred to /Olofsson et al. 2007/.

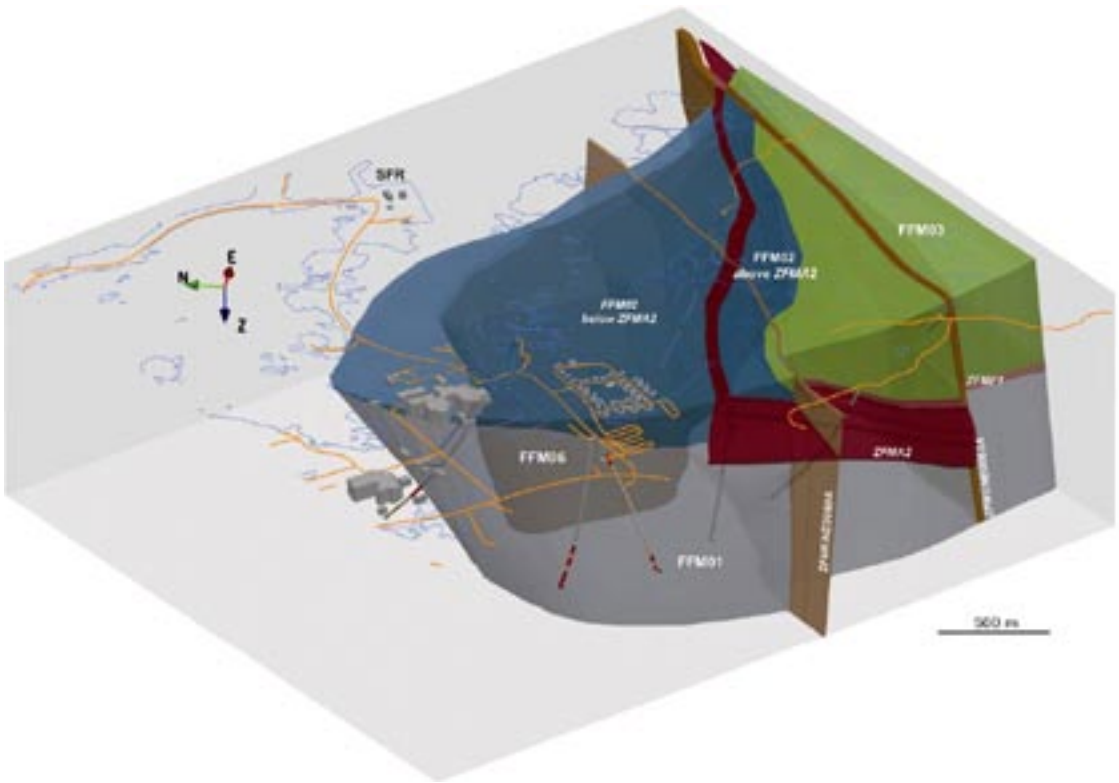

Figure 2-2. *View to the ENE showing the fracture domains within the target area (FFM01, FFM02, FFM03 and FFM06). Deformation zones ZFMA2, ZFMENE0060A, ZFMENE0062A and ZFMF1 are also shown in the figure. The figure is adapted from /Olofsson et al. 2007/.*

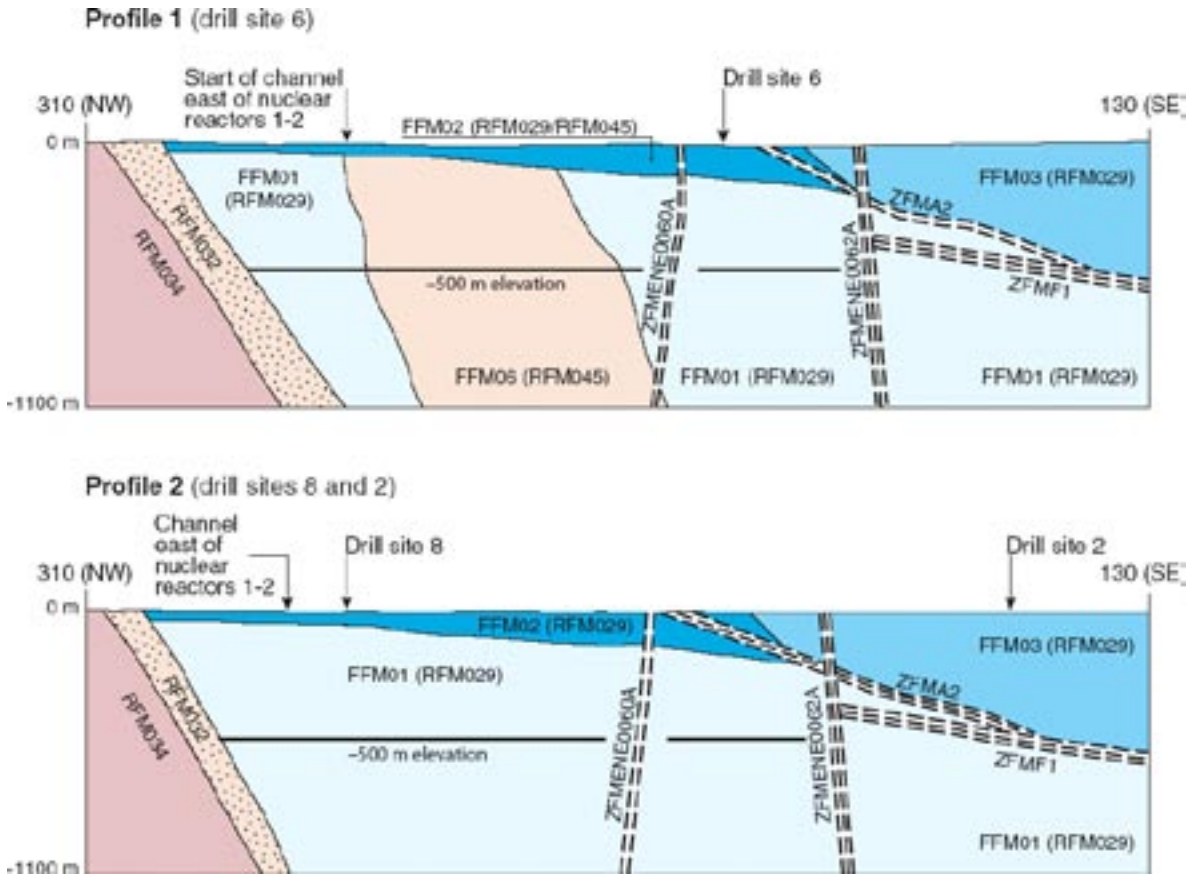

Figure 2-3. *Simplified profiles in a NW-SE direction (310°–130°) that pass through drill site 6 (upper profile) and drill sites 2 and 8 (lower profile). The labelled fracture domains (FFM01, FFM02, FFM03 and FFM06) occur inside rock domains RFM029 and RFM045. Only the high confidence deformation zones ZFMA2 (gently dipping), ZFMF1 (sub-horizontal), ZFMENE0060A (steeply dipping, longer than 3,000 m) and ZFMENE0062A (steeply dipping, longer than 3,000 m) are included in the profiles. The figure is adapted from /Olofsson et al. 2007/. The positions of the profiles, are showed in Figure 2-1.*

2.2 Sicada data

The data discussed in this report are available in the SKB database Sicada and located by the AP number (Table 2-2). The data are also available in the P-reports listed in Table 1-1. The evaluation of statistical data of fracture mineral distributions has made use of the following delivery from the Sicada database: Sicada_07_140.

Table 2-2. Controlling documents for the performance of the activities.

Activity plan	Number	Version
Sprickmineralogiska undersökningar	AP PF 400-04-32	1.0
	AP PF 400-06-077	1.0
Geokronologisk undersökning av sprickmineral	AP PF 400-07-047	1.0
Undersökning av bergets redox-kapacitet i	AP PF 400-05-047	1.0
anslutning till sprickor	AP PF 400-05-076	1.0

2.3 Mineral identification

Unknown minerals have been identified using hand lens, binocular microscope, polarizing microscope and scanning electron microscope with an energy dispersive spectrometer (SEM-EDS). X-ray diffraction (XRD) has been applied on phases difficult to identify or samples containing clay minerals. The XRD detection limit for a mineral depends on the specific mineral in question and other minerals present in the sample. The degree of crystallinity of the mineral also influences the detection limit. As a rough estimate, the detection limit for a mineral phase is mostly one to a few vol% /E. Jonsson, pers. comm. December 2007/. The analytical procedure for the XRD analyses is described in /Petersson et al. 2004/.

2.4 Calcite morphology

Determination of calcite morphology has been applied successfully in several studies to distinguish between different salinities in the formation water /e.g. Milodowski et al. 2002, 2005/. At Forsmark, only Palaeozoic calcites (cf Chapter 4) show well developed crystal shapes (mainly equant and scalenohedral). Unfortunately, recent calcites, which are of interest to study the latest hydrogeological evolution in the area, occur only as thin coatings together with clay minerals, and no crystal shapes have been possible to determine. Less emphasis has therefore been put on using this method so far.

2.5 Stable isotopes

Analyses of stable isotopes in fracture minerals (calcite, quartz, pyrite, asphaltite) provide information of the hydrogeochemical conditions prevailing during the periods of mineral precipitation. Calcite is favourable due to its relative fast response to changes in fluid chemistry and temperature etc /e.g. Wallin and Peterman 1999, Blyth et al. 2000, Tullborg et al. 2008/. Stable isotopic composition has also been used to distinguish different generations of calcite.

The isotopic ratios $^{18}O/^{16}O$ (in calcite and quartz), $^{13}C/^{12}C$ (in calcite and asphaltite), $^{34}S/^{32}S$ (in pyrite) and $^{87}Sr/^{86}Sr$ (in calcite) have been analysed and are expressed as δ-values relative to a standard (except for the $^{87}Sr/^{86}Sr$ ratio). The standards used are presented in Table 2-3. The δ-value is defined as follows using $\delta^{18}O$ as an example:

$$\delta^{18}O = \left[\frac{^{18}O/^{16}O_{\text{sample}}}{^{18}O/^{16}O_{\text{standard}}} - 1 \right] \times 10^3$$

Table 2-3. Standards used for the stable isotope analyses.

Isotopes	Mineral	Standard
$^{18}O/^{16}O$	Calcite	V-PDB* (Vienna PeeDee Belemnite)
$^{18}O/^{16}O$	Quartz	SMOW (Standard Mean Ocean Water)
$^{13}C/^{12}C$	Calcite, asphaltite	V-PDB
$^{34}S/^{32}S$	Pyrite	CDT (Canyon Diablo Troilite)

* Since the V-PDB standard is no longer available, the isotopic ratios are compared to the limestone material NBS19 which has a defined V-PDB value.

The $\delta^{18}O$ value in fracture minerals depends on the composition of the formation fluid and the formation temperature. If the temperature during precipitation is largely known, the $\delta^{18}O$ value of the precipitation fluid can be estimated reflecting its origin (e.g. meteoric or marine water). Due to the high oxygen content in silicates and oxides of the wall rock, water-rock interaction may also have an influence on the $\delta^{18}O$ value, especially under hydrothermal conditions and low water/rock ratio. The $\delta^{13}C$ value is not as temperature dependent as the $\delta^{18}O$ value and the interaction with the crystalline wall rock is negligible compared to the influence from HCO_3^- in the formation fluid. Instead, the $\delta^{13}C$ value reflects the source of the dissolved CO_2 inherited into the minerals. The $\delta^{34}S$ value in pyrite is, for example, used to separate magmatic/hydrothermal pyrite from pyrite precipitated due to bacterial or thermochemical reduction of sulphate /e.g. Hoefs 2004, Seal 2006/. Fractionation of strontium isotopes (^{87}Sr and ^{86}Sr) is negligible during calcite precipitation from fluids /e.g. Stuckless et al. 1991/. Since calcite does not accommodate ^{87}Rb, the radioactive parent of ^{87}Sr, in its crystal lattice, precipitated calcite preserves the $^{87}Sr/^{86}Sr$ ratio of the formation fluid. The $^{87}Sr/^{86}Sr$ ratio in groundwaters and hydrothermal fluids are largely determined by water-mineral interaction but also the origin of the fluids. Since the fraction of radiogenic ^{87}Sr is steadily growing in rocks and fracture minerals containing rubidium, higher $^{87}Sr/^{86}Sr$ ratios in the calcite may reflect younger ages of the fluid from which the calcite precipitated /Faure and Mensing 2004/.

The analytical errors of the stable isotopic analyses are $\delta^{13}C \pm 0.05‰$, $\delta^{18}O \pm 0.1‰$, $\delta^{34}S \pm 0.2‰$ and $^{87}Sr/^{86}Sr \pm 0.00002$, i.e. much smaller than the compositional variations between the samples. The analytical procedures are described in detail in /Sandström et al. 2004/. The preparation technique with calcite dissolution in HCl reduces the risk of contamination from more insoluble phases (e.g. from the wall rock).

2.6 Calcite trace element geochemistry

Trace elements in calcite can be used as indicators of formation temperature, redox conditions and dominating complexing agents etc /e.g. Möller and Morteani 1983, Tullborg et al. 2008/. The trace element composition of calcites has been obtained by HCl leaching of calcite and subsequent ICP-MS analysis, and by in situ laser ablation ICP-MS technique as described in /Sandström et al. 2004/ (ICP-MS) and /Sandström and Tullborg 2005/ (LA-ICP-MS).

2.7 Fluid inclusions

Analyses of fluid inclusions trapped within fracture minerals provide constraints on the formation temperature and salinity of the formation fluid. In Forsmark, only calcite has been found to be suitable for fluid inclusion studies (quartz is a common fracture coating mineral but the inclusions are too small for analysis). A major problem encountered is that many of the sampled calcites are either too deformed or are mixed with other minerals, thus rendering it difficult to carry out fluid inclusion studies. This is especially the case for the highly deformed hydrothermal calcites (generation 2, see Chapter 4.2). A low temperature technique has been used during sample preparation to avoid subsequence heating of the samples. However, the temperature was briefly raised to 70°C in order to melt the wax used during preparation. The fluid inclusion raw data will be published in /Sandström and Tullborg in prep/.

2.8 Geochemical analyses of bulk fracture coating material

Geochemical analyses of bulk fracture fillings, preferably from currently hydraulically conductive fractures and zones, are used to evaluate element mobility (e.g. variation in mobilisation and deposition with depth etc). Special focus has been put on the behaviour of chemical analogues for radionuclides (e.g. Cs, Sr, U, Th and REEs). Redox sensitive elements (e.g. Fe, Ce, Mn and U) can be used as indicators of how redox conditions vary with depth and how stable the conditions have been over time. The geochemistry of fracture minerals depends on the fluid from which they precipitated, as well as the chemical exchange during later water-rock interaction including also microbial processes. The geochemistry of fracture fillings provides a complement to the "snap shot" in time that the chemical analyses of groundwater represent. The analytical procedure is described in /Petersson et al. 2004/.

2.9 Radiometric dating of fracture minerals

Based on the interpreted relative sequence of fracture mineralisations, strategic minerals suitable for radiometric dating techniques have been sampled and analysed in order to constrain the radiometric ages of the mineralisation sequence /Sandström et al. 2006a, 2008/. A major problem with radiometric dating of fracture minerals is that minerals commonly used for radiometric dating of rocks are absent in most fracture systems (e.g. zircon, titanite, monazite, baddeleyite). In Forsmark, the most suitable mineral is adularia (low temperature K-feldspar) which can be dated by the high precision $^{40}Ar/^{39}Ar$ technique. Rb-Sr dating has also been carried out on an assemblage of altered wall rock, adularia, prehnite and calcite. The precision of this method is less precise than the $^{40}Ar/^{39}Ar$ dating. This may be due to the less constrained closure temperatures for the Rb-Sr system and that the different fracture minerals may have precipitated during a prolonged period. Analytical procedures are described in /Sandström et al. 2006a/.

2.10 U-series equilibrium

The uranium decay series nuclides ($^{238}U/^{234}U/^{230}Th$) can be applied, for example, to study the mobility of uranium during the last 1 Ma. Basically, disequilibrium (activity ratio $\neq 1$, see Chapter 8) between the nuclides in the uranium decay series indicate that mobilisation or deposition has occurred during the last 1 Ma. The analytical procedure is described in /Sandström and Tullborg 2006a/.

2.11 Orientation of fractures

BIPS (Borehole Image Processing System) /e.g. Graffner 2000/ is a method used for imaging 360° of the borehole wall and consists of a digital high resolution TV-camera that is lowered into the borehole. The resolution of the image is c. 1.0 mm. During the BIPS-based mapping of the drill core, orientation of fractures and other structures are put into the Boremap™ software. The orientation data can be viewed together with the borehole wall image with a BIPS Image Viewer™ (v.2.51) where the orientation and aperture of specific fractures can be obtained (Figure 2-4).

To visualise the orientation of fractures with different minerals, data obtained from the drill core mapping have been extracted from the SKB database Sicada (delivery: Sicada_07_140) and plotted in lower hemisphere, equal area stereographic projections in contoured plots with Terzhagi correction. In this report, only orientation of fractures outside deformation zones (DZ) are analysed. Orientations of fractures inside deformation zones are discussed in /Stephens et al. 2007/ and are not presented in this report.

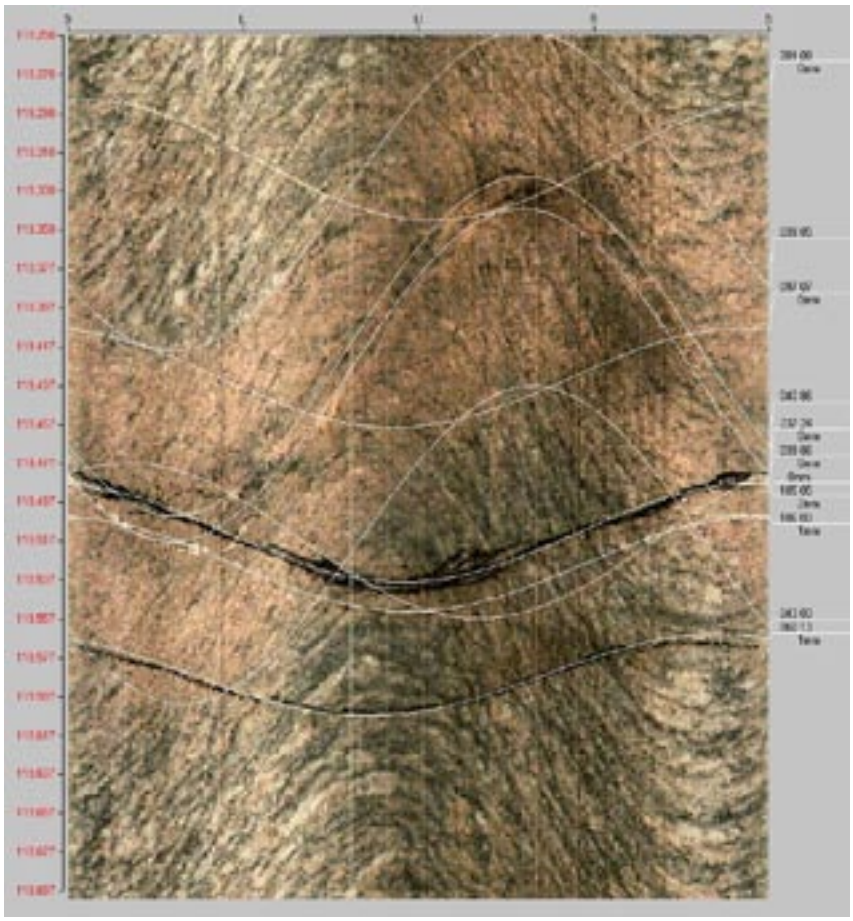

Figure 2-4. *Example of BIPS-image from KFM07A (adjusted depth on y-axle) showing 360° of the borehole wall. Among other features, a sealed fracture with red-stained/oxidised wall rock is cut by two younger open fractures. The white lines represent mapped features with orientations and aperture.*

3 Fracture minerals

3.1 Identified fracture minerals

The fracture minerals identified within the Forsmark area are presented below (the XRD and SEM-EDS data referred to here are published in /Petersson et al. 2004, Sandström et al. 2004, 2008, Sandström and Tullborg 2005, 2006a/). The chemical formulae for the minerals have been adapted from /Deer et al. 1992/. The abundance of different fracture minerals in all fractures (open and sealed) in Forsmark shows a large variation and the relative abundance can be summarised as follows: calcite and chlorite/corrensite >> laumontite > quartz, adularia, albite, clay minerals > prehnite, epidote > hematite and pyrite. Other minerals have only been found as minor occurrences but can be more common in particular intervals (e.g. asphaltite). A special mapping campaign where the absolute volumes of a number of fracture minerals of interest for safety assessment considerations is estimated, is currently being carried out by SKB and will be presented during 2008. The identified minerals are here presented in alphabetic order:

Albite (Na-Plagioclase) ($NaAlSi_3O_8$) is commonly found in fracture fillings together with hydrothermal K-feldspar (adularia). The fillings can be brick-red due to hematite-staining.

Allanite $(Ca,Mn,Ce,La,Y,Th)_2(Fe^{2+},Fe^{3+},Ti)(Al,Fe^{3+})_2O.OH[Si_2O_7][SiO_4]$ is a REE-rich epidote group member, which has been found in two open fractures where it occurs as a thin beige coating.

Analcime ($NaAlSi_2O_6 \cdot H_2O$) has colourless, usually trapezohedral crystals (like garnet). It is stable at temperatures up to 200°C in the presence of quartz, but can in other assemblages exist at temperatures up to 600°C /Liou 1971/. In Forsmark, relatively large crystals of analcime (in the order of 5 to 10 mm) have been found in some fractures.

Apophyllite ($(K,Na)Ca_4Si_8O_{20}F \cdot 8H_2O$) is a hydrothermal sheet silicate with a white to silvery surface. It has been detected in some fractures at Forsmark. Based on a few SEM-EDS analyses it seems to be a relatively pure K-Ca-apophyllite.

Asphaltite ("bergbeck" in Swedish). The term is used in a broad sense, meaning black, highly viscous to solid hydrocarbons with low U and Th content.

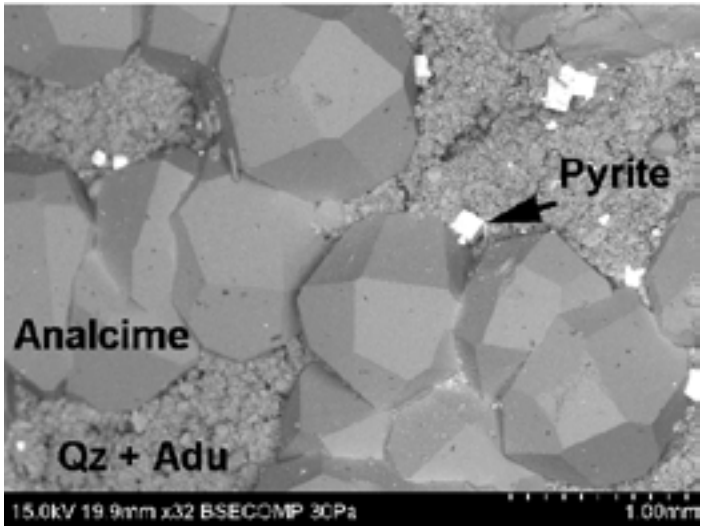

Figure 3-1. *Backscattered electron image of trapetzohedral analcime crystals together with pyrite on a coating of quartz (Qz) and adularia (Adu) from KFM08A 246.11–246.35 m.*

Figure 3-2. *Asphaltite (black) on fracture surface from KFM06B 90.60–90.85 m, the diameter of the drill core is ~ 5 cm.*

Barite ($BaSO_4$) has only been identified in a few samples (e.g. as small inclusions in galena).

Calcite ($CaCO_3$) occurs abundantly in Forsmark in different assemblages and with different crystal forms. The calcite analysed generally shows low contents of Mg, Mn and Fe. No other carbonate minerals have been identified.

Chalcopyrite ($CuFeS_2$) occurs in Forsmark as small grains together with pyrite, galena and sphalerite.

Chlorite ($(Mg,Fe,Al)_3(Si,Al)_4O_{10}(OH)_2$) occurs abundantly in Forsmark commonly as a dark-green mineral found in several associations. XRD identifies the chlorite as clinochlore but large variations in FeO/MgO ratios are indicated from SEM-EDS analyses (from 6 down to < 1). The occurrence of K, Na and Ca in many of the chlorite samples indicates ingrowths of clay minerals, mostly corrensite.

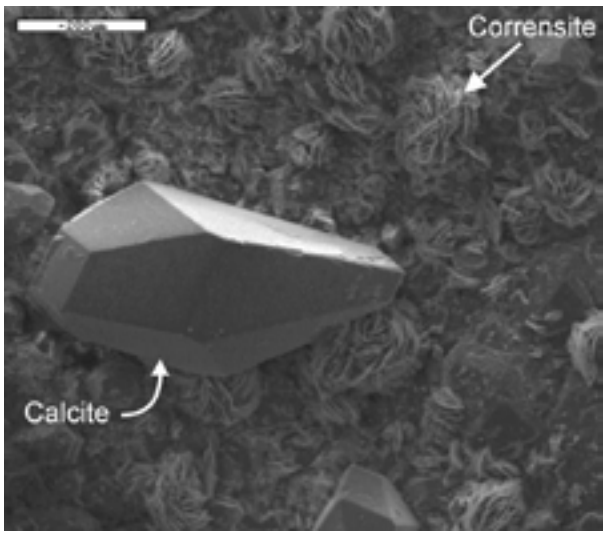

Figure 3-3. *Electron image of scalenohedral calcite crystal from KFM05A 146.40–146.57 m. Scale bar is 200 µm.*

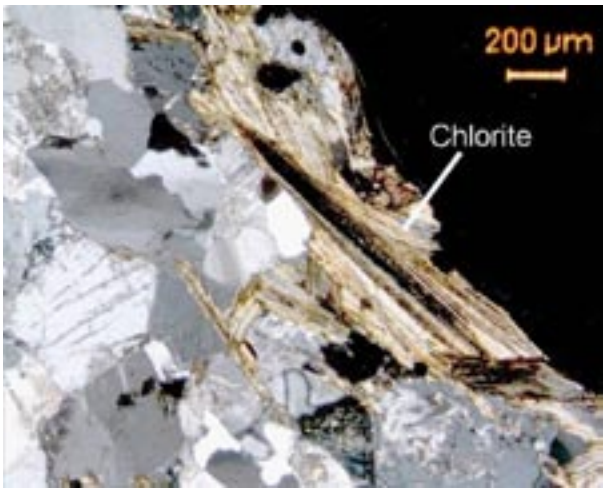

Figure 3-4. *Photomicrograph (crossed polars) of fracture coating chlorite, partly mixed with corrensite from KFM07A 118.18–118.31 m.*

Epidote ($Ca_2Al_2Fe^{3+}(SiO_4)(Si_2O_7)(O,OH)_2$) occurs as a green filling in sealed fractures. Epidote is normally found at temperatures above 200°C but has been reported in active geothermal systems at temperatures < 200°C /Bird et al. 1984, Bird and Spieler 2004/.

Fluorite (CaF_2). Violet fluorite is found in a few, mostly sealed, fractures.

Galena (PbS) is mainly found on fracture surfaces in the form of cubic or octahedral crystals. The mineral occurs together with pyrite in Forsmark and some galena crystals have small inclusions of barite.

Goethite (FeOOH) is found as a brownish to rust-red precipitate in some open fractures and is normally formed under oxidising conditions.

Hematite (Fe_2O_3) is common in the Forsmark fractures but the amount is relatively low (does not often turn up in the X-ray diffractograms). However, micro-grains of hematite cause intense red-staining of many fracture coatings. Small spherical aggregates of hematite have also been found in a few fractures.

K-feldspar ($KAlSi_3O_8$) is usually present along fractures in its low temperature form adularia, but is also found within wall rock fragments in breccias showing typical microcline twinning. The colour can be brick-red due to hematite-staining, but also greenish varieties occur in fine-grained mixtures with quartz.

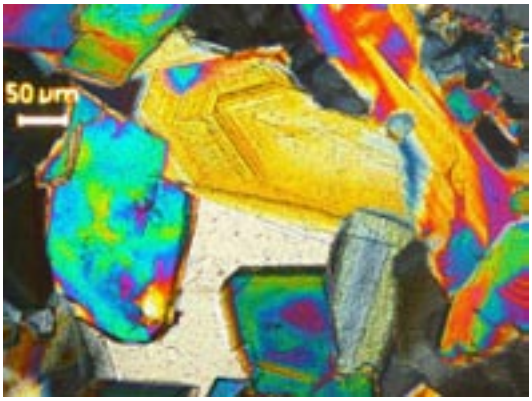

Figure 3-5. *Photomicrograph of epidote crystals (crossed polars) from KFM05A 428.00–428.13 m.*

Figure 3-6. *Fracture sealed with hematite stained adularia, KFM03A 184.34–184.50 m, the diameter of the drill core is ~ 5 cm.*

Laumontite ($CaAl_2Si_4O_{12} \cdot 4H_2O$) is a common zeolite mineral in the Forsmark area. It is brittle and the crystals show prismatic shapes. The mineral itself is white, but, at Forsmark, it is stained-red due to micro-grains of hematite, although white varieties are also present. Zeolites have open structures suitable for ion exchange processes. Laumontite is stable at temperatures somewhere between ~ 150° and 250°C /Liou et al. 1985/.

Pitchblende (UO_2) is an usually massive, non-crystalline, low temperature form of uraninite. At Forsmark, this mineral has only been possible to identify along one fracture together with hematite and chlorite.

Prehnite ($Ca_2Al_2Si_3O_{10}(OH)_2$) occurs as a light greyish green to grey or white, hydrothermal mineral. The stability field for prehnite is somewhere between 200° and 280°C at pressures below 3.0 kbar /Frey et al. 1991/.

Pyrite (FeS_2) is found in many fractures as small euhedral, cubic crystals grown on mostly open fracture surfaces, but also together with calcite in sealed fractures.

Quartz (SiO_2) has been identified in many of the analysed samples, commonly as very small and occasionally hematite-stained, euhedral crystals covering the fracture walls. They often have a greyish sugary appearance but can also be transparent and then appear to have the colour of the wall rock.

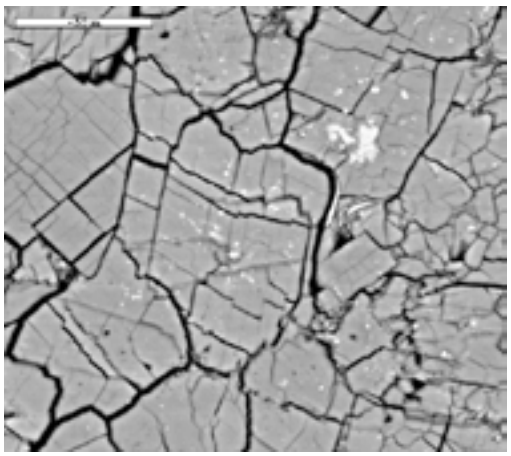

Figure 3-7. *Backscattered electron image of laumontite (grey) stained with small hematite grains (white) from KFM04A 244.46–244.58 m, scale bar is 50 µm.*

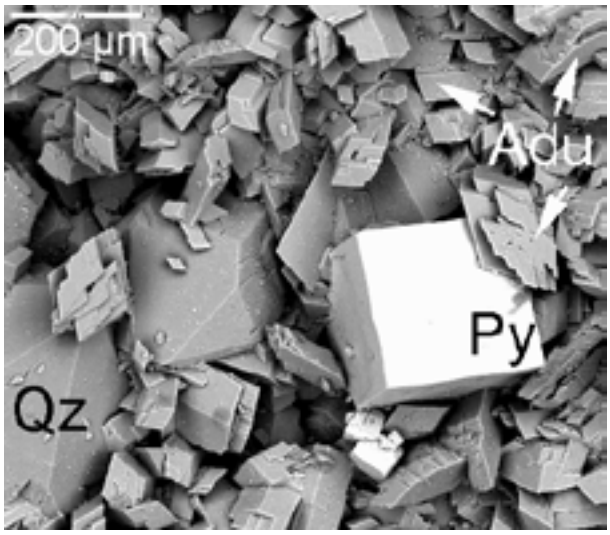

Figure 3-8. *Backscattered electron image of euhedral pyrite crystal (Py) together with quartz (Qz) and adularia (Adu) from KFM07A 882.95–883.05 m.*

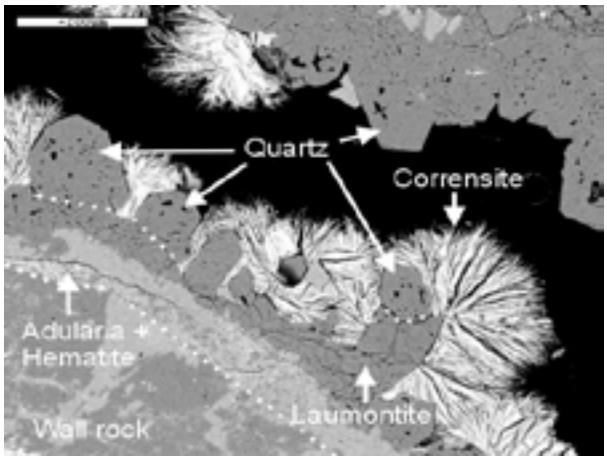

Figure 3-9. *Backscattered electron image of euhedral quartz crystals from KFM05A 938.00–938.18 m which have grown on hematite stained adularia and laumontite. Corrensite has later precipitated on the quartz. Scale bar is 200 µm.*

Sphalerite (ZnS) has been found in a few fractures and is commonly associated with galena.

Talc $(Mg_6)Si_8O_{20}(OH)_4$ has been identified in a few fractures along KFM11A.

Clay minerals

Corrensite ($(Mg,Fe)_9(Si,Al)_8O_{20}(OH)_{10} \cdot H_2O$) is a chlorite-like mixed-layer clay with layers of chlorite and smectite/vermiculite, usually with a ratio of 1:1. Based on XRD analyses, some of the corrensite samples show irregular ordering in the layering, indicating either that they have not reached perfect corrensite crystallinity or that they are altered. Corrensite is the clay mineral most commonly found and is, as mentioned above, commonly found together with chlorite. This is a swelling type of clay, similar to mixed-layer illite/smectite and saponite (see below).

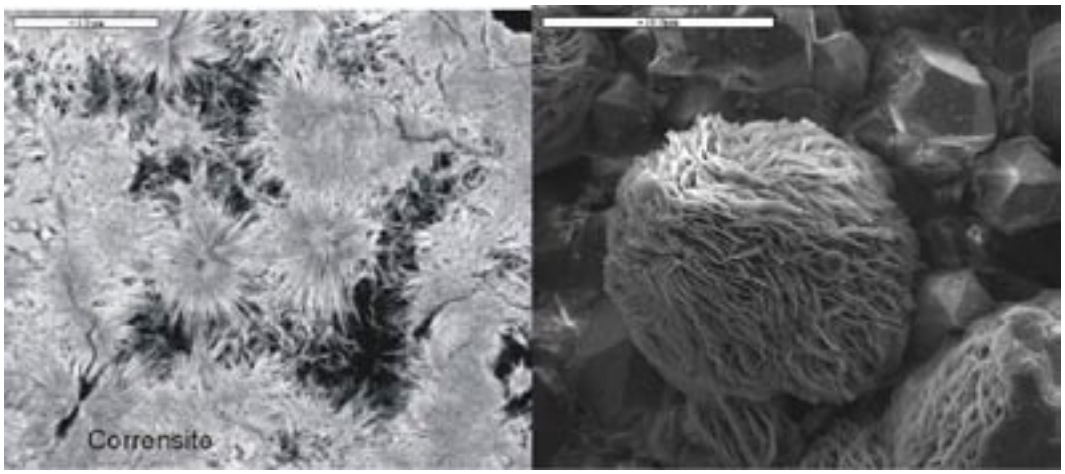

Figure 3-10. *Backscattered electron images of corrensite. The left image is from a thin section from KFM05A 428.00–428.13 m, scale bar is 50 µm. The right image is from KFM05A 938.00–938.18 m. Scale bar is 200 µm.*

Illite $(K,H_2O)Al_2[(Al,Si)Si_3O_{10}](OH)_2)$ occurs as micro – to cryptocrystalline, micaceous-flakes, and is usually light grey in colour. After corrensite, illite is the most common clay mineral in Forsmark.

Kaolinite $(Al_4[Si_4O_{10}](OH)_8)$ has only been identified in KFM01C. The XRD peaks indicate low crystallinity of the kaolinite.

Mixed layer clays. Mixed layer clay with layers of illite and smectite has been identified in some fractures. XRD analyses show a 3:2 ratio of illite/smectite.

Saponite $(Mg_3(Si_4O_{10})(OH)_2 \cdot nH_2O)$ is a variety of swelling smectite.

Smectite group $(½Ca,Na)_{0.7}(Al,Mg,Fe)_4[(Si,Al)_8O_{20}](OH)_4.nH_2O$ is a group of swelling clay minerals taking up water or organic molecules between their structural layers. They also show marked cation exchange properties /Deer et al. 1992/. Smectite group clay minerals are not common in Forsmark.

Vermiculite $((Mg,Ca)_{0.6–0.9}(Mg,Fe^{3+},Al)_{6.0}[(Si,Al)_8O_{20}(OH)_4.nH_2O)$ is similar to smectite.

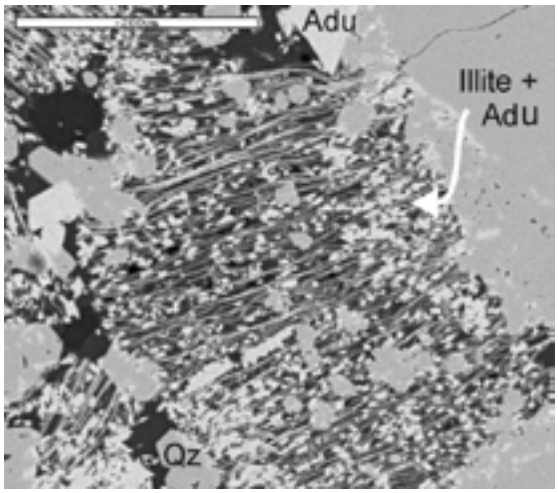

Figure 3-11. *Backscattered electron image of illite together with small adularia crystals (Adu), from KFM50A 111.56–111.60 m. Scale bar is 200 µm.*

3.2 XRD data

Qualitative X-ray diffraction (XRD) analyses have been carried out to identify unknown minerals, especially clay minerals, and to complement the geochemical analyses of material from hydraulically conductive fractures (and crushed zones).

The analysed fracture fillings from transmissive fractures and deformation zones commonly contain fine-grained material including fragments of wall rock together with a fraction of clay-sized particles. The most abundant minerals identified by XRD in samples with all fractions present are quartz, plagioclase, K-feldspar, calcite, chlorite and clay minerals. In the fine fraction (< 10 μm), feldspars and quartz are still found abundantly, but most samples are dominated by chlorite and clay minerals.

Clay minerals

It is often impossible to distinguish different clay minerals macroscopically, and no differentiation is made of different clay minerals during drill core mapping. However, some estimation of the relative abundance of different clay minerals has been made based on available XRD data. In addition, information from the examination of the drill cores carried out in connection with the sampling for the detailed mineralogical studies is taken into account. From this information it is evident that corrensite (chlorite/smectite or chlorite/vermiculite) is the dominant clay mineral followed by illite and mixed layer clays (e.g. illite/smectite). Non-mixed smectite, vermiculite and kaolinite have also been identified, but only in a few samples.

A histogram of clay minerals (and chlorite occurring in the fine fraction < 10 μm) identified by XRD is presented in Figure 3-12. Note that the selection of samples for XRD analysis often coincides with the presence of a Posiva Flow Log-anomaly (PFL), i.e. the fracture is hydraulically conductive, and the data presented in Figure 3-12 therefore underestimates the true relative abundance of specific clay minerals. Both corrensite (and chlorite) occur abundantly in fractures which show no PFL-anomaly. Depth distribution of different clay minerals is addressed in section 6.3.

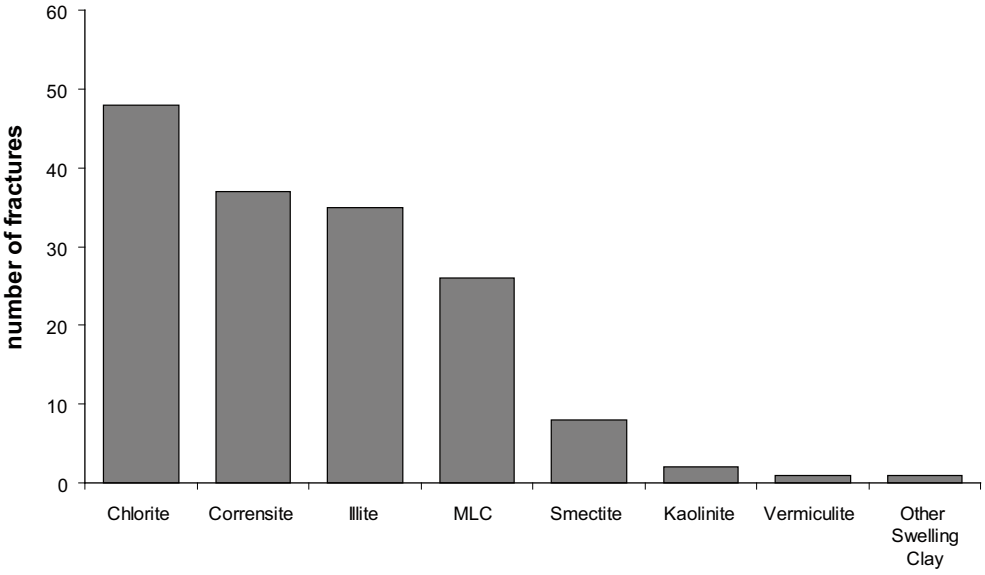

Figure 3-12. *Histogram showing number of fractures where clay minerals and chlorite have been identified by XRD-analysis of bulk fracture filling material in the fine fraction (< 10 μm). The representativity of the samples is discussed in the text. MLC = mixed layer clay.*

3.3 Concluding remarks

The confidence is high that all major fracture mineral phases have been identified within the Forsmark site. The relative abundance of different fracture minerals can be summarised as follows; calcite and chlorite/corrensite >> laumontite > quartz, adularia, albite, clay minerals > prehnite, epidote > hematite and pyrite. Other identified minerals have only been found as minor occurrences but can be more common in specific intervals (e.g. asphaltite, analcime and goethite) (see Chapter 6).

The most common clay minerals are corrensite > illite > mixed layer clays > smectite > kaolinite, vermiculite and other swelling clays. No other carbonates than calcite have been identified and the only sulphate mineral identified is barite which occurs in very small amounts (e.g. as inclusions in galena). Gypsum has not been identified along any fractures. Pyrite makes up more than 99% of the identified sulphides but galena, chalcopyrite and sphalerite have also been identified.

4 Sequence of fracture mineralisations, their ages and formation conditions

An estimation of formation temperatures during different episodes of mineral precipitation can be obtained from the mineralogy since different minerals are stable at different temperatures. The Ca-silicates epidote-prehnite-laumontite all have similar chemical compositions but precipitate under different, although overlapping, temperature regimes; epidote normally > 200°C /Bird et al. 1984, Bird and Spieler 2004/, prehnite between 200 and 280°C /Frey et al. 1991/ and laumontite between 150 and 250°C /Liou et al. 1985/ at low pressures (< 3 kbar). Furthermore, temperature information can be derived from fluid inclusions, which also provide salinities of the fluid involved. Finally, stable isotopes may provide temperature constraints, for example, the presence of organic carbon signatures indicate formation temperatures usually < 150°C. The age of the rock units in the Forsmark area has been well established /Hermansson et al. 2007, 2008/, providing a maximum age of the fractures. The most voluminous plutonic suite (dominated by granite and tonalite to granodiorite affected by penetrative ductile deformation) intruded at 1.89–1.87 Ga. A younger suite of undeformed granite and aplite as well as pegmatitic granite and pegmatite intruded the area at 1.86–1.85 Ga.

A summary of the relative sequence of fracture mineralisations is presented in Table 4-1. A more detailed description of the different fracture mineral generations follows below.

Table 4-1. Summary of the relative sequence of fracture mineralisations, their approximate formation temperatures, fluid salinity, stable isotopic composition of calcite and radiometric ages obtained.

	Dominating Minerals	Formation temp.[1]	Fluid salinity	$\delta^{18}O$ in calcite	$\delta^{13}C$ in calcite	$^{87}Sr/^{86}Sr$ in calcite	Obtained radiometric ages[2]
		°C	wt% $CaCl_2$ eq	(‰ PDB)	(‰ PDB)		Ma
Generation1	epidote, chlorite, quartz	> 200					
Generation 2	adularia, prehnite, laumontite, chlorite, calcite	~ 150–280	3.5 to 13.1	–8.2 to –23.9	–1.6 to –7.1	0.70731 to 0.71289	1,107 ± 7 1,093 ± 3 1,072 ± 3 1,034 ± 3 1,096 ± 100*
Generation 3	quartz, calcite, pyrite, corrensite, adularia, analcime, asphaltite	~ 50–190	7.3 to 19.3	–14.4 to –9.6	–53.1 to –2.4	0.71461 to 0.71679	< 460 276.9 ± 1.1
Generation 4	Clay minerals, chlorite, Calcite, ± pyrite, ± FeOOH	< 50		–15.0 to –7.4	–21.3 to +8.1	0.71375 to 0.71940	

[1)] Based on mineral stabilities and fluid inclusions in calcite.

[2)] Based on $^{40}Ar/^{39}Ar$ dating of adularia and one Rb-Sr errorchron age (*) determination of adularia, prehnite, calcite and wall rock.

4.1 Generation 1

The oldest generation of fracture minerals in the Forsmark area is dominated by fractures sealed with hydrothermally precipitated epidote, quartz and Fe-rich chlorite. The minerals occur also in sealed, brittle-ductile cataclasites (Figure 4-1). Stereoplots with the orientation of epidote-sealed fractures within different fracture domains are shown in Figure 4-2. Epidote commonly occurs in sub-horizontal to gently dipping and steep WNW-ESE to NW-SE fractures but is also found, to a lesser degree, in other steeply dipping fracture sets. Epidote can be mistaken for prehnite during the drill core mapping, and some bias in the data is therefore expected in the extracted Boremap data.

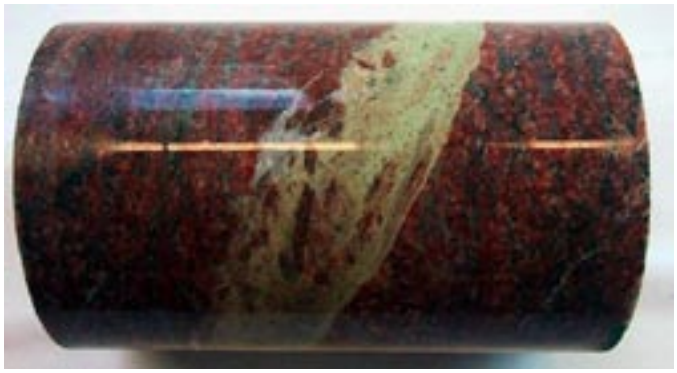

Figure 4-1. *Epidote-sealed cataclasite, KFM08A 605.08–605.16 m. The diameter of the drill core is ~ 5 cm.*

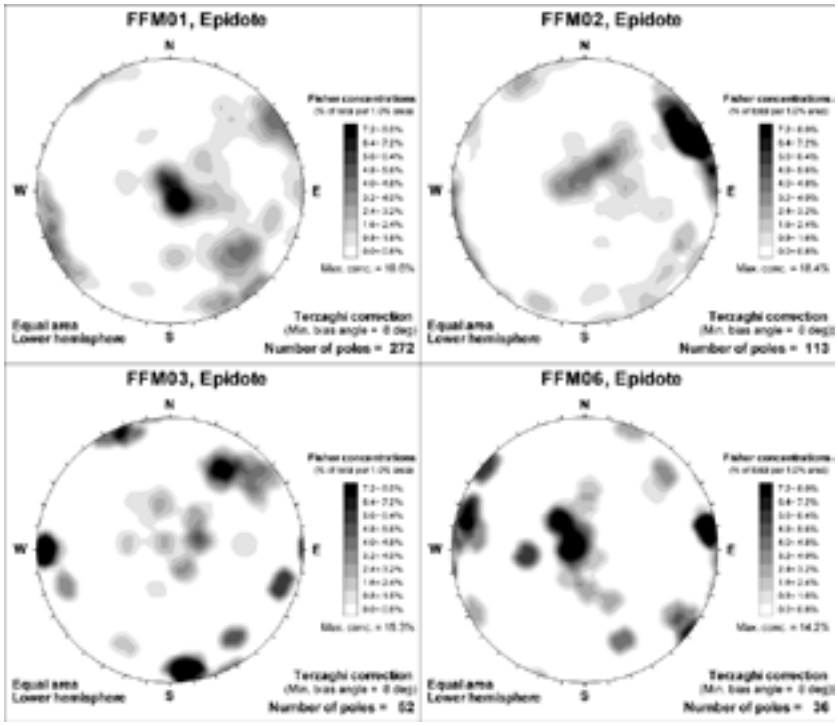

Figure 4-2. *Orientation of fractures sealed with epidote in fracture domains FFM01, FFM02, FFM03 and FFM06 (data from outside deformation zones). Fisher concentrations are shown as a percentage of the total number of poles per 1.0% of stereonet area. A Terzaghi correction has been applied to compensate for borehole orientations.*

Although epidote has been recorded at temperatures < 200°C in active geothermal systems, the mineral is normally formed at temperatures above 200°C /Bird et al. 1984, Bird and Spieler 2004/. Below this temperature prehnite is formed instead of epidote /Liou et al. 1983/. No radiometric ages of generation 1 minerals have been obtained. The $^{40}Ar/^{39}Ar$ hornblende and biotite ages (blocking temperatures at ~ 500° and 300°C respectively) indicate that the bedrock started to respond to brittle deformation between 1.80 and 1.73 Ga /Stephens et al. 2007, Söderlund et al. in press/. The oldest $^{40}Ar/^{39}Ar$ ages of adularia belonging to generation 2 (1.1 Ga, see below) provide a minimum age of the older generation 1 minerals. Therefore, it can be concluded that generation 1 minerals precipitated sometime between 1.8 and 1.1 Ga, possibly in response to late Svecokarelian and/or Gothian tectonothermal events /Sandström et al. 2006a, Stephens et al. 2007/.

4.1.1 Red-staining/oxidation of the wall rock

Fractures sealed with generation 1 and 2 minerals are associtated with red-staining of the wall rock due to hematite dissemination (Figure 4-3). This alteration shows strong spatial association with deformation zones /Stephens et al. 2007/, but is also common adjacent to single fractures within fracture domains. The character and properties of this altered (red-stained/oxidised) rock that occurs adjacent to generation 1 (and 2, see below) fractures have been described in a P-report by /Sandström and Tullborg 2006b/. The main focus of that study was to evaluate the remaing reducing capacity of the red-stained/oxidised wall rock. A scientific paper with focus on the processes associated with the rock alteration will be published /Sandström et al. in press/. For quantitative results the reader is referred to the P-report. The red-staining/oxidation of the wall rock occurres independently of depth /Stephens et al. 2007/. Other types of rock alteration in the Forsmark area (albitisation and development of vuggy rock associated with quartz dissolution) are not addressed within the scope of this report, the reader is instead referred to /Möller et al. 2003, Olofsson et al. 2004, Stephens et al. 2007/. However, based on the stable isotopic composition in calcite precipitated in voids in the vuggy rock, it can be concluded that the development of the vuggy rock is, at least, older than generation 2 minerals (see below) /Sandström and Tullborg 2006a/. Along single fractures, the red-staining/oxidation is the most common wall rock alteration.

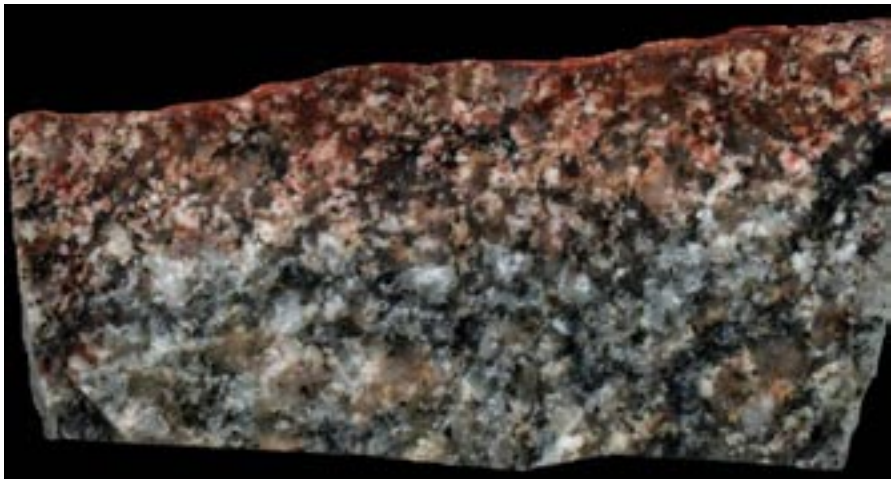

Figure 4-3. *Red-stained hydrothermally altered rock adjacent to a laumontite sealed fracture (generation 2, see below). The red-staining can be seen to gradually disappear ~ 1.5 cm out from the fracture. Sample KFM09A 145.84 m. The base of the picture is ~ 4.5 cm.*

The major mineralogical changes in the red-stained/oxidised rock are an almost complete saussuritisation of plagioclase (Figure 4-4), chloritisation of biotite (Figure 4-5) and to some extent hematisation of magnetite (Figure 4-6). The plagioclase of oligoclase composition has been replaced by a mineral assemblage consisting of albite, adularia, sericite, epidote, hematite and calcite. The red-staining is due to the dissemination of sub-microscopic hematite grains within and along the grain boundaries of the saussuritised plagioclase (Figure 4-4).

The hydrothermal red-staining normally extends a few centimetres perpendicularly out from the fractures, although more extensive zones also exist, often associated with penetrative networks of thin fractures and deformation zones /Stephens et al. 2007/. However, the alteration (especially the chloritisation) extends farther into the rock than the red-staining suggests, and the amount of rock mapped as "oxidised" should therefore be seen as a minimum value of the amount of altered rock.

The changes in geochemical composition between fresh and red-stained rock are relatively small. The major changes include an increase in Na_2O and LOI (Loss On Ignition) whereas CaO, FeO and SiO_2 decrease in the altered rock. Most trace elements have been immobile on the whole rock scale. However, on the micro-scale (between and within grains), the mobility of both major and trace elements have been more extensive /Sandström et al. in press/.

An increase in the connected porosity in the red-stained rock can be seen, most likely due to the chloritisation of biotite and an increase in the number of micro-fractures.

A small increase in the degree of oxidation can be seen in the red-stained rock but this change is not as evident as may be suggested by the red staining of the rock. The measured mean total oxidation factor (Fe^{3+}/Fe_{total}) increases from 0.20 in fresh rock to 0.28 in altered rock, indicating that most Fe is still in the Fe^{2+} oxidation state even in the altered rock.

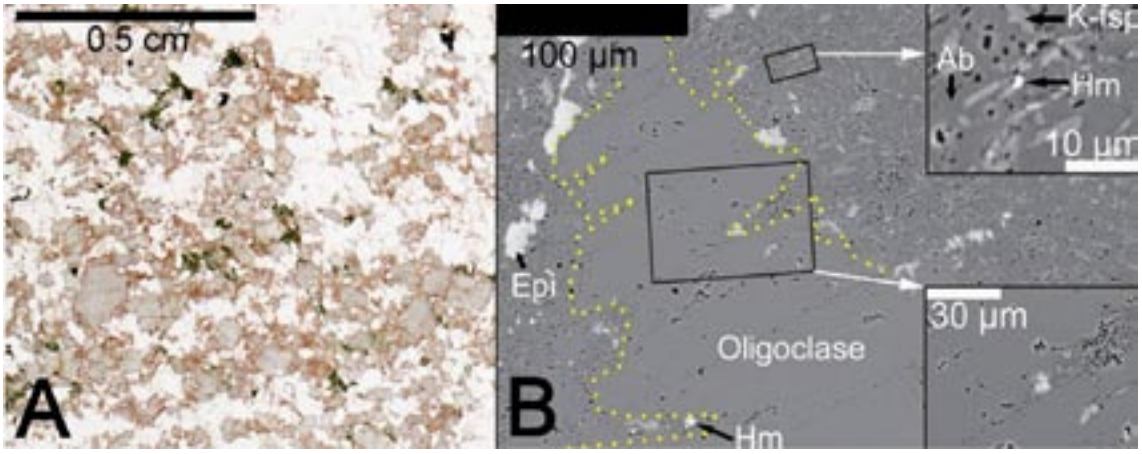

Figure 4-4. *Scanned thin section of altered rock showing how the red-staining is concentrated within and along grain boundaries of the saussuritised plagioclase. Sample KFM08A 623.13–623.35m. (B) Back-scattered electron image of a plagioclase crystal where a distinct front between fresh and saussuritised plagioclase is evident (marked with dashed line).*

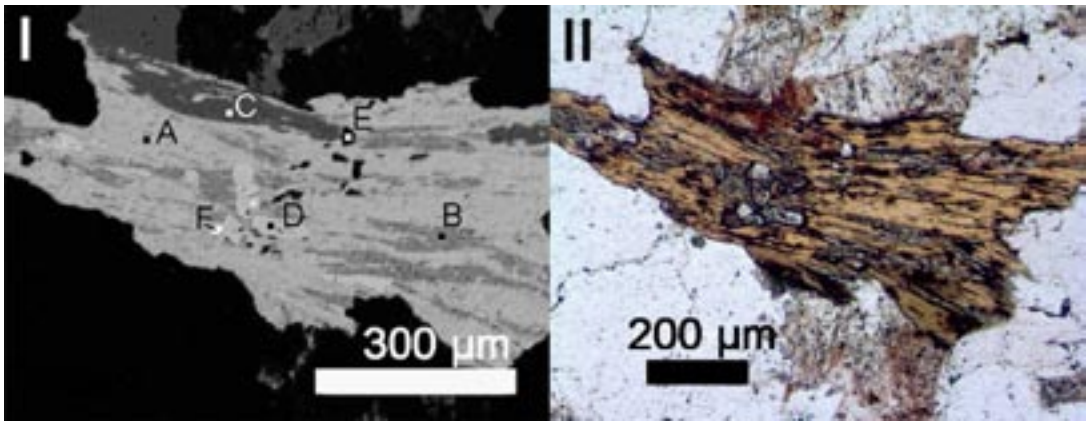

Figure 4-5. *(I) Backscattered electron image of chlorite with lenses of pumpellyite, adularia and titanite which pseudomorphically has replaced a biotite crystal. Small subhedral quartz and zircon crystals can also been seen in the image. A= chlorite, B= pumpellyite, C= adularia, D= titanite, E= quartz, F= zircon; (II) Microphotograph of the same chlorite crystal.*

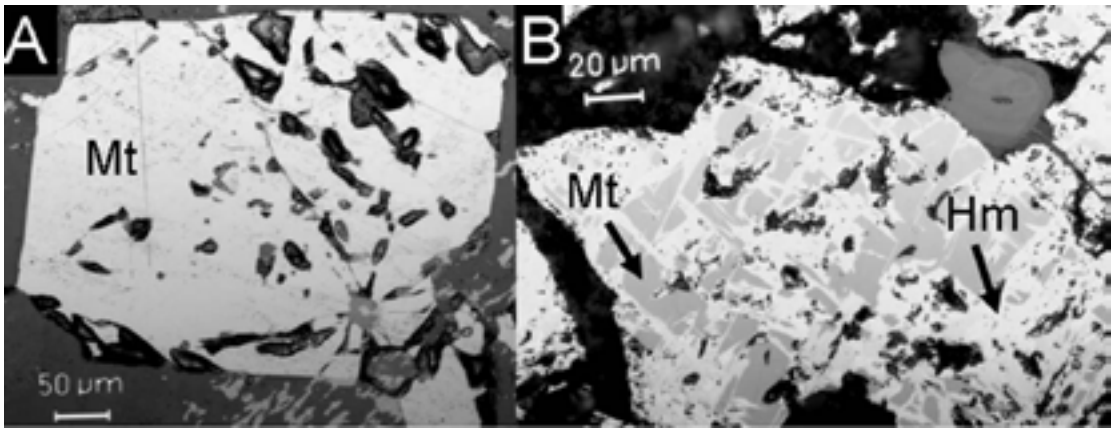

Figure 4-6. *(A) Microphotograph (reflected light) of a magnetite (Mt) crystal in fresh unaltered rock; (B) Microphotograph (reflected light) of magnetite partly replaced by hematite (Hm) in altered rock.*

4.2 Generation 2

Epidote-sealed fractures are cut by fractures sealed with a sequence of younger hydrothermal minerals. The sequence involves an initial phase with precipitation of hematite-stained adularia and albite together with small amounts of quartz, followed by prehnite and subsequently hematite-stained laumontite (Figure 4-7). Laumontite also occurs as sealings in breccias associated with the same hydrothermal event. Calcite, chlorite and corrensite are found coeval with all these phases. Trace amounts of pyrite have also been identified coeval with generation 2 minerals. Precipitation of generation 2 minerals is associated with the same kind of red-staining/ oxidation of the wall rock as associated with generation 1 minerals (see section 4.1.1).

Figure 4-7. *Generation 2 laumontite and calcite sealed fractures and breccias. Drill cores from KFM01C ~ 298–302 m.*

Due to highly deformed calcite and insufficient fluid inclusions, it was not possible to obtain homogenisation temperatures from the fluid inclusion studies of generation 2 calcites. However, homogenisation temperatures of ~ 200°C have been found in sample KFM08A 410.57 m (Figure 4-8) where calcite has grown in pores in vuggy granite (episyenite). The salinity of these fluid inclusions varies between 3.5 and 13.1 wt% (CaCl equivalents). Given the stable isotopic composition of this calcite (see section 5.3), it is plausible that it is associated with the same circulation of hydrothermal fluids responsible for the precipitation of generation 2 fracture minerals, and hence provides an approximate formation temperature. The stability fields for prehnite (~ 200–280°C at P < 3 kbar /Frey et al. 1991/) and laumontite (150–250°C /Liou et al. 1985/) also provide an estimation of the formation temperatures which overlap with the obtained homogenisation temperature in fluid inclusions.

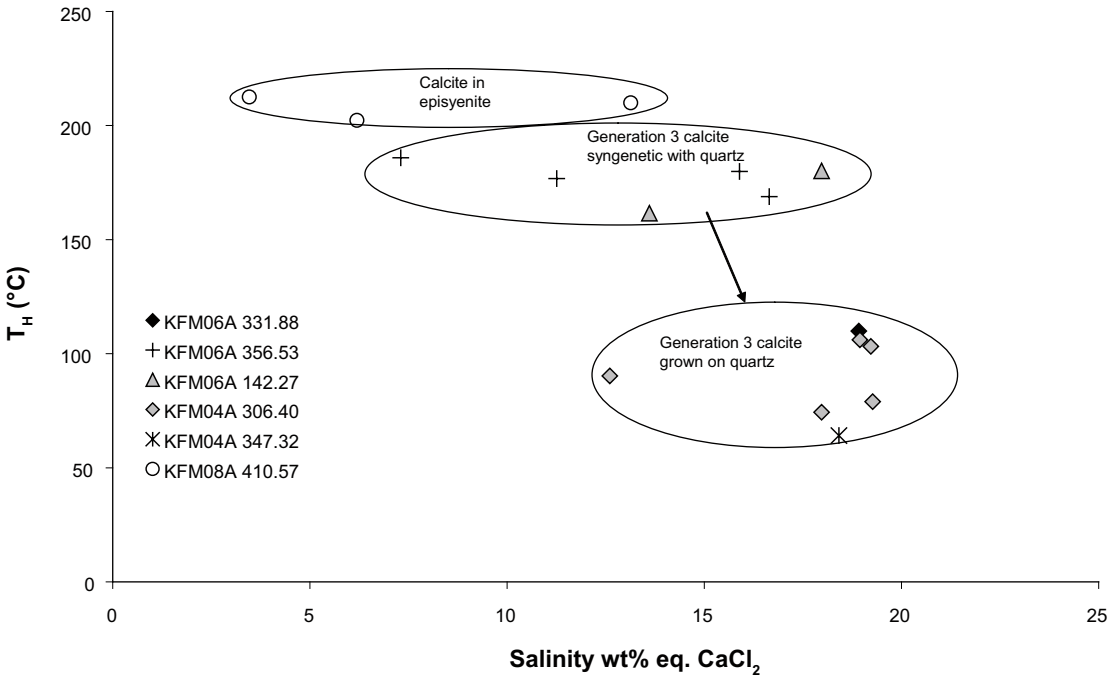

Figure 4-8. *Homogenisation temperature versus salinity of fluid inclusions in calcite /Sandström and Tullborg, in prep/.*

Based on $\delta^{13}C$ and $\delta^{18}O$ values in generation 2 calcite, a hydrothermal origin of the formation fluid is strongly suggested. A high degree of fluid-rock interaction is indicated by an oxygen shift in the $\delta^{18}O$ values in calcite (see section 5.1) as well as the alteration (red-staining/oxidation) of wall rock adjacent to fractures with generation 2 minerals (see section 4.1.1).

The obtained $^{40}Ar/^{39}Ar$ ages from generation 2 minerals (Table 4-1) can be interpreted as: a) crystallisation ages of the minerals, b) timing of thermal resetting of the isotopic systems, or c) cooling ages when the dated minerals passed through the closing temperature. A formation temperature of ~ 200°C for generation 2 minerals as suggested by the obtained homogenisation temperatures in fluid inclusions disagree with the cooling age hypothesis. However, it is possible that temperatures locally in the fracture system were higher than 200°C as suggested by the presence of prehnite (stable above ~ 200°C /Frey et al. 1991/).

The $^{40}Ar/^{39}Ar$ ages (and one Rb-Sr errorchron) between 1.1 and 1.0 Ga of generation 2 adularia suggest that this generation of fracture minerals was formed in connection with early Sveconorwegian tectonothermal activity /cf Bingen et al. 2005/. Another possibility is complete resetting of the isotopic systems during this period which would mean that at least the adularia is pre-Sveconorwegian. U/Pb geochronology of titanite in the bedrock shows a disturbance in the U/Pb system at 909 ± 200 Ma /Hermansson et al. 2008/, suggesting that even the rock matrix was thermally influenced during this episode. $^{40}Ar/^{39}Ar$ cooling ages from K-feldspar in the rock matrix indicate that the rock matrix passed the closure temperature for K-feldspar at ~ 1.5 Ga /Stephens et al. 2007/.

Although adularia-sealed fractures often are cut by prehnite- and laumontite-sealed fractures, the minerals are also found coeval in many fractures making a distinct separation between the different phases (parageneses) of generation 2 difficult. One possibility is that the different phases represent different conditions (P-T-x) during a single but prolonged and complex tectonothermal event. This is supported by observations of adularia and prehnite which have grown synchronously (Figure 4-9) and gradual transitions between prehnite and laumontite (Figure 4-10). Another scenario is that adularia, prehnite and laumontite precipitated during different tectonothermal events and that the obtained Sveconorwegian $^{40}Ar/^{39}Ar$ ages of adularia represent a resetting of the isotopic system during the youngest event, i.e. circulation of the hydrothermal fluids responsible for precipitation of laumontite.

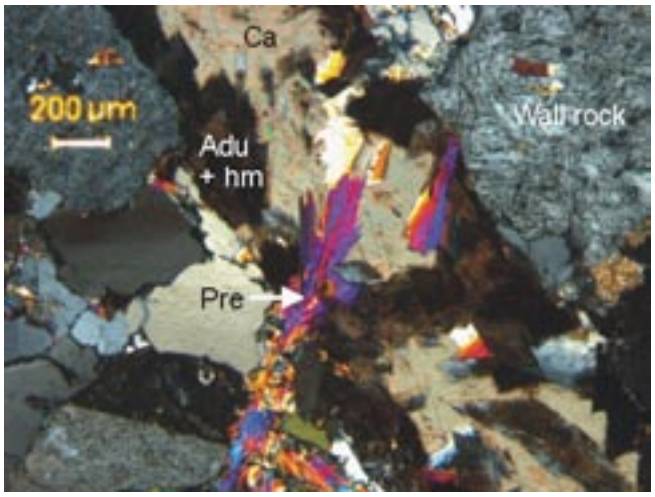

Figure 4-9. *Photomicrograph of prehnite crystals (Pre) which have grown together with hematite-stained adularia (Adu + hm). The fracture has later been sealed with calcite.KFM05A 692.00–692.15 m.*

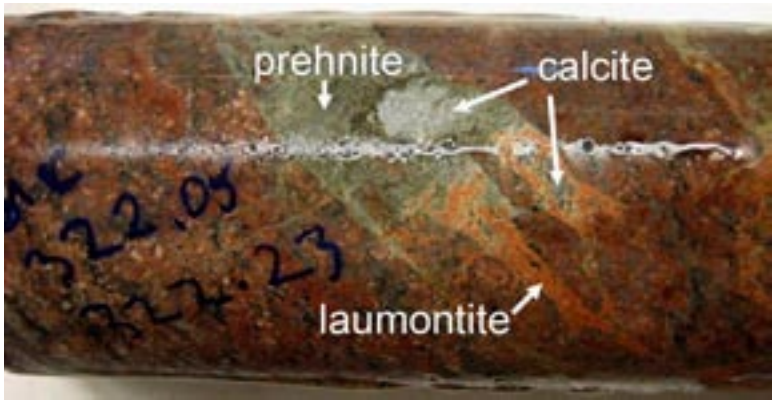

Figure 4-10. *Gradual transition between generation 2 prehnite and laumontite. Calcite occurs together with both phases. KFM01C 233.05–322.23 m. The diameter of the drill core is ~ 5 cm.*

Three samples of K-feldspar fragments from the wall rock in tectonic breccias sealed with laumontite have been dated by the $^{40}Ar/^{39}Ar$ method. One sample did not give a plataue age, one sample gave a well-defined plataue age showing that the K-Ar isotopic system in the wall rock fragments was resetted during the 1.1–1.0 Ga event, and the third sample gave a less developed plataue age of ~ 1.35 Ga. The obtained age of ~ 1.35 Ga is not interpreted as the age of the breccia formation, but as an age representing cooling of the K-feldspar in the wall rock below the closing temperature of K-feldspar /Sandström et al. 2008/.

Generation 2 minerals are commonly found in steep fractures trending ENE-WSW to NNE-SSW and NNW-SSE (as shown by adularia and laumontite in Figure 4-11 and Figure 4-12). Generation 2 minerals occur as the first precipitated minerals in most fractures (Figure 4-9), indicating formation of new fractures prior to precipitation of these fracture minerals (after precipitation of generation 1 minerals) or a complete dissolution of older fracture filling minerals in these fractures prior to precipitation. No evidences for dissolution of older (generation 1) fracture minerals have been found in fractures with generation 2 minerals during the detailed fracture mineral studies. Nevertheless, dissolution can still have occurred in many fractures since steep fractures which strike WNW-ESE to NW-SE (which often are lined with generation 1 minerals) mainly are found outside the target volume and thus poorly represented in the drill cores. Many breccias and cataclasites are sealed with generation 2 laumonite (Figure 4-7), suggesting that fracturing/reactivation of fractures in the rock occured during the same event responsible for precipitation of generation 2 minerals. No significant differences in the orientation of fractures with generation 2 minerals can be seen between the different fracture domains. Although adularia occurs in more than this generation, the abundance of hematite-stained generation 2 adularia compared to the few occurrences of generation 3 adularia, makes adularia applicable as an index mineral for the orientation of fractures with generation 2 minerals.

4.2.1 Dissolution of fracture minerals

A period of dissolution of older fracture fillings followed the precipitation of generation 2 minerals. This can be seen as partly dissolved laumontite and calcite in some fractures. The timing and cause of this dissolution are still unknown.

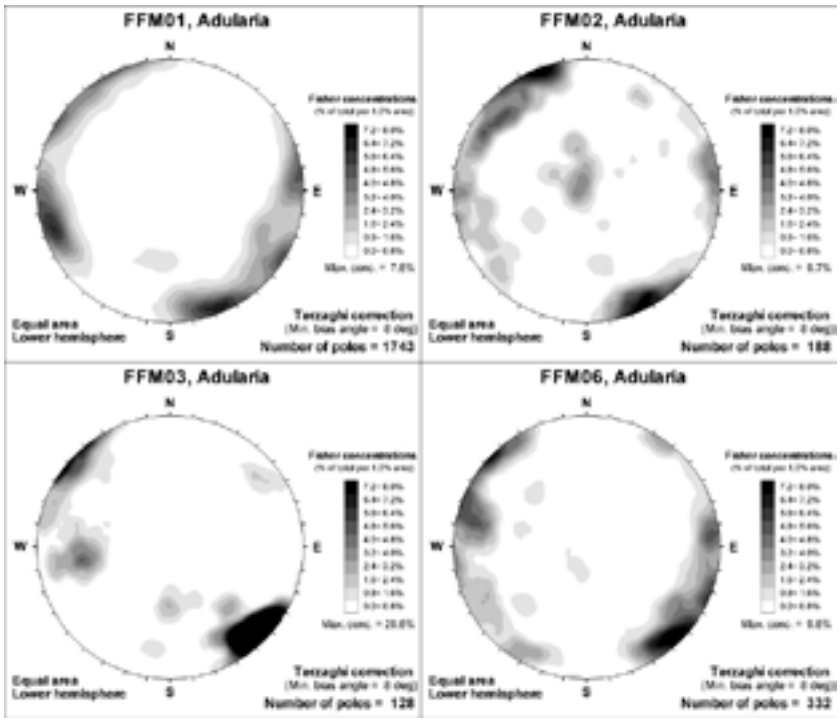

Figure 4-11. *Orientation of fractures sealed with adularia in fracture domains FFM01, FFM02, FFM03 and FFM06 (data from outside deformation zones). Fisher concentrations are shown as a percentage of the total number of poles per 1.0% of stereonet area. A Terzaghi correction has been applied to compensate for borehole orientations.*

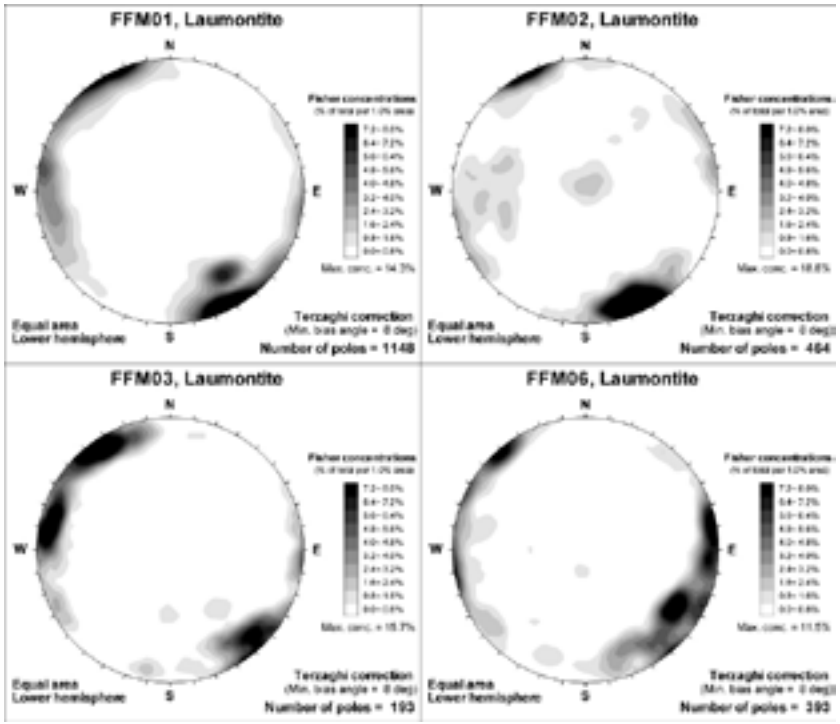

Figure 4-12. *Orientation of fractures sealed with laumontite in fracture domains FFM01, FFM02, FFM03 and FFM06 (data from outside deformation zones). Fisher concentrations are shown as a percentage of the total number of poles per 1.0% of stereonet area. A Terzaghi correction has been applied to compensate for borehole orientations.*

4.3 Generation 3

Generation 3 consists of minerals precipitated under low-temperature conditions and is dominated by calcite, quartz and pyrite (Figure 4-13). Asphaltite (a bitumen) occurs abundantly in the upper 150 metres of the bedrock, but has also been found at depths down to ~ 400 m close to the Forsmark deformation zone outside the target area. The occurrence and origin of the asphaltite have been addressed by /Sandström et al. 2006b/. Analcime, corrensite and adularia belonging to generation 3 are also found although less abundantly. Trace amounts of galena, fluorite, sphalerite, chalcopyrite and barite have also been identified. Quartz occurs as thin fracture coatings precipitated as the first mineral in fractures or as overgrowths on older fracture minerals (Figure 4-14). Calcite, pyrite and the other generation 3 minerals have later precipitated on these coatings. Quartz is also found intergrown and cogenetic with calcite and asphaltite in some of the fractures (Figure 4-15). Analcime occurs as the latest precipitated mineral in the generation 3 sequence.

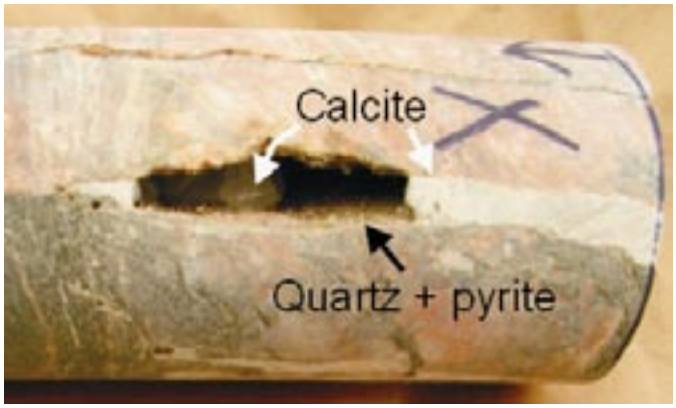

Figure 4-13. *Generation 3 calcite precipitated together with pyrite on a thin coating of quartz. Sample KFM04A 306.40–306.55 m, the diameter of the drill core is ~ 5 cm.*

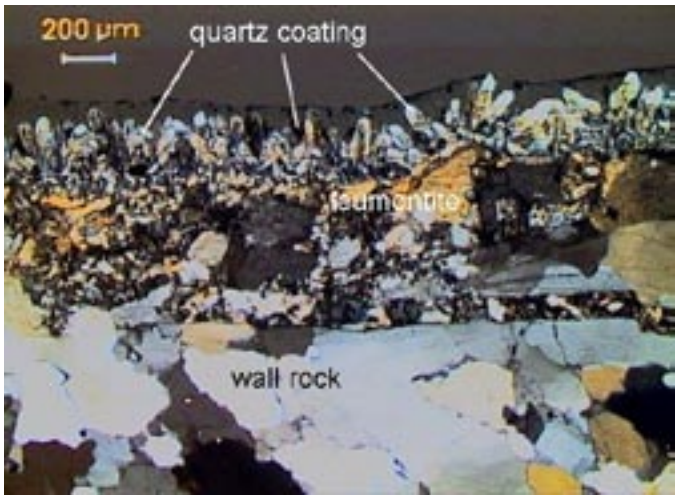

Figure 4-14. *Photomicrograph with crossed polars of thin coatings of euhedral generation 3 quartz precipitated on older generation 2 laumontite. Sample KFM04A 306.40–306.55 m.*

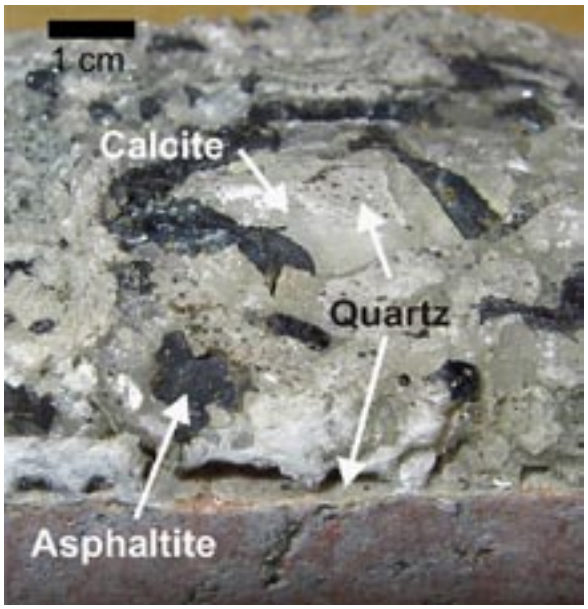

Figure 4-15. *Fracture filled with calcite, asphaltite and thin coatings of quartz. Sample KFM06C 103.19–103.28 m.*

Homogenisation temperatures (T_H) obtained from fluid inclusions in generation 3 calcite separate into two groups; T_H 161–186°C and T_H 64–109°C (Figure 4-8). Whether this separation is real or an artefact due to the small number of analysed inclusions can not be determined from this data. However, the higher T_H´s are found in calcite which is syngenetic and intergrown with quartz and shows salinities between 7 and 18 wt% (CaCl equivalents). Fluid inclusions with the lower T_H's are found in calcites which have grown on top of quartz coatings and display a shift toward more saline compositions (12–19 wt% CaCl eq.) (see Figure 4-8 and Figure 4-13)

Asphaltite, probably gilsonite, which occurs in the upper part of several boreholes has, based on $\delta^{13}C$ values (~ –30‰ PDB) and biomarker analyses, been confirmed to be of organic origin. Downward migration of fluids from the organic-rich early Palaeozoic Scandinavian Alum Shale is, based on e.g. similar biomarkers and the absence of another known organic source rocks, suggested as the most plausible source of the asphaltite /Sandström et al. 2006b/.

Generation 3 calcites can be distinguished from older calcite by their higher $^{87}Sr/^{86}Sr$ values (section 5.3). Most generation 3 calcites show $\delta^{13}C$ values between –7 and –30‰ (PDB) (section 5.1), indicating an organic influence on the formation fluid /cf Tullborg et al. 1999, Wallin and Peterman 1999/. A few samples with extreme $\delta^{13}C$ values (< –30‰) indicate microbial activity, probably due to oxidation of organic material, producing extreme $\delta^{13}C$ values in CO_2/HCO_3^- which have been incorporated in the precipitating calcite. The positive $\delta^{34}S$ values in generation 3 pyrite (section 5.2) could be due to mobilisation, and subsequent precipitation, of sulphur emanating from Cambrian-Carboniferous sedimentary pyrite, which has been shown to be enriched in ^{34}S /Strauss 1997/, in agreement with the proposed Palaeozoic age of generation 3 minerals. The $\delta^{18}O$ values of generation 3 quartz vary between 18.4 and 21.9‰ (SMOW) /Sandström and Tullborg 2006a/ which is in agreement with a low temperature origin for generation 3 /cf Chacko et al. 2001/.

Microbial and/or thermochemical reduction of sulphate, in the presence of organic material and subsequent precipitation of pyrite and calcite in a reduced system, is a plausible process for the precipitation of generation 3 minerals. Sulphate and organic matter are suggested to have emanated from overlying organic rich sediments and the source of the elevated temperatures, suggested by the fluid inclusion analyses, could be heat due to burial by the overlying sediments. It could also have resulted from the opening of fractures that allowed deeper, hotter fluids, to rise from depth. However, no isotopic indications of deep hot fluids have been found in generation 3 calcites.

Generation 3 minerals suitable for radiogenic dating (adularia) are only found sporadically. Only two samples of fracture filling adularia clearly belonging to generation 3 have been identified and dated by the $^{40}Ar/^{39}Ar$ method /Sandström et al. 2006a/. The position of the two dated samples within the relative sequence is well known based on genetic relations with other generation 3 minerals and represent one early and one late phase of the precipitation of generation 3 minerals. The inferred older sample gave an $^{40}Ar/^{39}Ar$ step-heating spectrum typical for excess argon (u-shaped) /cf Kelley 2002/. Thus, the obtained age of ~ 460 Ma can only be considered as a maximum age for the adularia. The other (inferred younger) analysed adularia sample has grown together with analcime on top of generation 3 pyrite and represents a late stage of the precipitation of generation 3 minerals. Thus, the interpretation is that the main phase(s) of precipitation of generation 3 minerals occurred prior to the obtained $^{40}Ar/^{39}Ar$ age of 276.9 ± 1.1 Ma.

Altough the radiometric age data is very limited for generation 3 minerals, the good relative geochronological control on the dated samples constrains the main event(s) of precipitation of generation 3 minerals to the Palaeozoic period. Precipitation of generation 3 minerals occurred at several events during the Palaeozoic as shown in Figure 4-16, where calcite mixed with quartz and pyrite represents an older event of precipitation followed by precipitation of pure calcite. $\delta^{13}C$ values in calcite from both these events of precipitation show an organic influence on the formation fluid (section 5.1.2.).

A plausible tectonic scenario responsible for the penetration of fluids from a sedimentary overburden is the development of an overpressured aquifer in an overlying sedimentary basin /cf Hunt 1990, Gleeson et al. 2003, Sircar 2004/ in response to the development of a Caledonian foreland basin during the Palaeozoic /cf Larson et al. 1999/. The obtained $^{40}Ar/^{39}Ar$ age of 276.9 ± 1.1 Ma correlates with the formation of the Oslo rift /e.g. Sundvoll et al. 1990/ implying that this event also could have influenced the stress situation in Forsmark during the late Palaeozoic, causing fracturing or reactivation of older fractures.

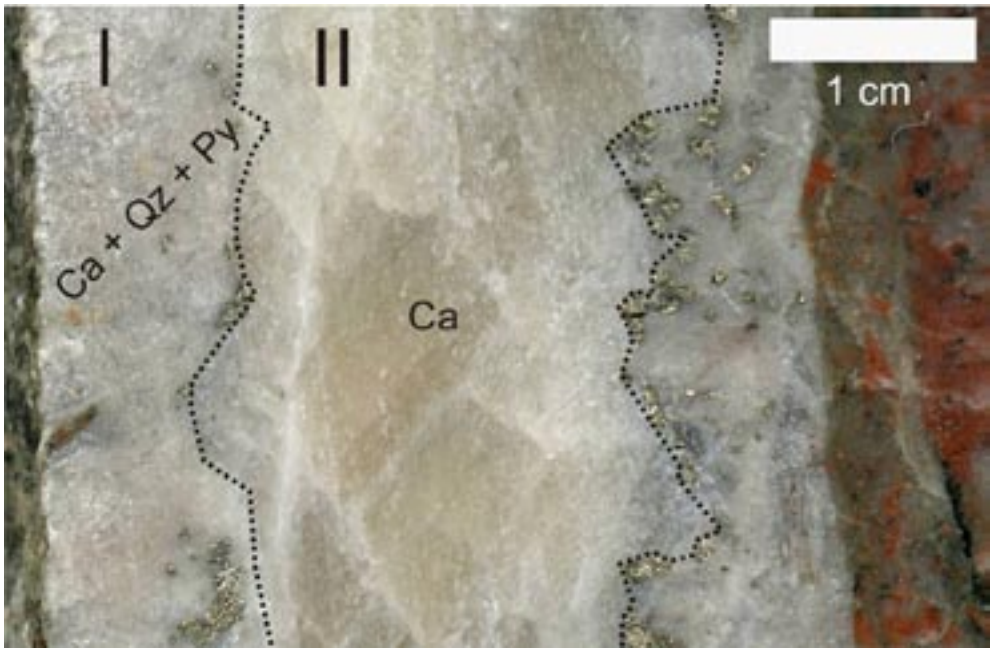

Figure 4-16. *Palaeozoic generation 3 frature fillings showing precipitation during two different events; first precipitation of calcite (Ca) together with quartz (Qz) and pyrite (Py) (I) and later precipitation of pure calcite (II).*

Pyrite occurs almost exclusively as a generation 3 mineral and is therefore, beside asphaltite, which exclusively belongs to this generation, used as index minerals to show the orientation of fractures with generation 3 minerals based on the Boremap data (Figure 4-17 and Figure 4-18). It is evident from the orientation of these fractures, and the occurrence of generation 3 minerals in fractures with older generation 2 minerals (section 4.2), that the circulation of fluids responsible for precipitation of generation 3 minerals occurred in reactivated steep NE trending fractures. The more sub-horizontal to gently dipping fractures filled with generation 3 minerals in the shallow fracture domains FFM02 and FFM03 suggest that reactivation of older structures (generation 1, section 4.1) was significant in the upper part of the present bedrock during the Palaeozoic. Reactivation of the older, steep NW trending structures is also suggested by the presence of pyrite and asphaltite in these fractures, especially in fracture domains FFM02, FFM03 and FFM06. When fractures inside deformation zones also are considered /Stephens et al. 2007/ it is apparent that more sub-horizontal to gently dipping fractures are coated with generation 3 minerals than is evident from Figure 4-17 and Figure 4-18.

Fractures with pyrite (generation 3 mineral) that do not contain a generation 1-2 mineral and/or do not have altered wall rock (which is associated with generation 1 and 2 mineral precipitation) can be interpreted as possibly younger than those sealed with generation 1 and 2 minerals. The Boremap system used during the drill core mapping only allows four different fracture minerals to be recorded for each fracture (altered wall rock is mapped as a fracture mineral in Boremap). If four or more minerals are recorded in a fracture, additional information (such as wall rock alteration) is available in Sicada as comments in the data file: bm_comment. Therefore, the content in the comment file has also been considered during the interpretation of the Boremap data. Minerals/alterations in the Boremap data here considered as representative for the generation 1-2 precipitation events are: hematite, adularia, red feldspar, laumontite, prehnite, epidote, oxididised walls, bleached walls, epidotised walls and saussuritised walls. However, there is a large degree of bias in this data since e.g. faint alteration easily can have been overlooked during the drill core mapping.

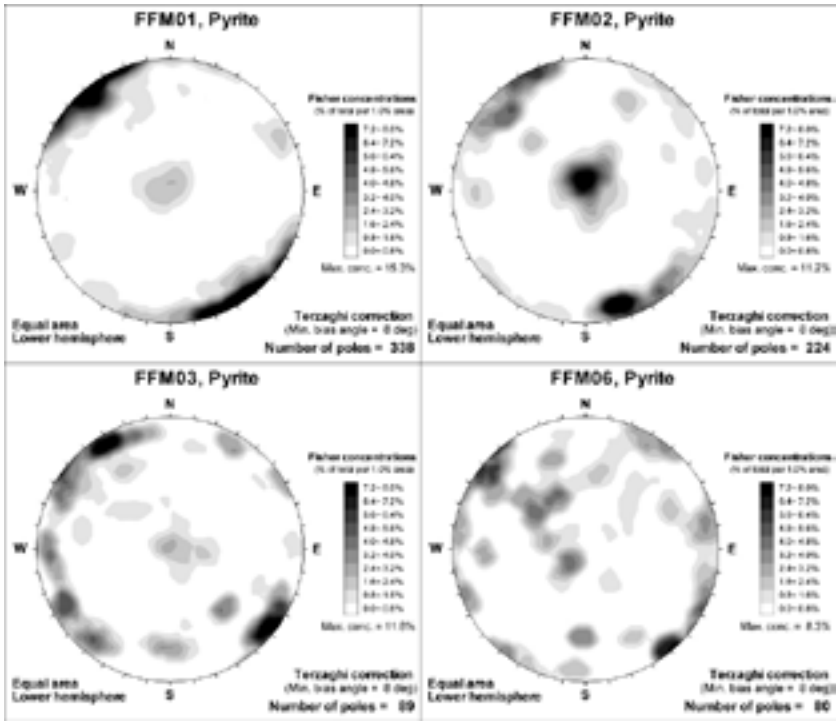

Figure 4-17. *Orientation of fractures with pyrite in fracture domains FFM01, FFM02, FFM03 and FFM06 (data from outside deformation zones). Fisher concentrations are shown as a percentage of the total number of poles per 1.0% of stereonet area. A Terzaghi correction has been applied to compensate for borehole orientations.*

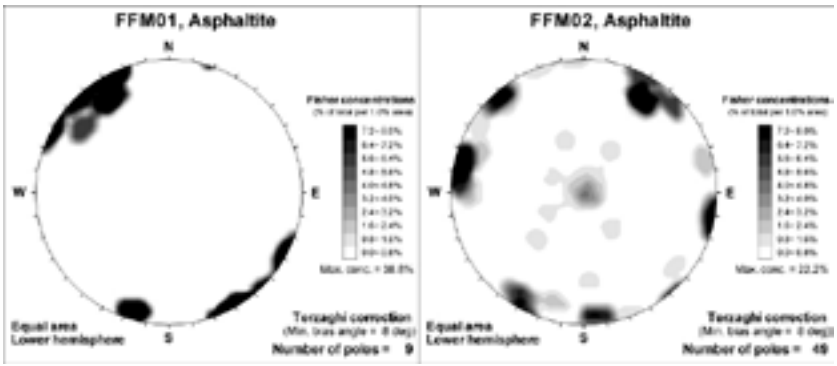

Figure 4-18. *Orientation of fractures with asphaltite in fracture domains FFM01 and FFM02 (data from outside deformation zones). No occurrences of asphaltite have been identified in FFM03 and FFM06. Fisher concentrations are shown as a percentage of the total number of poles per 1.0% of stereonet area. A Terzaghi correction has been applied to compensate for borehole orientations. Observe that only 9 poles are used in the plot of fractures with asphaltite in FFM01.*

Considering the available data, formation of new fractures after the precipitation of generation 1 and 2 minerals is suggested by the presence of a significant number of fractures with pyrite but without altered wall rock or generation 1 and 2 minerals (Figure 4-19). Formation of new fractures was probably more extensive in the upper part of the bedrock during this period as suggested by the higher abundance of fractures with pyrite without altered wall rock or generation 1-2 minerals in fracture domains FFM02 and FFM03 and FFM06. Formation of new fractures is also indicated within the older deformation zones. No difference can be seen between open/partly open fractures and sealed fractures.

The orientation of fractures with pyrite and no wall rock alteration and/or generation 1-2 minerals is shown in Figure 4-20. The orientation data are not unambiguous regarding formation of fractures after the generation 1-2 fracture mineral precipitation events, many of the fracture orientations showed in Figure 4-20 are similar to those of fractures lined with generation 1 and 2 minerals (cf Figure 4-2, Figure 4-11 and Figure 4-12). This could be due to that some of the fractures plotted in Figure 4-20 have altered wall rock which has not been recorded during the drill core mapping but also formation of new discrete fractures within older deformation zones dominated by older minerals. However, in the upper part of the bedrock (fracture domain FFM02) (Figure 4-20), fractures with pyrite and no wall rock alteration and/or generation 1-2 are preferably sub-horizontal to gently dipping, although other fracture sets are also represented.

Considering the available data, the following conclusions of the conditions prevailing during precipitation of generation 3 minerals can be made:

- Precipitation of quartz and calcite occurred at an early stage from a fluid with temperatures in the vicinity of 161–186°C and salinities between 7 and 18 wt% ($CaCl_2$ eq.). Calcite found on quartz coatings precipitated at temperatures between 64 and 109°C and from a fluid with a salinity between 12 and 19 wt% ($CaCl_2$ eq.). It is possible that the differences in formation temperature and salinity are indicative for local variations in temperature and composition of the fluid, but it is also possible that the minerals with the higher formation temperatures are significantly older. However, the majority of generation 3 calcites precipitated under lower temperature conditions.
- The isotopic composition of calcite, pyrite and asphaltite strongly indicates an organic influence on the formation fluid. The occurrence of asphaltite in the upper part of the bedrock implies a downward penetration of the fluid emanating from an organic rich sedimentary cover /Sandström et al. 2006b/.
- $^{40}Ar/^{39}Ar$ ages of adularia show that the main events of precipitation of generation 3 fracture minerals occurred during the Palaeozoic, after the late Ordovician (< 460 Ma) and with a late phase of mineral growth during the early Permian (around 277 Ma).

- Pyrite in many of the fractures, and also the presence of organic material (asphaltite), indicate reducing conditions in large parts of the fracture system during this period.
- Circulation of fluids responsible for precipitation of Generation 3 minerals occurred in older reactivated structures, but also in fractures formed after precipitation of generation 1 and 2 minerals, especially in the upper part of the bedrock.
- A plausible tectonic scenario responsible for the penetration of fluids from a sedimentary overburden is elevated pressure in response to the development of a Caledonian foreland basin during the Palaeozoic.

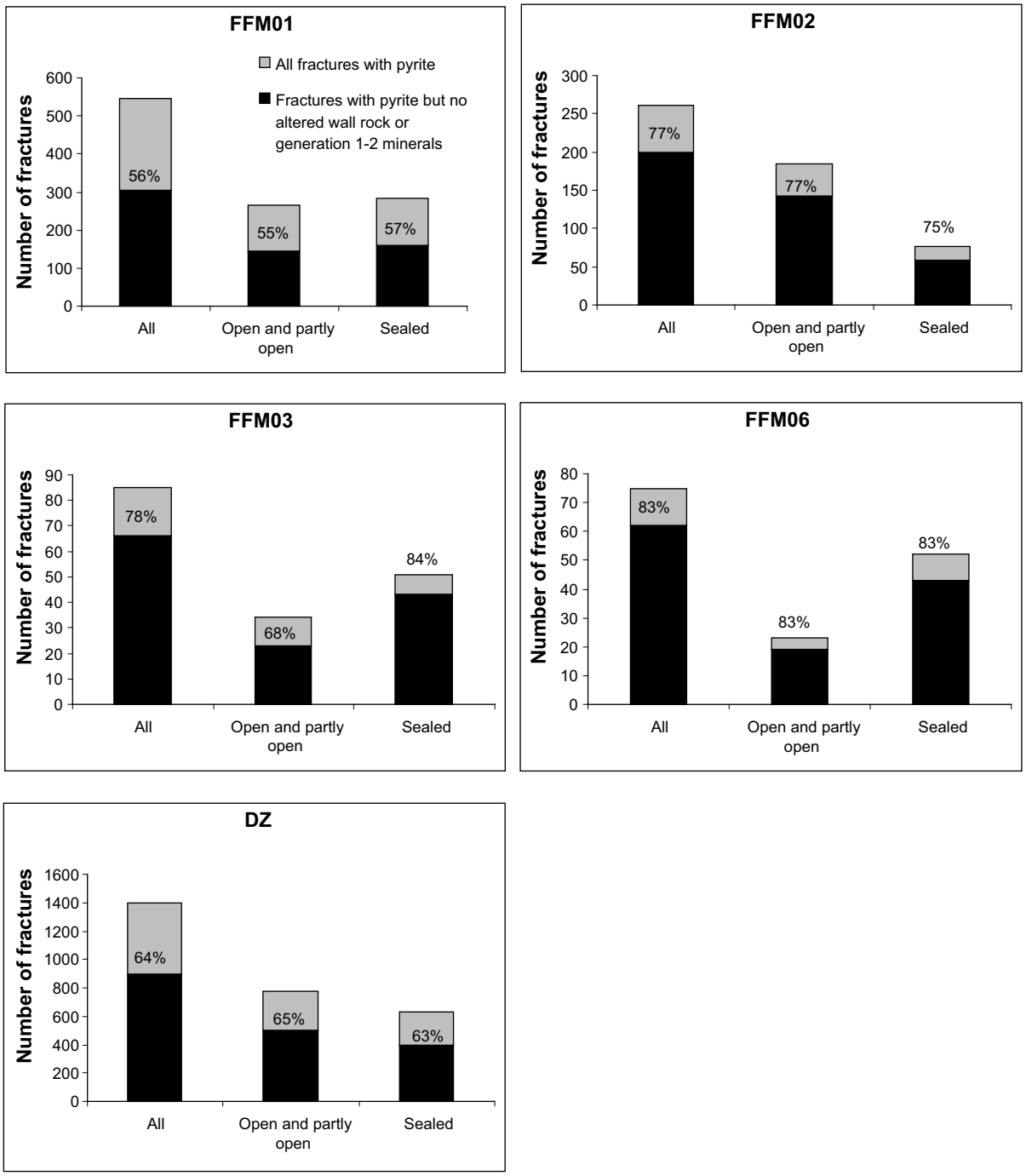

Figure 4-19. *Percentages of fractures within fracture domains FFM01, FFM02, FFM03, FFM06 and deformation zones (DZ) with pyrite that have no wall rock alteration and/or do not contain any generation 1 or 2 minerals. Grey bars represent the total number of fractures with pyrite.*

	Open and partly open fractures	Sealed fractures
FFM01 Pyrite without generation 1-2 minerals and/or no wall rock alteration	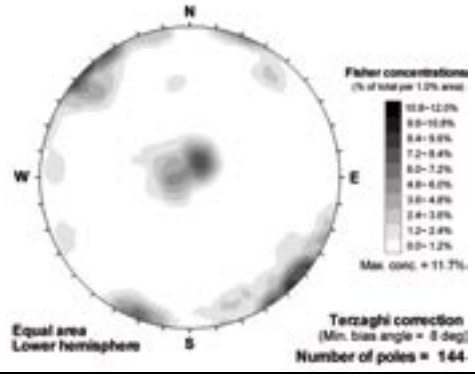	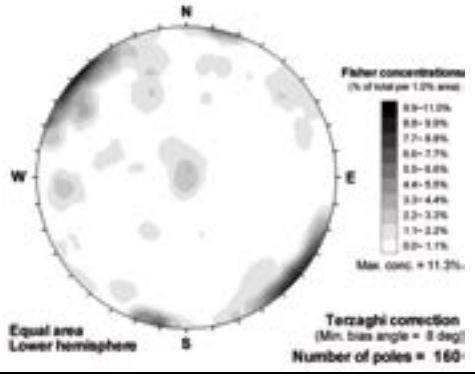
FFM02 Pyrite without generation 1-2 minerals and/or no wall rock alteration	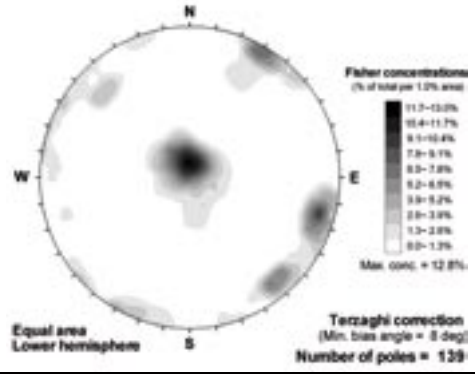	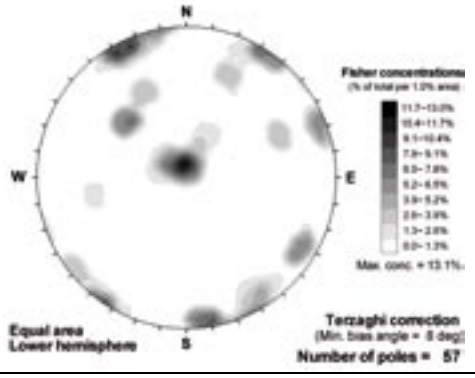
FFM03 Pyrite without generation 1-2 minerals and/or no wall rock alteration	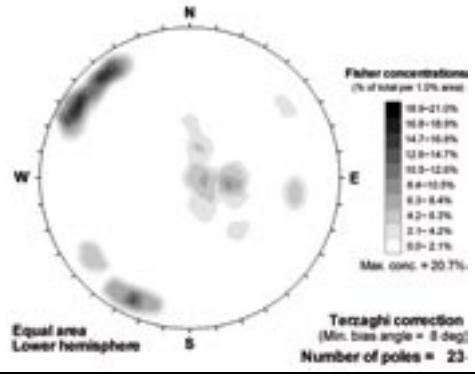	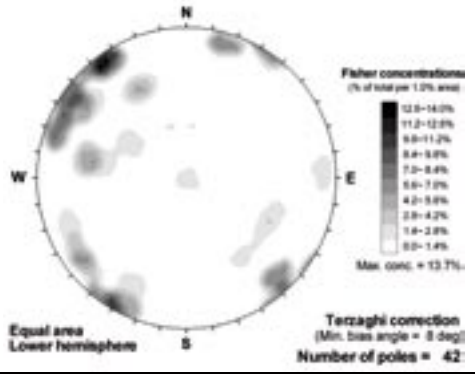
FFM06 Pyrite without generation 1-2 minerals and/or no wall rock alteration	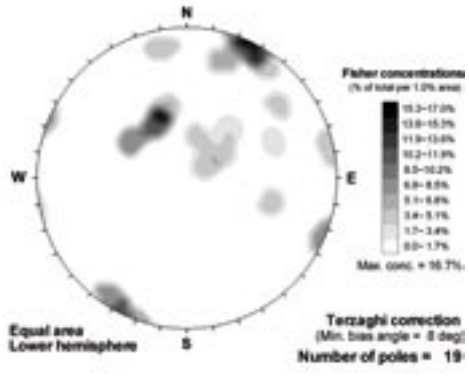	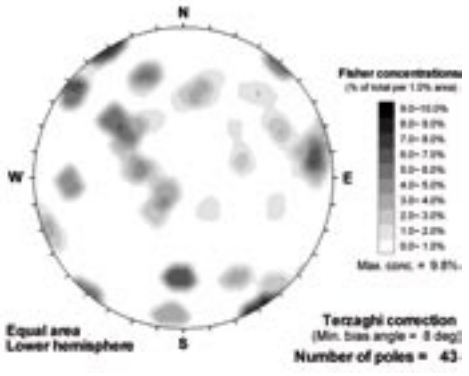

Figure 4-20. *Orientation of fractures with pyrite that have no wall rock alteration and/or do not contain any generation 1 or 2 minerals. Data from fracture domains FFM01, FFM02, FFM03 and FFM06 (Data from outside deformation zones). Fisher concentrations are shown as a percentage of the total number of poles per 1.0% of stereonet area. A Terzaghi correction has been applied to compensate for borehole orientations.*

4.4 Generation 4

Generation 4 mainly consists of clay minerals, chlorite/corrensite and thin coatings of calcite, preferentially found in hydraulically conductive fractures and fracture zones (Figure 4-21 and Figure 4-22). Many of these fractures and zones are older reactivated structures containing remnants of generation 1, 2 and 3 minerals. Small amounts of goethite and pyrite are also found in some of these fractures. Although it is often difficult to distinguish this younger pyrite from older generation 3 pyrite, the present reducing conditions suggest that pyrite precipitation could be an ongoing process /Gimeno et al. 2008/. The most abundant clay minerals are corrensite, illite, mixed layer clays and smaller amounts of smectite, kaolinite, vermiculite and other swelling clays (see section 3.2). However, clay minerals have also been formed during previous events (generations) and it is difficult to distinguish clay minerals formed during generation 4 from the older ones.

Generation 4 calcites show similar $\delta^{18}O$ and $\delta^{13}C$ signatures as generation 3 calcites, but a shift toward higher $\delta^{18}O$ and $\delta^{13}C$ values can be seen (section 5.1). Only one calcite has been identified with a $\delta^{18}O$ value and a $^{87}Sr/^{86}Sr$ ratio corresponding to precipitation at equilibrium with present day groundwater at ambient temperatures. However, a few sampled calcites may have been precipitated from groundwaters recharged during a slightly cooler climate regime (section 5.1).

Analyses of U-series disequilibrium in bulk fracture mineral samples, mostly collected from hydraulically conductive fractures and fracture zones (see also Chapter 8), interpreted as belonging to generation 4, indicate that many of these fractures have been open to uranium redistribution during the last 1 Ma, mainly in the upper 200 m but also at greater depth.

Figure 4-21. *Fracture surface with thin coating of generation 4 calcite and clay minerals. Sample KFM01C 90.63–90.73 m. The diameter of the drill core is ~ 5 cm.*

Figure 4-22. *Fracture filled with generation 4 clay minerals (illite and mixed layer clay) together with chlorite, calcite, quartz, plagioclase, K-feldspar and titanite. Minerals have been identified by XRD-analysis. Sample KFM01C 12.43–12.5 m. The diameter of the drill core is ~ 5 cm.*

Generation 4 minerals are commonly found in sub-horizontal to gently dipping fractures (exemplified by clay minerals and goethite in Figure 4-23 and Figure 4-24), but also in steep NNE, ENE and NW trending fractures. Almost all these fractures are reactivated older structures (predominantly Proterozoic) which have been hydraulically conductive at different episodes, for example, due to shifts in the stress field in the area. It is also plausible that some preferred formation of near-horizontal fractures occurred later in response to loading and unloading cycles related to sedimentation episodes and glaciations /cf Stephens et al. 2007/.

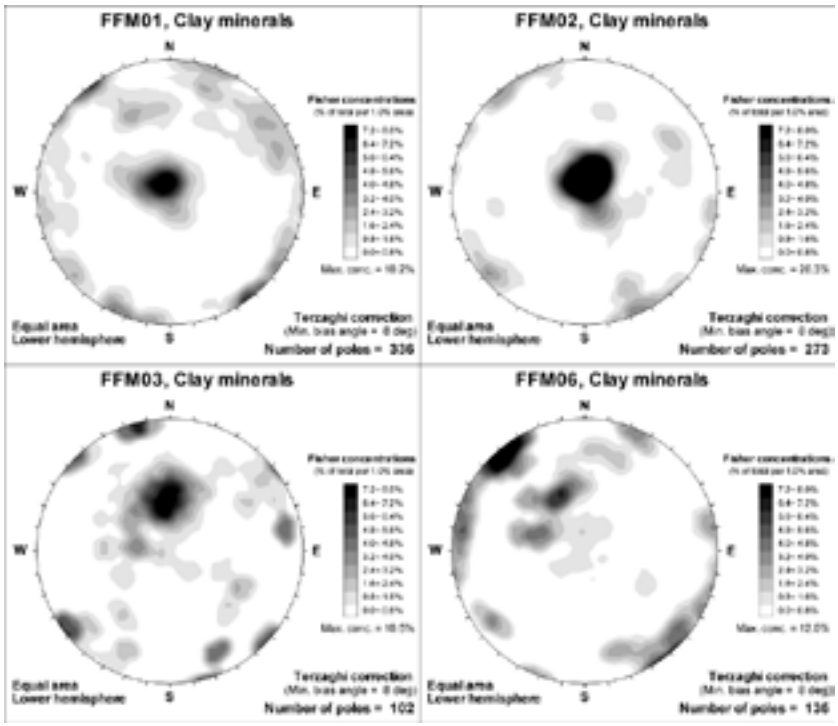

Figure 4-23. *Orientation of fractures with clay minerals in fracture domains FFM01, FFM02, FFM03 and FFM06. Data from outside deformation zones. Fisher concentrations are shown as a percentage of the total number of poles per 1.0% of stereonet area. A Terzaghi correction has been applied to compensate for borehole orientations.*

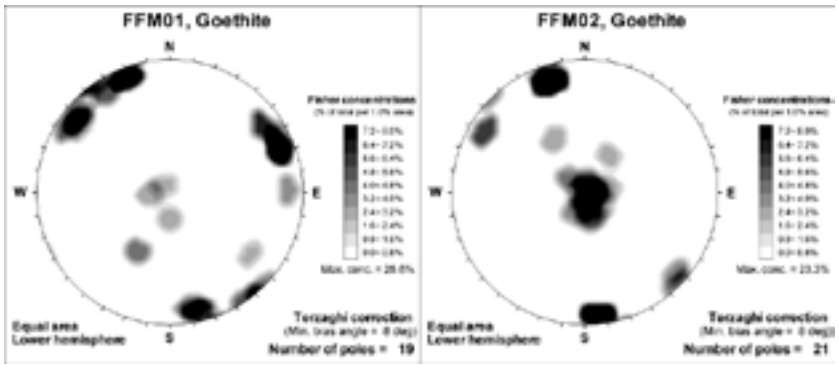

Figure 4-24. *Orientation of fractures with goethite in fracture domains FFM01 and FFM02 (only one goethite occurrence has been mapped in FFM03 and none in FFM06). Data from outside deformation zones. Fisher concentrations are shown as a percentage of the total number of poles per 1.0% of stereonet area. A Terzaghi correction has been applied to compensate for borehole orientations.*

Fractures mapped as “no mineral”, i.e. fractures where minerals could not be identified macroscopically during the drill core mapping, are present in the Boremap data. Although several of these fractures may be drilling or mapping artefacts /Stephens et al. 2007/, natural fractures without any mineral coatings are possibly of late origin and may be connected with stress release close to the bedrock surface /Stephens et al 2007/. It is evident from Figure 4-25 that most fractures mapped as “no mineral” are found in sub-horizontal and gently dipping fractures. The orientations are similar to those fractures with clay minerals, especially in FFM01 and FFM02. In FFM03 and FFM06, several “no mineral”-fractures also occur along steep fractures. In order to understand the geological importance of fractures mapped as “no mineral” further analysis of the Boremap data, detailed microscopic examination of the fracture surfaces and evaluation of groundwater chemistry regarding dissolution/precipitation of minerals at present conditions are needed.

4.5 Concluding remarks

Four different generations of fracture mineralisations have been distinguished with a high confidence.

Generation 1 consists of epidote, quartz and chlorite, and brittle-ductile cataclasites are sealed with these minerals (T > 200°C). They are conspicuous in sub-horizontal and gently dipping fractures or in steep, WNW-ESE to NW-SE fractures. However, they are also present along fractures in other steeply dipping sets. This generation formed between 1.8 and 1.1 Ga, and is possibly related to late Svecokarelian and/or Gothian tectonothermal events. Red-staining/oxidation of the wall rock is associated with precipitaton of generation 1 minerals.

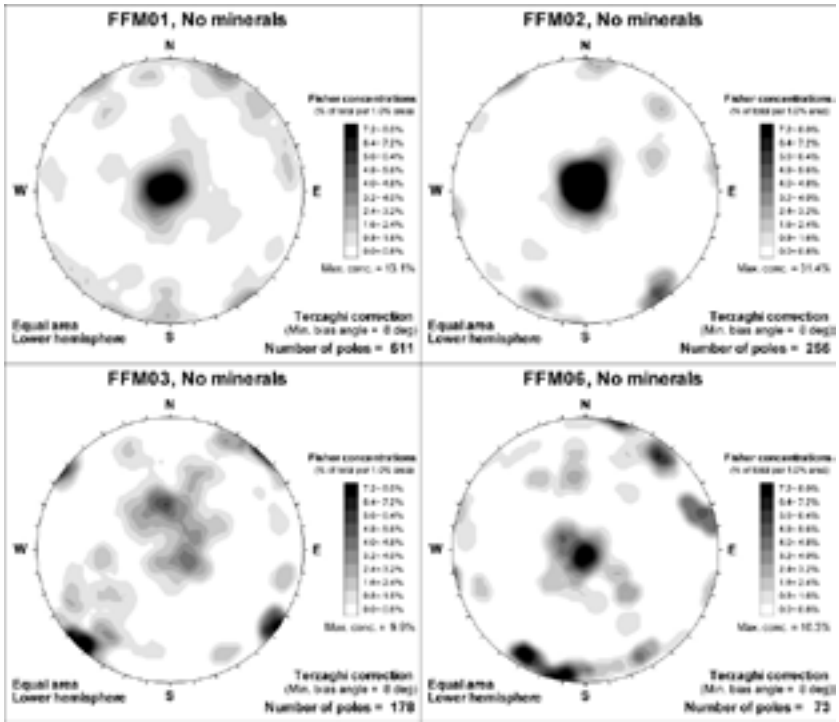

Figure 4-25. *Orientation of fractures with no visible minerals in fracture domains FFM01 and FFM02 (only one goethite occurrence has been mapped in FFM03 and none in FFM06). Data from outside deformation zones. Fisher concentrations are shown as a percentage of the total number of poles per 1.0% of stereonet area. A Terzaghi correction has been applied to compensate for borehole orientations.*

Generation 2 consists of a sequence of hydrothermal fracture minerals (T ~ 150–280°C) dominated by adularia, albite, prehnite, laumontite, calcite, chlorite and hematite. Generation 2 minerals are particularly common along steep, ENE-WSW to NNE-SSW and NNW-SSE fractures. $^{40}Ar/^{39}Ar$ ages from adularia indicate a major influence of early Sveconorwegian tectonothermal activity at 1.1 to 1.0 Ga on the development of fracture systems that are coated or filled by this mineral. Both reactivation of older fractures and formation of new fractures are inferred during the Sveconorwegian tectonothermal event. Red-staining/oxidation of the wall rock is also associated with precipitaton of generation 2 minerals. Dissolution of fracture minerals occurred before the formation of generation 3 minerals.

Generation 3 consists of minerals precipitated under low-T conditions during the Palaeozoic. The most abundant minerals are calcite, quartz, pyrite, corrensite and asphaltite. Stable isotopes in calcite and the presence of asphaltite indicate that the formation fluid was influenced by organic material, which may have emanated from an overlying sedimentary cover. The orientation of fractures with generation 3 minerals suggests reactivation of fractures filled with older minerals but new fractures were also formed.

Generation 4 is dominated by chlorite/clay minerals and thin precipitates of calcite in predominantly hydraulically conductive fractures and fracture zones. These minerals are prominent along sub-horizontal and gently dipping fractures, but are also present in different sets of steeply dipping fractures. It is inferred that most of the hydraulically conductive fractures are ancient structures and that precipitation of generation 4 minerals has most likely occurred during a long period of time (after the Palaeozoic). However, some of the near-surface, sub-horizontal fractures, which include sheet joints formed in connection with stress release, may be Quaternary in age. Fractures without any visible minerals (mapped as “no mineral” during the drill core mapping) are also interpreted to belong to generation 4, although the abundance of these fractures needs to be addressed in a special study. Precipitation of generation 4 minerals has probably been controlled by, for example, variations in water flow pathways under different stress situations.

In the pioneering work by /Wiman 1927, 1930, 1941/ on fracture minerals in the Uppsala region, many of the same fracture minerals that now have been identified in Forsmark were described in similar sequences (e.g. epidote, prehnite, laumontite, quartz, calcite, chlorite, adularia). Similar fracture minerals and approximately the same stable isotope signatures of calcites were also identified during fracture mineral investigations at the Finnsjön test site, ~ 17 km WNW of the Forsmark site /Tullborg and Larson 1982/. Although the large amount of high quality drill core material from the Forsmark site investigation together with more detailed analyses have made more detailed and far-reaching conclusions possible at Forsmark, the identification of the similar fracture minerals and mineral sequences in the region suggests that the low to moderate temperature evolution here described for the Forsmark site is possibly relevant to a much larger region in central Sweden.

5 Stable isotopes and calcite geochemistry

Since stable carbon and oxygen isotope analyses can be carried out on very small sample volumes (150–200 µg), a relatively large number (175) of $\delta^{18}O$ and $\delta^{13}C$ analyses have been carried out. Larger amounts of samples are needed for $^{87}Sr/^{86}Sr$ (30–40 mg) and therefore relatively few samples (especially of generation 4 calcites) have been analysed.

Representative samples for generation 2 and 3 calcite have been selected for trace element analysis. Generation 4 calcite occurs in very small amounts, often mixed with other phases; these factors and the relatively large amount of sample needed for the ICP-MS analyses (10–20 mg) make analysis of this late calcite difficult.

Most fracture filling calcite in Forsmark is of either hydrothermal (generation 2; Precambrian) or "warm brine" origin (generation 3; Palaeozoic). Younger calcite (generation 4) occurs only in small amounts and is mostly found in near surface fractures and hydraulically conductive zones. For a detailed description of the different generations (parageneses), see Chapter 4. Detailed descriptions of the analysed calcite and pyrite samples are available in the P-reports listed in Table 1-1.

5.1 Carbon and oxygen isotopes

5.1.1 Generation 2

Hydrothermal generation 2 calcites show relatively small variations in $\delta^{13}C$ with values between –1.6 and –7.1‰ (PDB). The majority of these calcites have low $\delta^{18}O$ values (< –14‰ PDB) although calcites showing a shift toward higher $\delta^{18}O$ values are also found (Figure 5-1). Low $\delta^{18}O$ values and $\delta^{13}C$ values between –1 and –7‰ PDB are typical for calcite precipitating under hydrothermal conditions or precipitation from glacial waters /e.g. Tullborg et al. 1999, Hoefs 2004/. However, in Forsmark, the hydrothermal parageneses with coeval adularia, prehnite and laumontite clearly implies a hydrothermal origin of this calcite. The trend toward higher $\delta^{18}O$ values in many calcites is probably due to an "oxygen shift" where interaction with the wall rock increases the $\delta^{18}O$ value of the fluid /e.g. Drever 1997/ which is inherited by the calcite during precipitation. Intensive water-rock interaction is supported by the observed wall rock alteration associated with precipitation of the hydrothermal calcite (4.1.1). No significant correlation between $\delta^{18}O$ in calcite and the formation temperature of coexisting minerals (adularia, prehnite or laumontite) can be seen. This is probably due to the influence from the wall rock on the $\delta^{18}O$ value in generation 2 calcites which predominates over a possible temperature dependent fractionation of ^{18}O during the calcite precipitation. Different intensities of water-rock interaction in different fractures result in high spatial variations of $\delta^{18}O$ in groundwaters; a signature later inherited by precipitated calcites.

5.1.2 Generation 3

Palaeozoic generation 3 calcite shows a narrower span in $\delta^{18}O$ values (–9.6 and –14.4‰ (PDB) compared with the older generation 2 calcite. In contrast to relatively homogeneous values in $\delta^{18}O$, extreme variation in $\delta^{13}C$ values spanning from –2.4 to –53.1‰ PDB (Figure 5-1) is shown. The variations seen in the $\delta^{18}O$ values could be due to different temperatures during precipitation and/or variation in the isotopic composition of the fluid. A moderate interaction with the wall rock is also possible. A few generation 3 calcites show $\delta^{18}O$ values in equilibrium with the present groundwater at ambient temperatures. However, the composition of the formation fluid during the Palaeozoic was most likely very different from the present and, furthermore, temperature indicators (e.g. fluid inclusions) indicate formation temperatures well above the

present. Therefore, comparison between generation 3 calcite and the present groundwater is not valid. $\delta^{13}C$ values in calcite between –7 and –30‰ PDB indicate an organic influence on the fluid /cf Tullborg et al. 1999, Wallin and Peterman 1999/ which is in agreement with the proposed downward penetration of fluids from an organic rich sedimentary cover as proposed by the presence of asphaltite in the upper parts of the bedrock /Sandström et al. 2006b/ (see also section 4.3). More extreme $\delta^{13}C$ values (< –30‰ PDB) are probably due to microbial oxidation of organic matter under in situ non-equilibrium conditions, resulting in extreme depletion of ^{13}C in the produced HCO_3^-/CO_2 which subsequently is inherited into the precipitating calcite /cf Pedersen et al. 1997, Budai et al. 2002/. There is evidence for more than one event of calcite precipitation during the Palaeozoic (section 4.3). However, it is not possible to distinguish between these calcites based on stable isotopic composition. In Figure 5-1, calcites representing an early event of generation 3 calcite precipitation (cf section 4.3) are marked with arrows; both events are characterised by an organic $\delta^{13}C$ signature and show similar $\delta^{18}O$ values.

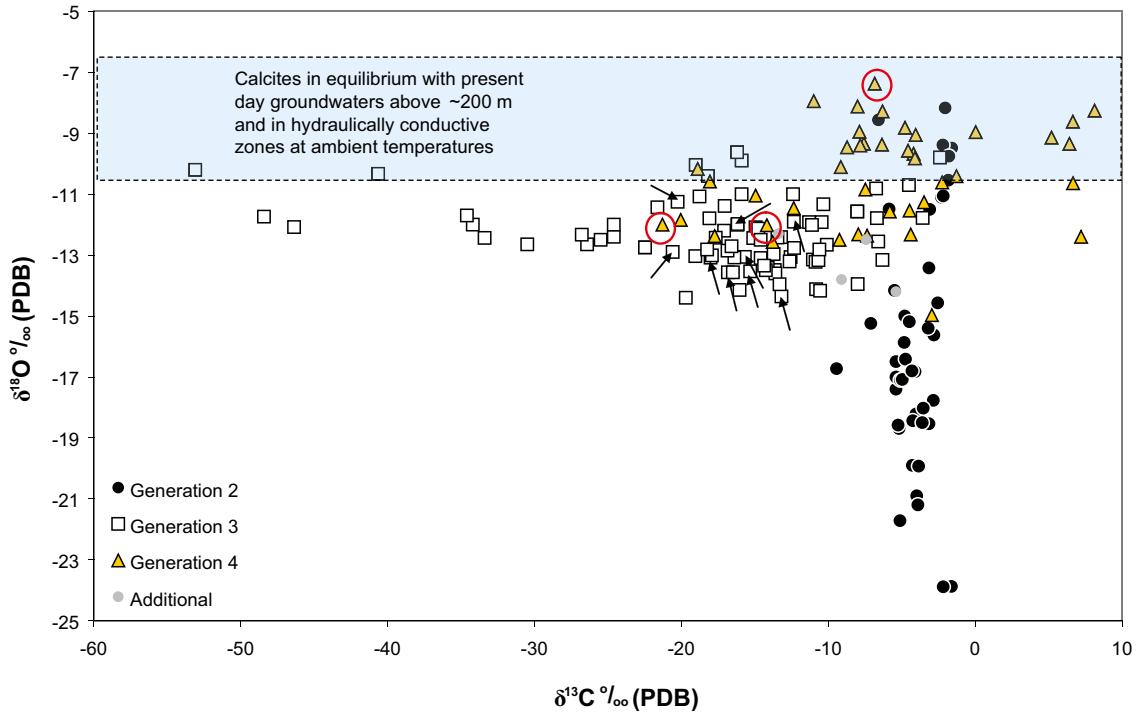

Figure 5-1. *$\delta^{13}C$ versus $\delta^{18}O$ in fracture filling calcite. The isotopic composition of groundwaters above ~ 200 m and in hydraulically conductive zones is presented in /Smellie at al. 2008, Sicada/ and are dominated by brackish-marine waters (–10 to –8.5 ‰ SMOW) and, in the upper 100 m, by fresh meteoric water (–12 to –10.5‰ SMOW). For calculation of $\delta^{18}O$ in calcite in equilibrium with these waters, the fractionation formula by /O'Neil et al. 1969/ has been applied at a temperature of ~ 7°C. Calcites marked as 'Additional' have not been possible to relate to the relative sequence of fracture mineralisations. Three generation 4 calcites with $^{87}Sr/^{86}Sr$ overlapping with the present groundwaters are marked with red circles. The samples marked with arrows represent calcite found coeval/intergrown with quartz and represent an early event of generation 3 calcite precipitation. Analytical errors are within the size of the symbols.*

5.1.3 Generation 4

The youngest calcites (generation 4) overlap in both $\delta^{13}C$ and $\delta^{18}O$ values with the Palaeozoic (generation 3) calcite, although a shift towards higher values can be seen in both $\delta^{13}C$ and $\delta^{18}O$ values. Some of this overlap could be due to overgrowth of younger calcite on older Palaeozoic calcite but a large part of the variation can be assumed to correspond to precipitations from very different waters. Generation 4 calcite represents calcites formed mainly during the Caenozoic. During this period marine-brackish to meteoric waters have recharged during temperate and cool climate conditions and these may have taken part in the calcite dissolution/precipitation processes. Calcites with $\delta^{18}O$ values between –11 and –7‰ PDB may have precipitated from waters similar to the present groundwater in the upper 200 m (Figure 5-1). Calcites with lower $\delta^{18}O$ could have been precipitated from a water influenced by a larger glacial component. A few calcites display positive $\delta^{13}C$ values, possibly due to in situ microbial activity involving CH_4–CO_2 fractionation processes.

Three of the generation 4 calcite samples have values overlapping with the $^{87}Sr/^{86}Sr$ ratios in the present groundwaters (section 5.3) indicating a recent age, and these could thus have precipitated during conditions similar to the present. Only one of these calcites has a $\delta^{18}O$ value in equilibrium with the present groundwater at ambient temperatures (Figure 5-1), but the other may reflect precipitation from water influenced by a slightly colder climate.

5.1.4 Carbon and oxygen isotope variation with depth

The $\delta^{13}C$ values in calcite vary with depth as seen in Figure 5-2, with the most extreme values between 30 and 200 m. The closed conditions necessary for extreme ^{13}C fractionation have probably not been possible to obtain in the uppermost 30 m of the bedrock. No correlation between $\delta^{18}O$ and depth can be seen (Figure 5-3).

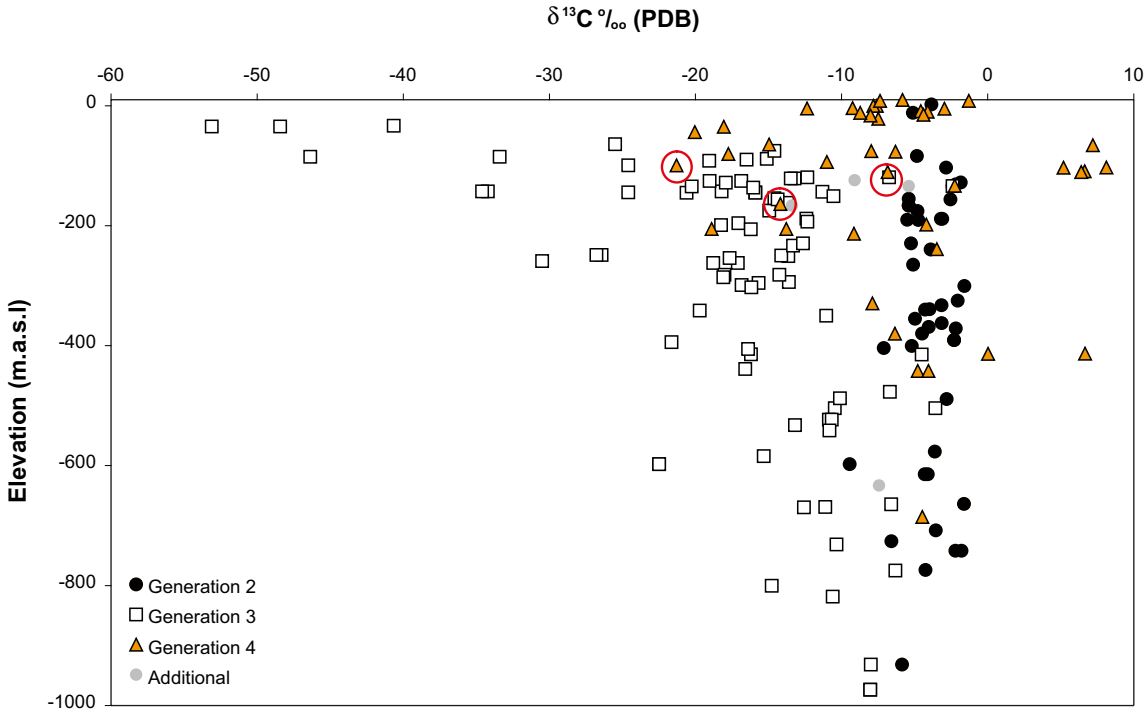

Figure 5-2. *$\delta^{13}C$ versus depth (elevation) in calcite. Analytical errors are within the size of the symbols. Three generation 4 calcites with $^{87}Sr/^{86}Sr$ overlapping with the present groundwaters are marked with red circles.*

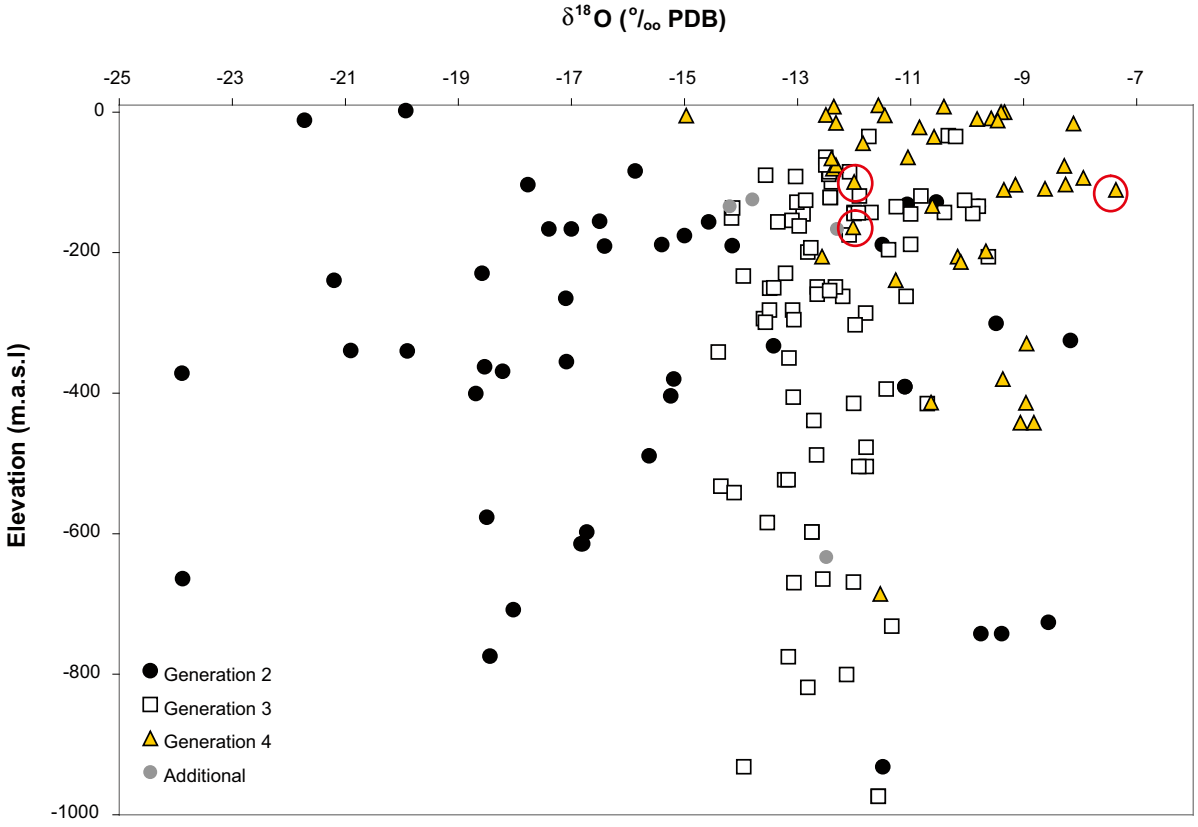

Figure 5-3. *$\delta^{18}O$ versus depth (elevation) in calcite. Analytical errors are within the size of the symbols. Three generation 4 calcites with $^{87}Sr/^{86}Sr$ overlapping with the present groundwaters are marked with red circles.*

5.2 Sulphur isotopes

Pyrite is associated mostly with the generation 3 paragenesis; younger generation 4 pyrite is also found although only in small amounts. Some pyrite can also be of possibly late magmatic or hydrothermal origin. Most analysed pyrites show $\delta^{34}S$ values between +5 and +31.5‰ (CDT) (Figure 5-4), compared to $\delta^{34}S$ values typically close to 0‰ CDT (Canyon Diablo Troilite) for hydrothermal/magmatic pyrite /e.g. Hoefs 2004/. The large variation (even within a single sampled fracture surface) and the positive values are interpreted as a result of Rayleigh fractionation in a closed system /cf Hoefs 2004/ where sulphate enriched in ^{34}S has been reduced during the oxidation of organic matter by microbial or thermochemical processes. The large variation and the lack of any depth trend support in situ microbial activity. The reduced S^{-} was subsequently precipitated as pyrite on the fracture surfaces. A possible explanation for the high $\delta^{34}S$ values in the Palaeozoic pyrite could be the enrichment in ^{34}S seen in Cambrian-Carboniferous sediments /Strauss 1997/. This is in accordance with the suggested influence from an organic rich Palaeozoic sedimentary cover on the formation fluids responsible for the precipitation of generation 3 minerals (section 4.3).

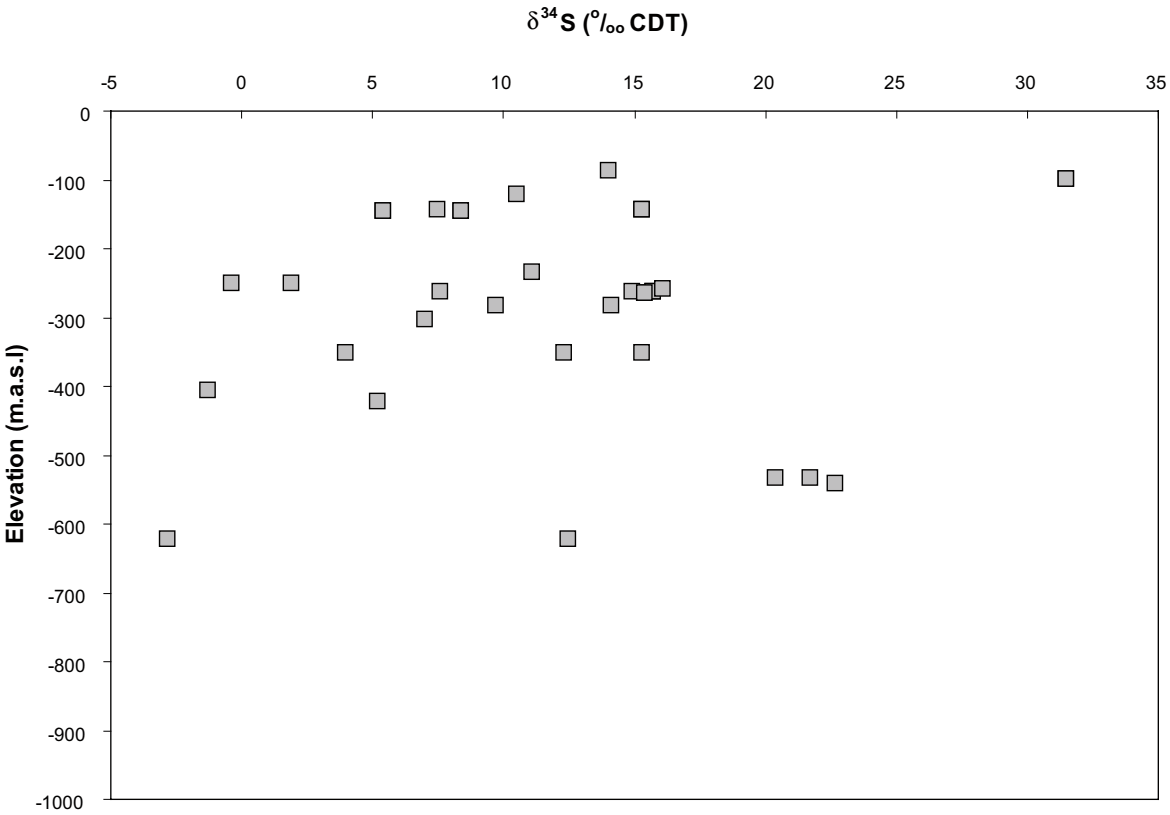

Figure 5-4. *$\delta^{34}S$ values versus depth (elevation) of pyrite in fractures. Analytical errors are within the size of the symbols.*

5.3 Strontium isotopes

Hydrothermal calcites (generation 2) show significantly less radiogenic $^{87}Sr/^{86}Sr$ ratios than younger calcites. The ratio in the early calcite ranges from 0.7073 to 0.7129 (Figure 5-5) in all but one sample (0.7151); the rather large variation is probably due to water-rock interaction during the circulation of the hydrothermal fluids responsible for the calcite precipitation. The wall rock alteration adjacent to fractures with generation 2 minerals is characterised by almost complete saussuritisation of plagioclase releasing Ca and Sr from the plagioclase (cf section 4.1.1). This would have a significant impact on the Sr isotopic composition of the fluid; on the other hand, the wall rock alteration also includes formation of chlorite from the breakdown of biotite, so radiogenic Sr was also released from the wall rock during the alteration. The overlapping $^{87}Sr/^{86}Sr$ ratios in calcite coeval with adularia, prehnite and laumontite indicate that these minerals did not precipitate during distinctly separated periods (Figure 5-5). One generation 2 calcite coeval with prehnite differs from the rest of the Generation 2 samples with a high $^{87}Sr/^{86}Sr$ ratio (0.7151), no evident explanation for this deviation has been identified.

Most Palaeozoic (generation 3) calcites have $^{87}Sr/^{86}Sr$ ratios between 0.7149 and 0.7164. The limited range in Sr isotopic composition indicates a relatively homogeneous Sr isotope ratio in the fluid, possibly due to that the calcite precipitated from an old water/brine which had equilibrated with mineral phases in the rock.

Eight samples of the younger generation 4 calcites have been analyzed for $^{87}Sr/^{86}Sr$, of these, five samples show values similar to the Palaeozoic calcites, although three show more radiogenic signatures. Only one calcite has been identified that is in equilibrium with both $\delta^{18}O$ and $^{87}Sr/^{86}Sr$ in the present groundwater at ambient temperatures. Two calcites have been identified which have $^{87}Sr/^{86}Sr$ ratios overlapping with the present groundwaters, but are not in equilibrium with the $\delta^{18}O$ values measured in groundwaters above 200 m. These calcites *can* have precipitated recently during a colder climate, but can also have precipitated during different

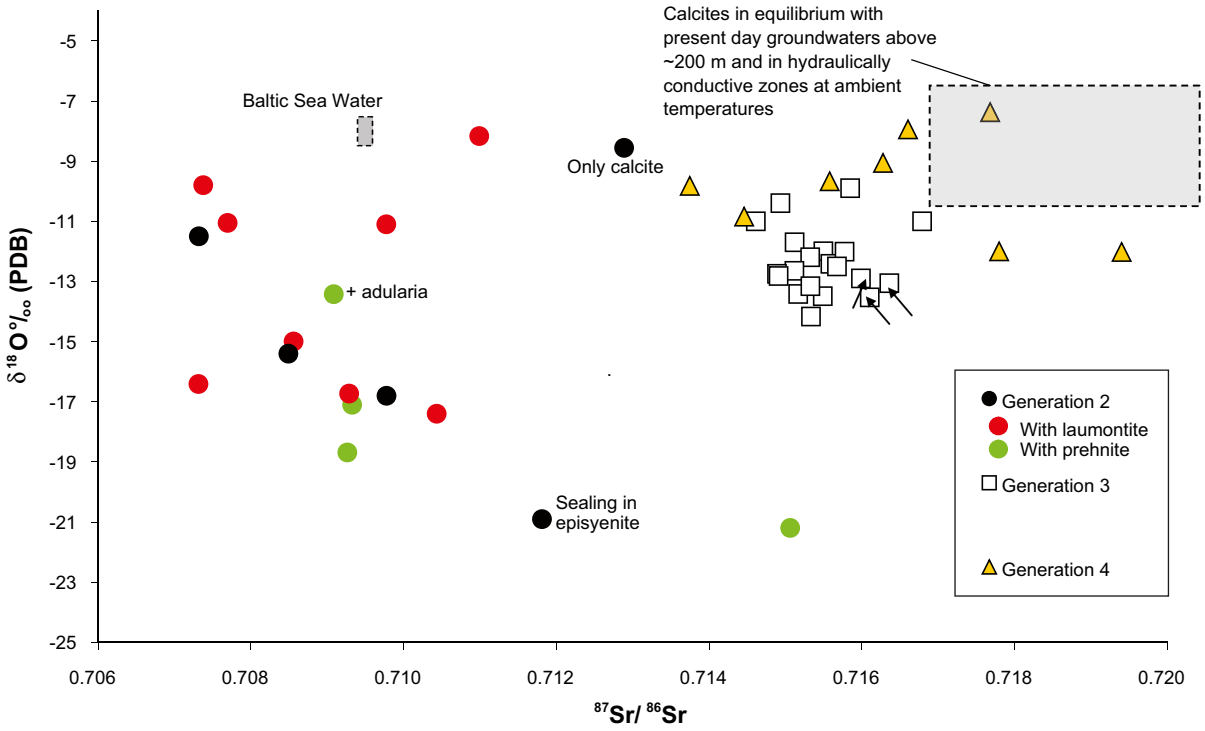

Figure 5-5. *$^{87}Sr/^{86}Sr$ ratio versus $\delta^{18}O$ (PDB) in fracture filling calcite. Cogenetic minerals for generation 2 calcites are marked by the colour of the dots. Notice the overlap in $^{87}Sr/^{86}Sr$ ratios in calcite cogenetic with prehnite and laumontite. The isotopic composition of Baltic Sea Water and groundwaters down to ~ 200 m depth and in hydraulically conductive zones is presented in /Smellie et al. 2008, Sicada/ and are dominated by brackish-marine waters (–10 to –8.5‰ SMOW) and, in the upper 100 m, fresh meteoric water (–12 to –10.5‰ SMOW). For calculation of $\delta^{18}O$ in calcite in equilibrium with these waters, the fractionation formula by /O'Neil et al. 1969/ has been applied at a temperature of ~ 7°C. Analytical errors are within the size of the symbols.*

climatic periods when the groundwater had a similar composition. The $^{87}Sr/^{86}Sr$ ratio of Baltic Sea water (~ 0.7094–0.7095) is also marked in Figure 5-5. However, infiltrating waters are strongly influenced by ion exchange with fracture minerals, such as clay minerals, and acquires their $^{87}Sr/^{86}Sr$ ratio very early in the flow path /Peterman and Wallin 1999/. The generation 4 calcites are mainly distinguished on textural grounds and by their slightly higher $\delta^{18}O$ values. As mentioned in section 4.4 the amounts of generation 4 minerals are relatively small and it has only been possible to sample a small set of samples for both $\delta^{18}O$ and $^{87}Sr/^{86}Sr$ isotopes.

The $^{87}Sr/^{86}Sr$ ratio in rock samples from Forsmark varies highly depending, for example, on the initial Rb/Sr ratio of the rock type. The analysed rock samples give $^{87}Sr/^{86}Sr$ ratios between 0.7116 and 0.8059 (n = 5) /Sandström et al. 2006a/. An overlap can be seen between $^{87}Sr/^{86}Sr$ ratios in late precipitated calcite and the host wall rock. However, the $^{87}Sr/^{86}Sr$ ratios in the metagranite (to granodiorite) that dominates the area (0.7525–0.8059) are significantly higher than the ratios found in the calcite (Table 5-1). The fact that relatively recent calcites precipitated in fractures have not inherited the radiogenic signature of the wall rock, indicate that the amount of possibly recent water-rock interactions have been limited during the fluid circulation responsible for precipitation of this calcite. Alternatively, the water is reacting preferenctially with unradiogenic mineral phases such as plagioclase. However, no mineralogical evidences for water-rock reactions during this low temperature circulation are found in the wall rock. Thus, interaction with fracture mineral coatings and possibly also the Quaternary cover is suggested as the main influence on the $^{87}Sr/^{86}Sr$ composition of the fluid responsible for precipitation of generation 4 calcite.

Table 5-1. Compilation of Ca/Sr (by weight) and $^{87}Sr/^{86}Sr$ ratios in different generations of calcite, rock types and groundwaters at the Forsmark site. Rock data have been extracted from Sicada as the data file p_geochemistry.xls, and water chemistry has been obtained from /Smellie et al. 2008, Sicada/. Rock type 101057 is the dominating rock within the Forsmark target area and host of the majority of the sampled fractures.

Samples	Ca/Sr (by weight)	$^{87}Sr/^{86}Sr$
Generation 2 calcite	1,258 – 2,247	0.7073 – 0.7151
Generation 3 calcite	6,828 – 19,545	0.7146 – 0.7168
Generation 4 calcite	n.a.	0.7137 – 0.7194
Granite (to granodiorite) (rock type 101057)	72 – 125	0.7525 – 0.8059 (n = 3)
Granodiorite, tonalite and granite (rock type 101051)	56 – 171	0.7116 (n = 1)
Surface waters	70 – 1,106	0.7121 – 0.7381
Groundwater	81 – 185	0.7169 – 0.7244
Baltic Sea Water	63 – 74	0.7094 – 0.7095 (0.7107*)

* Outlier

5.4 Trace elements in calcite

Due to the small amounts of generation 4 calcite and mixtures with mainly clay minerals, it has only been possible to analyse the trace element geochemistry of generation 2 and 3 calcites. The data have been presented in /Sandström et al. 2004, Sandström and Tullborg 2005/ and the results are summarised below.

The Fe and Mn content in the analysed calcites are generally low (below 0.2 wt%) and no significant differences can be seen between generation 2 and generation 3 calcites. No elevated concentrations of U or Th have been found in the calcite; the concentrations of both elements are usually < 0.2 ppm.

Hydrothermal (generation 2) calcites show Sr concentrations between 112 to 334 ppm, which are considerably higher than in the more abundant Palaeozoic generation 3 calcites (concentrations below 54 ppm). Radioactive Sr is one of the possible nuclides that could be mobilised in case of canister failure and immobilisation of Sr by coprecipitation in carbonates can be a possibility. However, calcite precipitated at low precipitation rates (e.g. at present conditions at Forsmark) does only incorporate small amounts of Sr /Morse and Bender 1990/, suggesting that a significant deposition of Sr by incorporation during ongoing precipitation of calcite is not plausible in the Forsmark fracture system. The Ca/Sr ratios (by weight) in groundwater samples from cored and percussion boreholes in Forsmark vary between 81 and 185 /Smellie at al. 2008, Sicada/ (Table 5-1). The hydrothermal calcites (generation 2) show Ca/Sr ratios between 1,258 and 2,247 (n = 3) whereas the Palaeozoic (generation 3) calcites show higher ratios between 6,828 and 19,545 (n = 8). None of these calcites are interpreted to be in equilibrium with present groundwater. The partition coefficient for Sr^{2+} in calcite is influenced by, for example, temperature, precipitation rate and solution and solid composition /Morse and Bender 1990/, making it difficult to calculate a palaeofluid composition since precipitation rate and fluid composition are very difficult to estimate. The partition coefficient for Sr^{2+} in calcite has in various experiments under different conditions been shown to vary between 0.02 and 0.40 /Curti 1999 and references therein/. A compilation of the Ca/Sr ratios in different calcites, waters and rocks are presented in Table 5-1.

Generation 2 calcites show uniform chondrite normalised REE-profiles (Figure 5-6). These profiles are typical for hydrothermal fluids with HCO_3^- as a dominant complexing agent /cf Landström and Tullborg 1995, Drake and Tullborg 2004/. A negative Ce anomaly is evident in many of the hydrothermal calcites indicating oxidising conditions where Ce^{3+} has been oxidised to Ce^{4+} and subsequently separated from the fluid prior to calcite precipitation. The Palaeozoic calcite (generation 3) show more fractionated REE-profiles with enrichment of the LREEs possibly due to organic complexation under low temperature conditions /cf Landström and Tullborg 1995, Drake and Tullborg 2004/. The negative Eu anomaly is more pronounced in these calcites, probably due to the reducing conditions prevailing during the Palaeozoic as shown by the presence of coeval pyrite (see section 4.3). Eu^{3+} can be reduced to Eu^{2+} under reducing conditions. No Ce anomalies can be seen in generation 3 calcite, further supporting the supposition of reducing conditions during precipitation of this calcite.

In situ laser ablation ICP-MS analysis of fracture filling calcite has been applied to detect possible zonation or inhomogeneity of the trace element geochemistry in fracture filling calcite. Due to the relatively large spot size of the laser beam (100 µm) it has not been possible to analyse any possible recent generation 4 calcite due to e.g. mixtures with clay minerals and the thin precipitates of this calcite. A profile has been analysed intersecting a fracture sealed with generation 3 calcite containing calcite from two precipitation events (Figure 5-7) (cf section 4.3). The results show that the REE-profile in calcite from the two events differs; the younger calcite is slightly more enriched in HREE. However, the difference between the two generation 3 events is small compared to the difference between generation 2 and 3 calcite (Figure 5-6).

5.5 Concluding remarks

Different generations of calcite can be distinguished based on their stable isotopic composition. Three general types of calcite have been identified: A) hydrothermal calcite (generation 2, Precambrian), B) warm-brine type calcite originating from a fluid influenced by organic material (generation 3, Palaeozoic), and C) low temperature calcite precipitated from different groundwaters under temperatures close to present groundwater ambient conditions (generation 4, late Palaeozoic to present). Calcites of the latter type occur only in small amounts but have been preferentially sampled for stable isotope analyses since they may provide information of the latest groundwater evolution in the area.

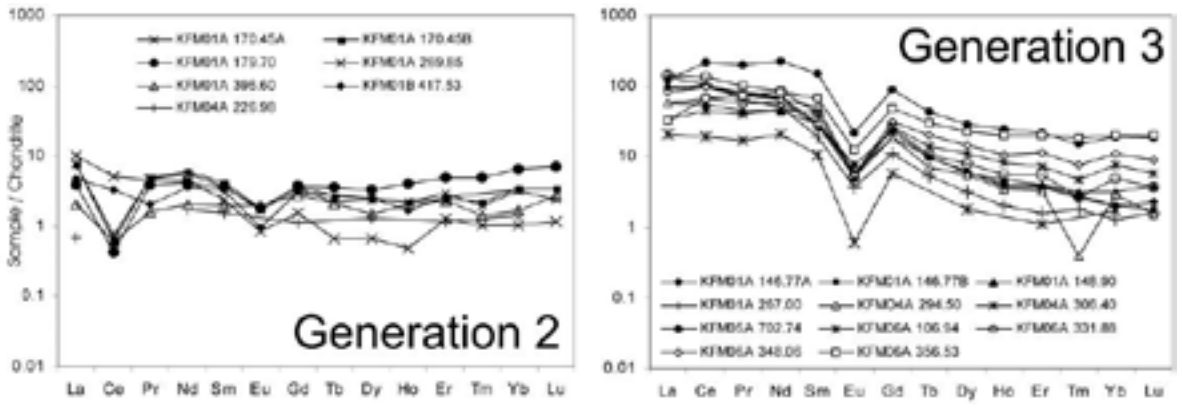

Figure 5-6. *Chondrite normalised REE profiles of fracture filling calcites. Chondrite values from /Evansen et al. 1978/. The negative Tm anomalies are due to analytical error.*

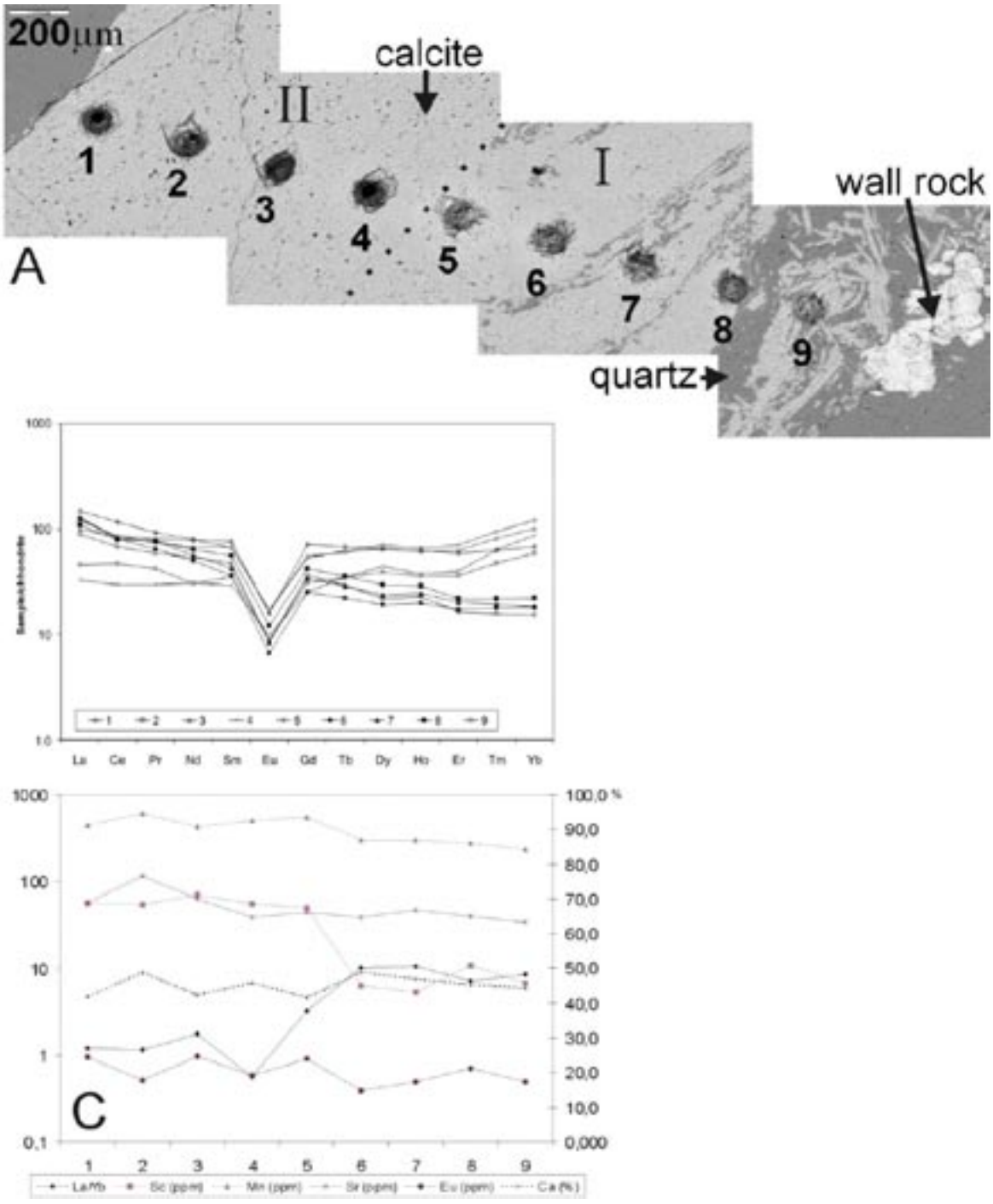

Figure 5-7. *Sample from KFM06A 142.27–142.39 m. A) Backscattered electron image showing a LA-ICP-MS traverse across a calcite sealed fracture. The calcite consists of one older phase mixed with quartz (I) cut by a younger calcite (II). The craters represent analysed spots. B) Chondrite normalised REE-profiles for the analysed spots. Note the enrichment of HREEs in samples 5-9. Chondrite values from /Evansen et al. 1978/. Tb, Ho and Tm are extrapolated values and have not been analysed. C) Selected trace elements plotted along the calcite traverse; the enrichment in HREEs in the left part of the traverse can be seen in the low La/Yb ratio. The Sc concentration also differs greatly between the two calcite phases while the Sr, Eu and Ca concentrations are relatively constant. The Mn content decreases slightly in the left part of the traverse. The figure is adapted from /Sandström and Tullborg 2005/.*

The differences between calcite and groundwater composition regarding both $^{87}Sr/^{86}Sr$ and the Ca/Sr ratios indicate that dissolution of fracture filling calcite does not significantly limit the chemical composition of groundwater in respect of these parameters. This is in agreement with the SEM studies which have not shown any dissolution structures of the calcites and, furthermore, the mass balance calculations show that the groundwaters are generally saturated in respect of calcite /Gimeno et al. 2008/. However, the situation in the soil cover may be quite different (e.g. /Tröjbom et al. 2007/). In the groundwaters the interaction with the silicate minerals (including ion exchange) seems to have the largest influence on both the Ca/Sr ratio and the Sr-isotope ratios. Due to the small amount of generation 4 calcites, it has been difficult to obtain good constraints on the Sr-isotope ratios in these, possibly young, calcites. This is not surprising since a large span in ages and formation fluids can be expected for these calcites

The calcites in the Forsmark fractures in general, contain small amounts of FeO, MgO and MnO (< 1 wt%) and the Sr content is below 300 ppm; both U and Th occur in concentrations below 0.2 ppm.

6 Distribution of fracture minerals

6.1 Occurrences of fracture minerals in different fracture domains

As described in Chapter 2, the Forsmark area has been divided into different fracture domains (Figure 2-2) and it is of interest to know whether or not the fracture mineralogy varies between these fracture domains or not. The fracture mineralogy of fracture domains FFM01, FFM02, FFM03 and FFM06 are shown in Figure 6-1 to 6-4. The data have been extracted from Sicada as the fracture data file p_fract_core. The fracture data have been assigned to the different fracture domains according to the classification in the FRACTURE_DOMAIN column. Occurrences of fracture minerals within drill core lengths classified as crushed zones and sealed networks are not included in this data set. Only occurrences of fracture minerals outside deformations zones are dealt with in this chapter. Fracture mineralogy within deformation zones (DZ) is addressed in /Stephens et al. 2007/.

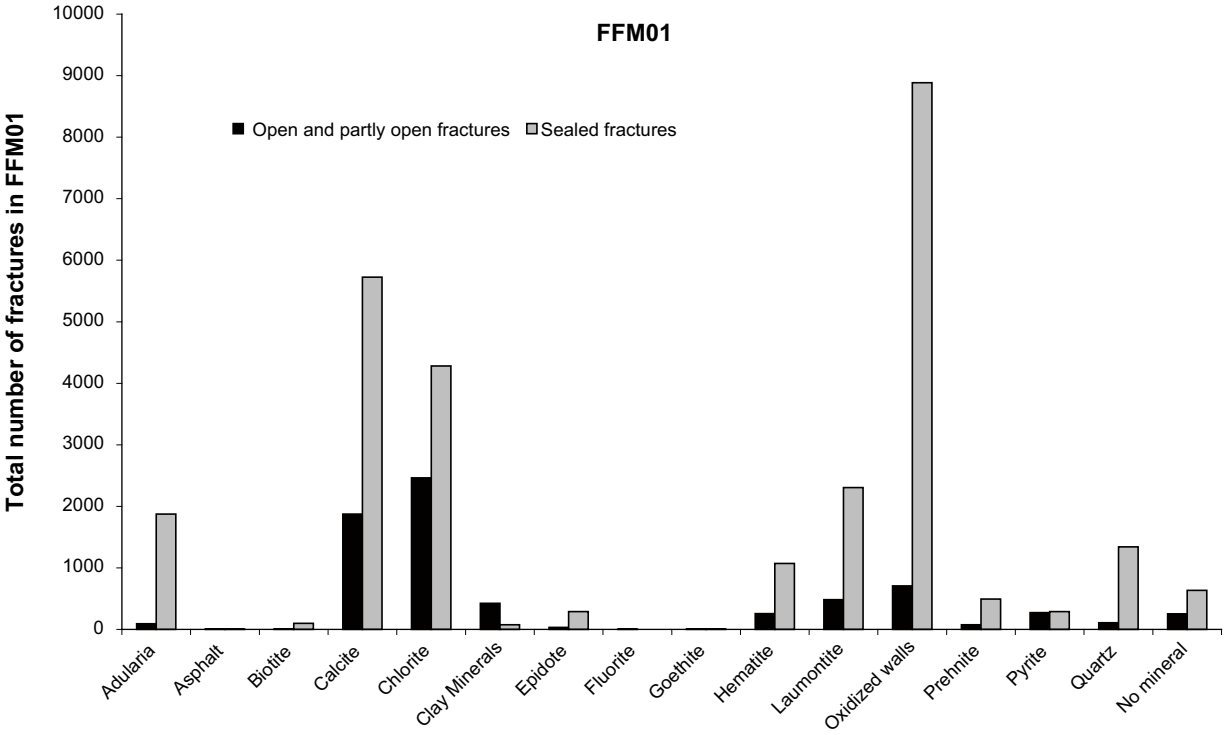

Figure 6-1. *Numbers of fractures where the listed fracture minerals have been identified during the drill core mapping in fracture domain FFM01. Fractures in deformation zones (DZ) have not been included.*

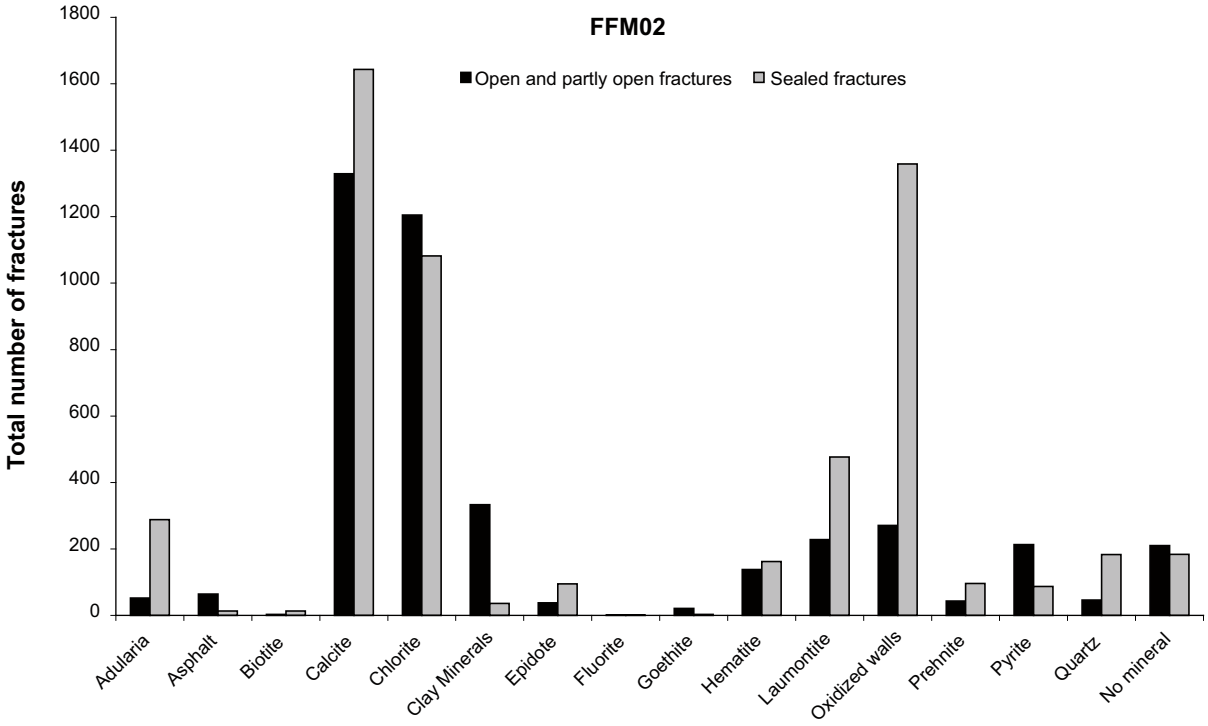

Figure 6-2. *Numbers of fractures where the listed fracture minerals have been identified during the drill core mapping in fracture domain FFM02. Fractures in deformation zones (DZ) have not been included.*

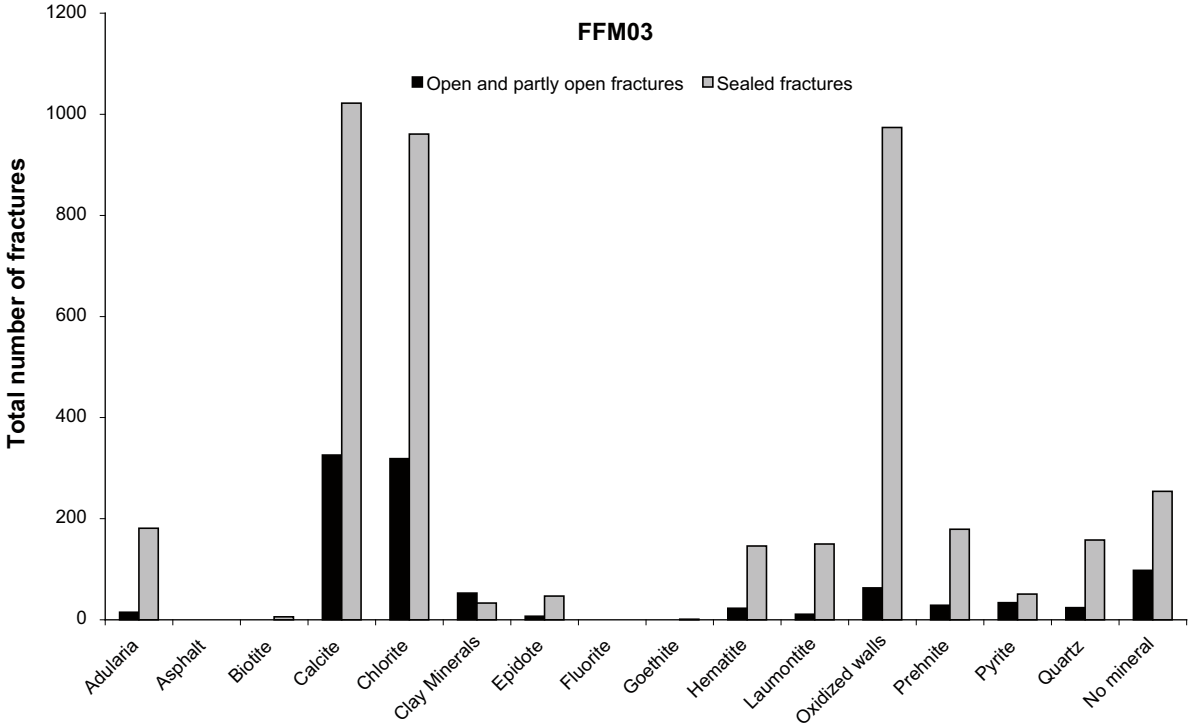

Figure 6-3. *Numbers of fractures where the listed fracture minerals have been identified during the drill core mapping in fracture domain FFM03. Fractures in deformation zones (DZ) have not been included.*

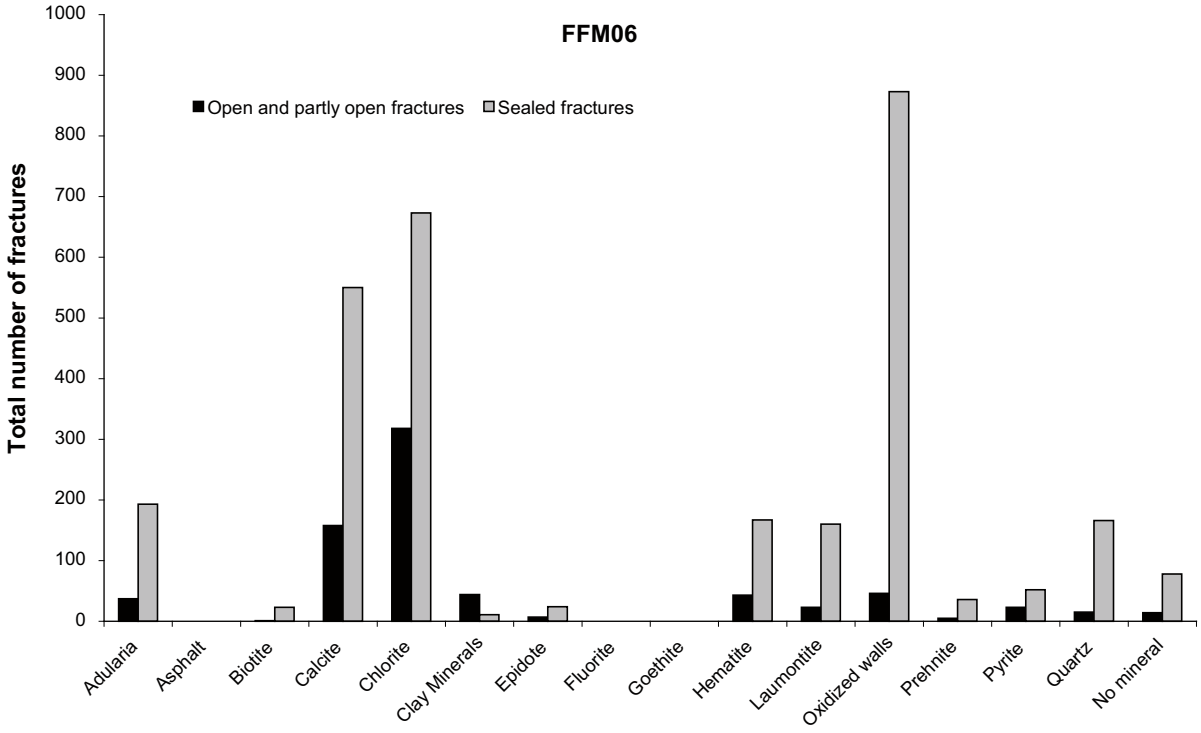

Figure 6-4. *Numbers of fractures where the listed fracture minerals have been identified during the drill core mapping in fracture domain FFM06. Fractures in deformation zones (DZ) have not been included.*

The following conclusions regarding the differences in mineralogy between the fracture domains can be made:

- With the exception of asphaltite and goethite, which almost exclusively are found in open fractures within fracture domain FFM02, there is no significant difference in fracture mineralogy between the fracture domains FFM01, FFM02, FFM03 and FFM06, although the proportion of the different minerals may vary. Asphaltite and goethite are probably also present in the upper part of FFM03, but there are only data from one borehole in the upper part of this fracture domain and the data available are insufficient.
- Clay minerals occur most abundantly in open fractures in FFM02 but are also found in all other fracture domains within the target area.
- Fracture domains FFM02 and FFM03 show relatively low ratios between fractures with oxidised walls and fractures with calcite (in sealed fractures) compared with domains FFM01 and FFM06. The oxidation (red-staining) of wall rock is associated with Precambrian fracture fillings (generation 1 and 2 minerals, see section 4.1.1). On the basis of these considerations and the observation that younger calcite (generation 4) is only found in open fractures (see section 4.4), together with the data analysis in section 4.3, it is concluded that most calcite in sealed fractures without wall rock alteration is inferred to belong to generation 3 and is Palaeozoic in age.

6.2 Variation of fracture mineralogy with depth in near-surface cored boreholes

The variation of fracture mineralogy with depth is discussed within the framework of the geological site descriptive model stage 2.2 /Stephens et al. 2007/. Boremap data from drill cores from near-surface levels (i.e. < 100 m from the bedrock surface) exist from seven boreholes in Forsmark (Table 6-1). Mineralogical data from shallow levels are critical for studies of the evolution of the redox front in the bedrock during the Pleistocene and Holocene hydrogeological evolution (cf Tullborg et al. 2008). However, no drill cores from these boreholes have been mapped completely from the bedrock-Quaternary surface. Boremap data available from these drill cores start between 5.20 and 15.56 m in borehole length. The lack of data from borehole lengths above 5.20 m is due to installed casing or lack of BIPS-images (Borehole Image Processing System). More detailed mapping of drill cores including the bedrock surface is needed to further evaluate if a past or present redox front(s) can be detected in the fracture system. Occurrences of fracture minerals within drill core lengths classified as crushed zones are not included in the data presented below.

The vertical distribution of the redox sensitive minerals goethite, pyrite and pH sensitive calcite from open and partly open fractures in these boreholes is shown in Figure 6-5 to Figure 6-7. Based on the available data, the following conclusions can be made about the frequency and distribution of these minerals in fractures from the upper 100 metres of bedrock:

- Calcite occurs abundantly in all boreholes, and no signs of calcite dissolution have been observed in the available data.
- Most of the goethite observations are from the near-surface extensions of the gently dipping deformation zone ZFMA2 (in KFM01B) and ZFMA8 (in KFM06B), from fracture domain FFM02 in KFM06B, and from the vertical- to steeply-dipping deformation zone ZFMENE1208B in KFM09A and KFM09B. The other occurrences are commonly found in fracture domain FFM02 but scattered occurrences are also found in FFM01.
- No correlation between pyrite occurrence and depth can be seen and there are no signs of pyrite disappearance close to the bedrock surface. Pyrite occurs in the same deformation zones as goethite (see above), possibly indicating complex redox evolution in fracture zones in the upper part of the bedrock, e.g. development of micro-environments.
- It is possible that groundwater flow in the sub-horizontal and gently dipping deformation zones does not favour formation of a typical redox transition zone. Instead, there may be a strong channelling of the recharging, partly oxidising water, when entering the highly transmissive deformation zones. At present, most of the oxygen consumption takes place in the Quaternary cover but, during earlier periods of the Quaternary, the situation may have been quite different. It is also possible that the upper 5 metres, which are not included in the corelogging, show calcite and/or pyrite dissolution together with goethite formation; this has simply not been possible to evaluate

Table 6-1. Cored boreholes with data from elevation > –100 m. See Table 2-1 for additional information.

Borehole	Start level (core length) of drill core mapping (m)
KFM01B	15.56
KFM01C	11.96
KFM03B	5.82
KFM06B	6.34
KFM07B	5.20
KFM08B	5.72
KFM09A	7.80
KFM09B	9.22

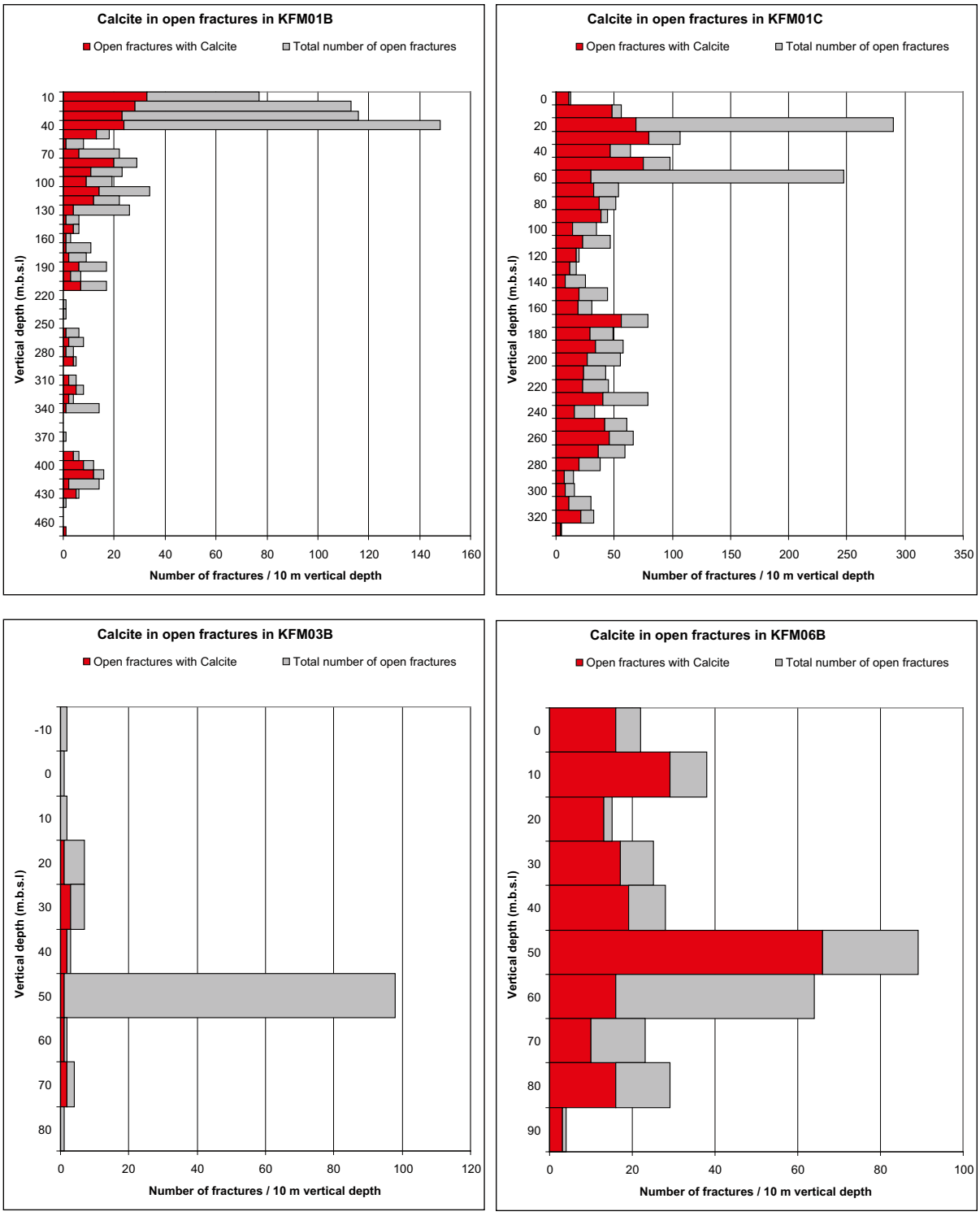

Figure 6-5. *Variation with depth of calcite in open (and partly open) fractures in cored boreholes where data are available from depths < 100 m. Note the different scales.*

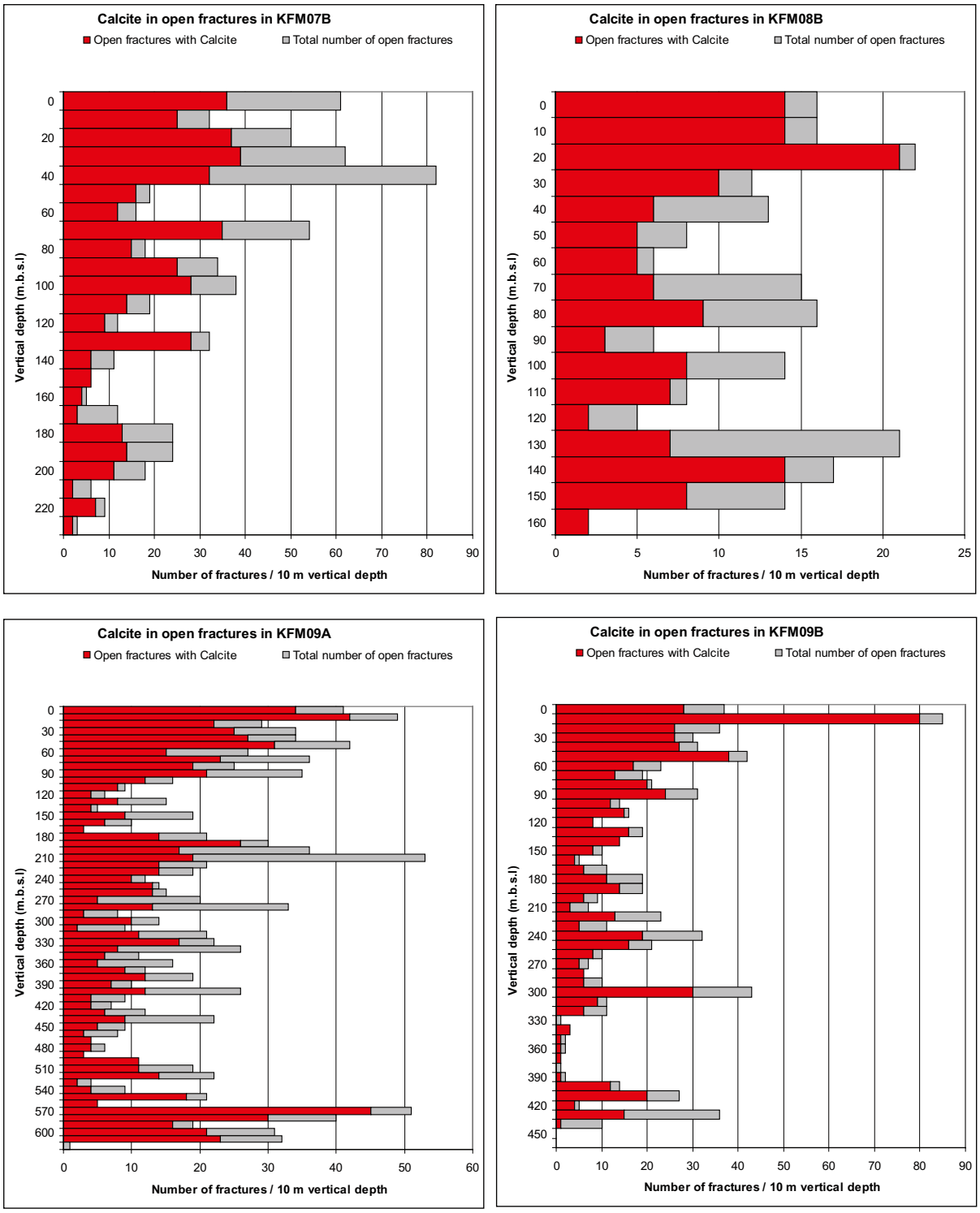

Figure 6-5. *Cont.*

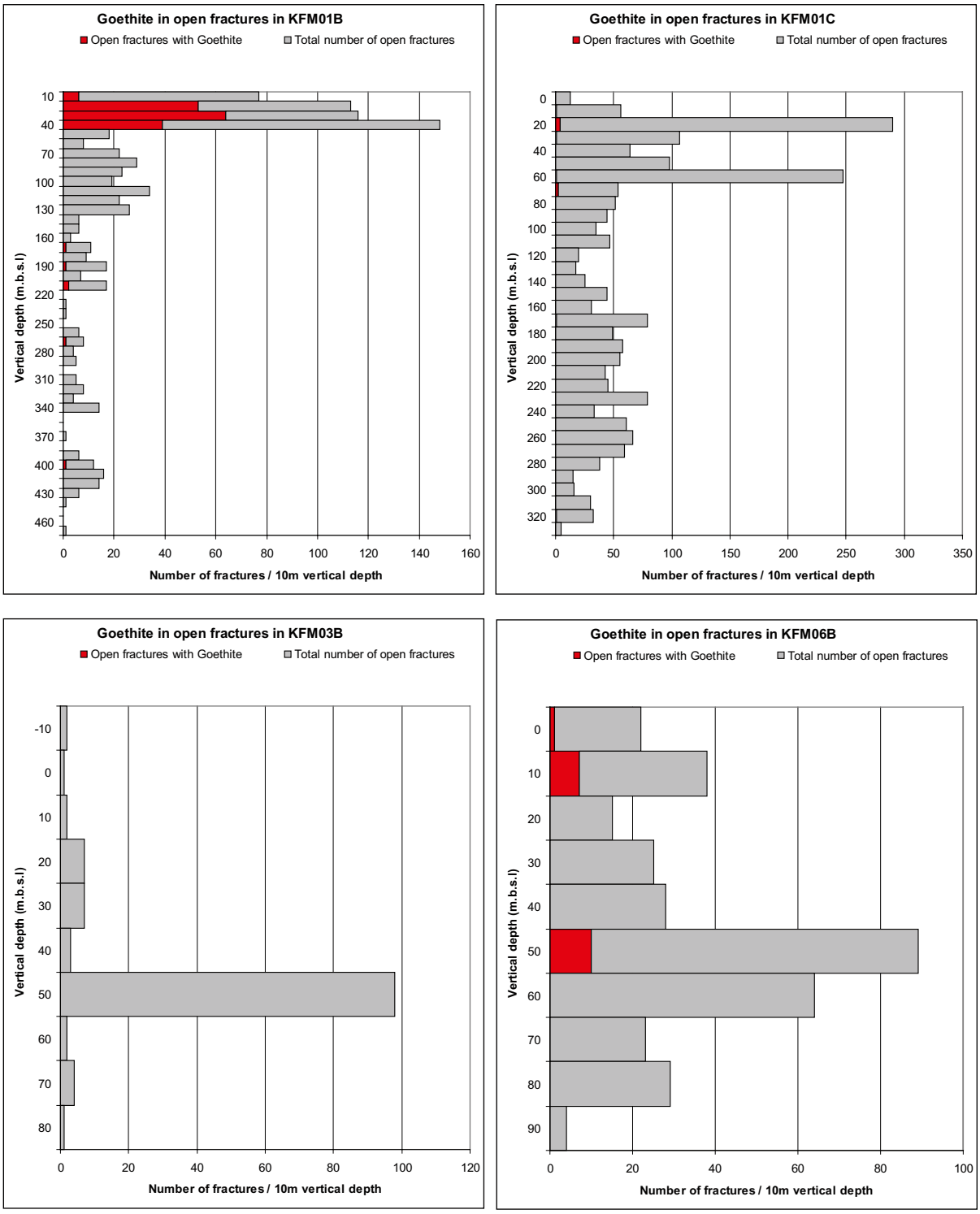

Figure 6-6. *Variation with depth of goethite in open (and partly open) fractures in cored boreholes where data are available from depths < 100 m. Note the different scales.*

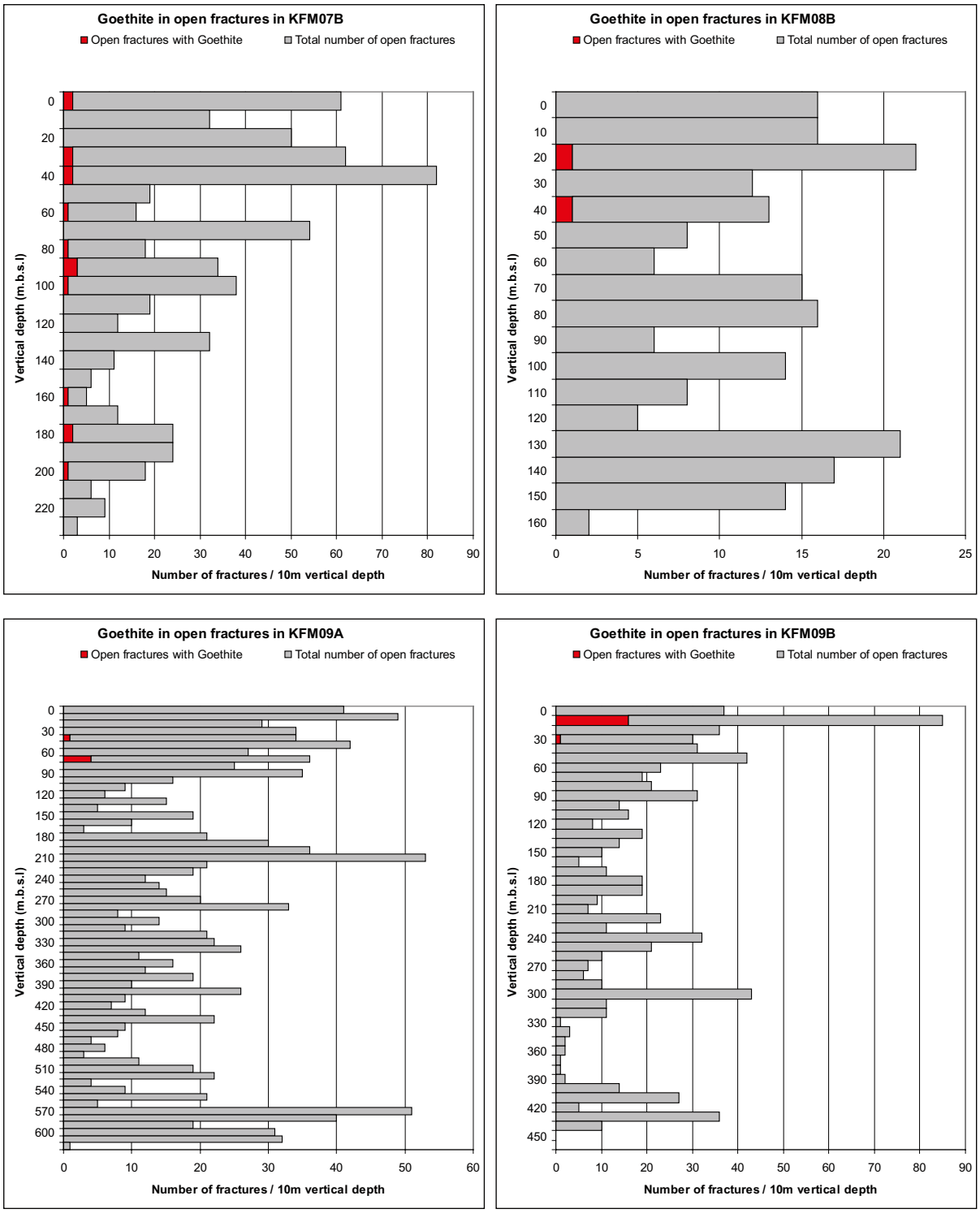

Figure 6-6. *Cont.*

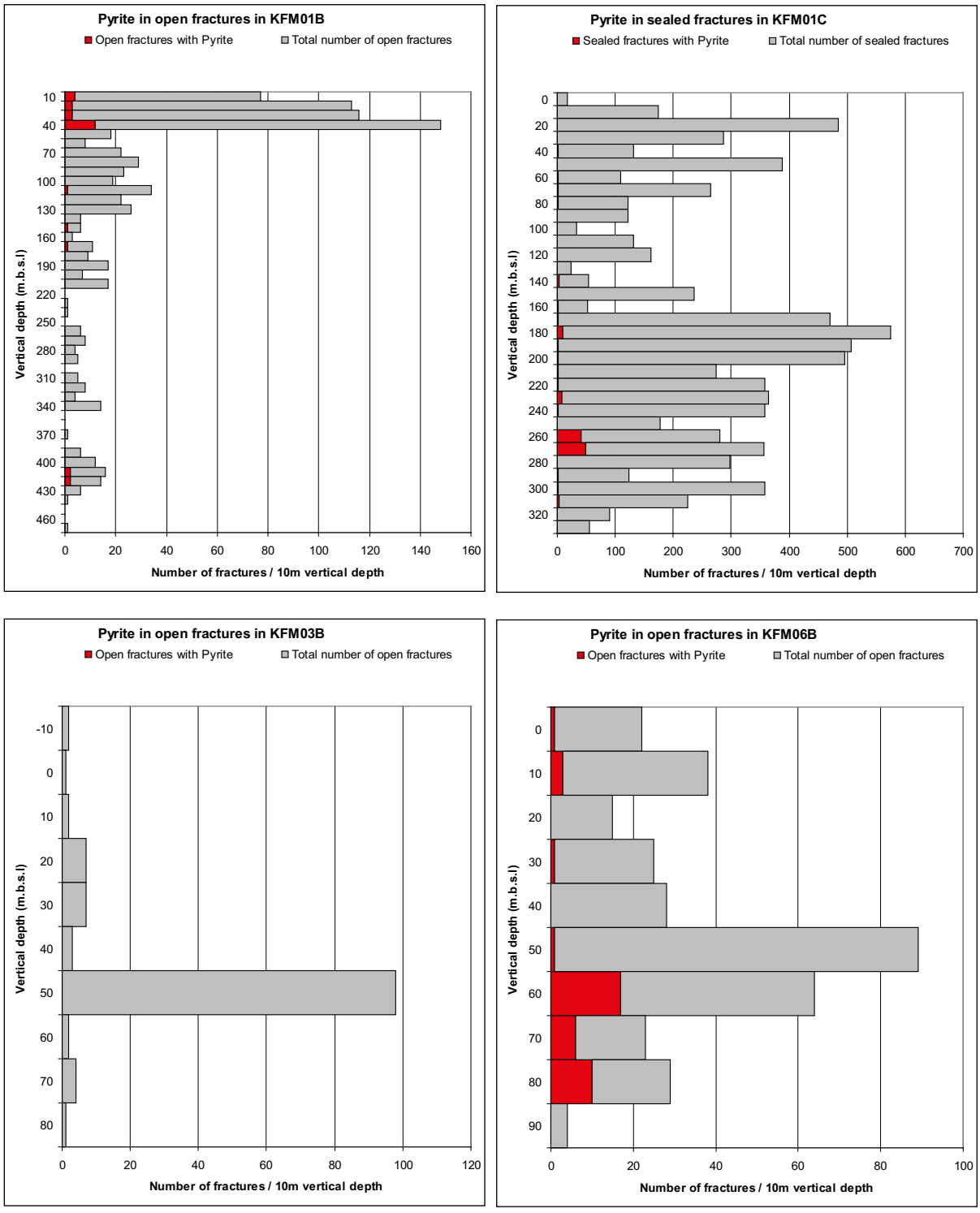

Figure 6-7. *Variation with depth of pyrite in open (and partly open) fractures in cored boreholes where data are available from depths < 100 m. Note the different scales.*

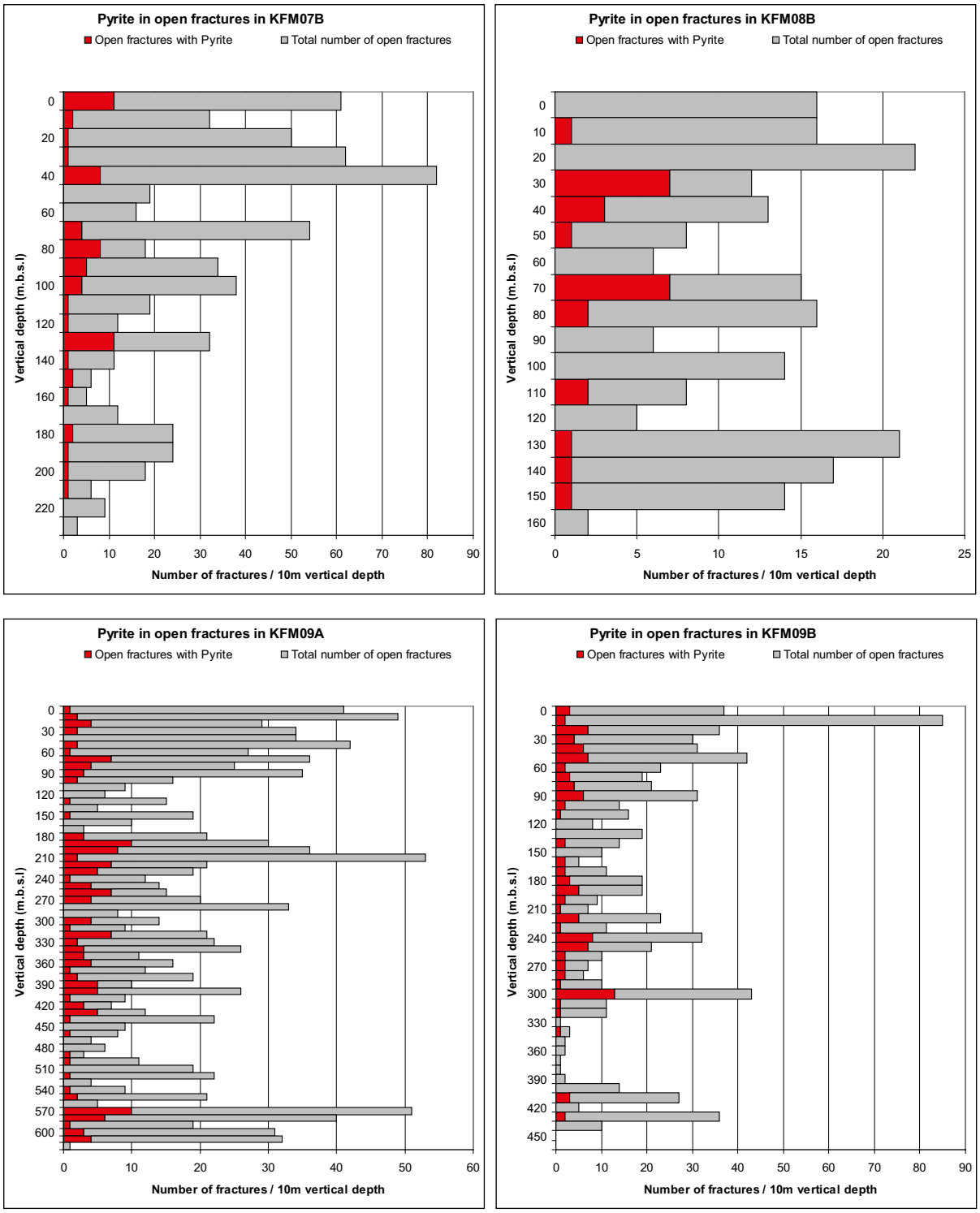

Figure 6-7. *Cont.*

6.3 Distribution of clay minerals with depth

The distribution of different clay minerals at depth is plotted in Figure 6-8 (based on XRD analyses). No samples with corrensite have been identified in the upper 75 m of the bedrock. However, only a few cored borehole data are available from the upper 75 m, the confident assessment of this is therefore limited. More detailed mapping of the occurrence of clay minerals would be needed to confirm this observation. Only a few samples with kaolinite (n = 2) and unmixed vermiculite (n = 1) have been identified showing that these clay minerals are rare at Forsmark. No other significant trends can be identified in the available data but it can be mentioned that the two observations of kaolinite belong to shallow depth. The repesentativity of the XRD data is discussed in section 3.2.

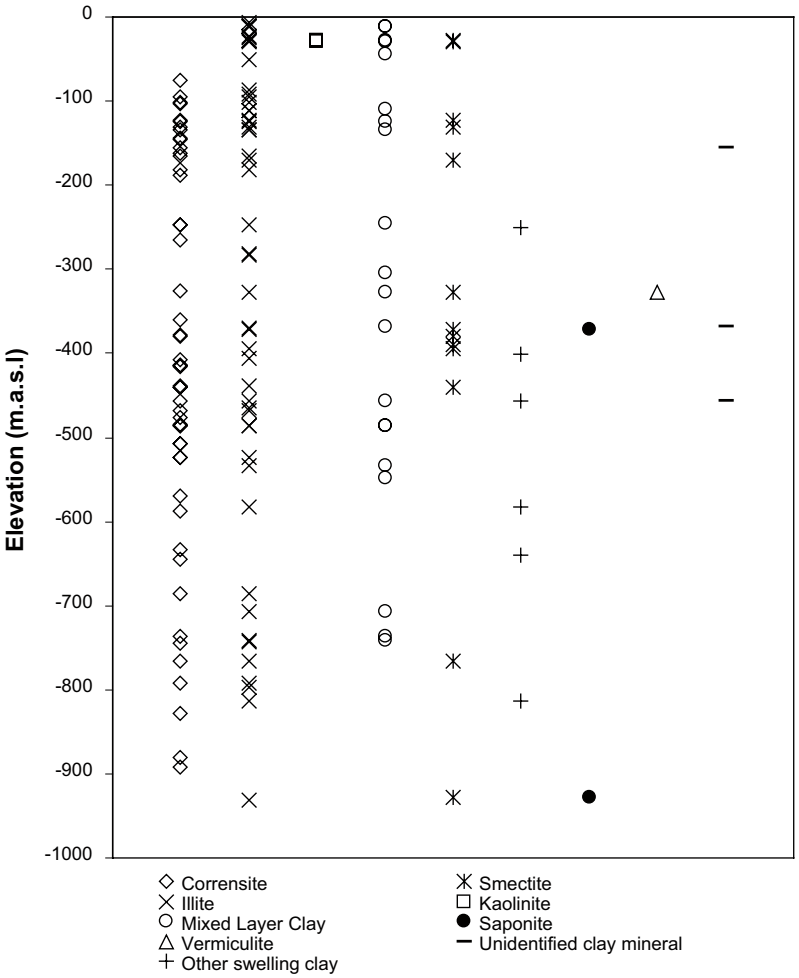

Figure 6-8. *Depth distribution of different clay minerals identified by XRD. The representativity of the samples is discussed in section 3.2.*

6.4 Fracture mineralogy in hydraulically conductive fractures

For the assignment of bedrock transport properties and the creation of a retardation model for the Forsmark area /Byegård et al. 2008/, ten sets of different mineral assemblages have been defined for open and partly open fractures from both deformation zones, and fracture domains, and plotted according to depth (Figure 6-9). The subdivision is based on the detailed studies reported in this report (e.g. the description of the different parageneses for generations 1-4, Chapter 4) but are also based on experience as to which significant units to extract from the Sicada database of the drill core loggings, for detailes, see /Byegård et al. 2008/. From this plot, it is evident that the most common fracture mineral assemblages are: chlorite + calcite ± other, chlorite ± other, laumontite ± other, calcite ± quartz ± pyrite, and chlorite + clay ± other. Other minerals in this context include prehnite, epidote, adularia and albite. From Figure 6-9, it is evident that laumontite is less common in the upper 100 metres, probably due to later reactivation and alteration. Calcite coated fractures are more common in the upper ~ 350 m and so are fractures lacking any mineral filling (even though the portion of these fractures is low at all depth).

When only fractures which are hydraulically conductive (showing PLF flow log anomalies) are considered (Figure 6-10), the most striking feature is the small number of fractures containing laumontite. The dominating fracture assemblages in the hydraulically conductive fractures are chlorite + calcite ± other and calcite ± quartz ± pyrite. A number of fractures without visible fracture coatings are also present in the PFL anomalies.

It is well known that only a small number of the open fractures are well connected and have a measurable transmissivity (e.g. from the Posiva Flow Log (PFL)), i.e. most open fractures are not hydraulically connected. Figure 6-10 shows the frequency of the different fracture minerals in transmissive fractures. Most groundwater flows along fractures within sub-horizontal and gently dipping zones /Follin et al. 2007/. Thus, most of today's groundwater flow occurs along fractures where fluids also circulated during the Palaeozoic, and most of the mineral coatings in these fractures are of Palaeozoic origin (generation 3, section 4.3). The steeply-dipping fractures normally containing laumontite belong to generation 2 (section 4.2) and are to much lesser extent, presently hydraulically conductive. However, many of the fractures with generation 3 minerals that precipitated during the Palaeozoic are reactivated older fractures and the absence of, for example, laumontite in the fractures, which today are hydraulically conductive, may be due to dissolution of this easily weathered mineral.

6.5 Concluding remarks

With the exception of asphaltite and goethite, which almost exclusively are found in open fractures within fracture domain FFM02 (and probably the upper part of FFM03), the same fracture mineralogy is found in FFM01, FFM02, FFM03 and FFM06, although the proportion of the different minerals may vary. Asphaltite and goethite are almost exclusively found in the upper part of the bedrock whereas other minerals (e.g. chlorite) show no or very little variation with depth. Clay minerals are found more abundantly in fractures in the upper part of the bedrock but are also found at greater depths. The calcite ± quartz ± pyrite assemblage is most common in the upper 350 m of the bedrock. No signs of calcite or pyrite dissolution can be seen in the upper 100 m of the bedrock, but the presence of goethite in hydraulically conductive deformation zones suggests channelled flows of oxygenated water in certain zones and development of micro-environments at some occasions, not necessarily the present. The conditions in the upper 5 m of the bedrock have not been included in the core mapping and have therefore not been evaluated.

The dominating fracture assemblages in hydraulically conductive fractures are chlorite + calcite ± other and calcite ± quartz ± pyrite (i.e. typical assemblage of the generation 3 fracture minerals which precipitated during the Palaeozoic).

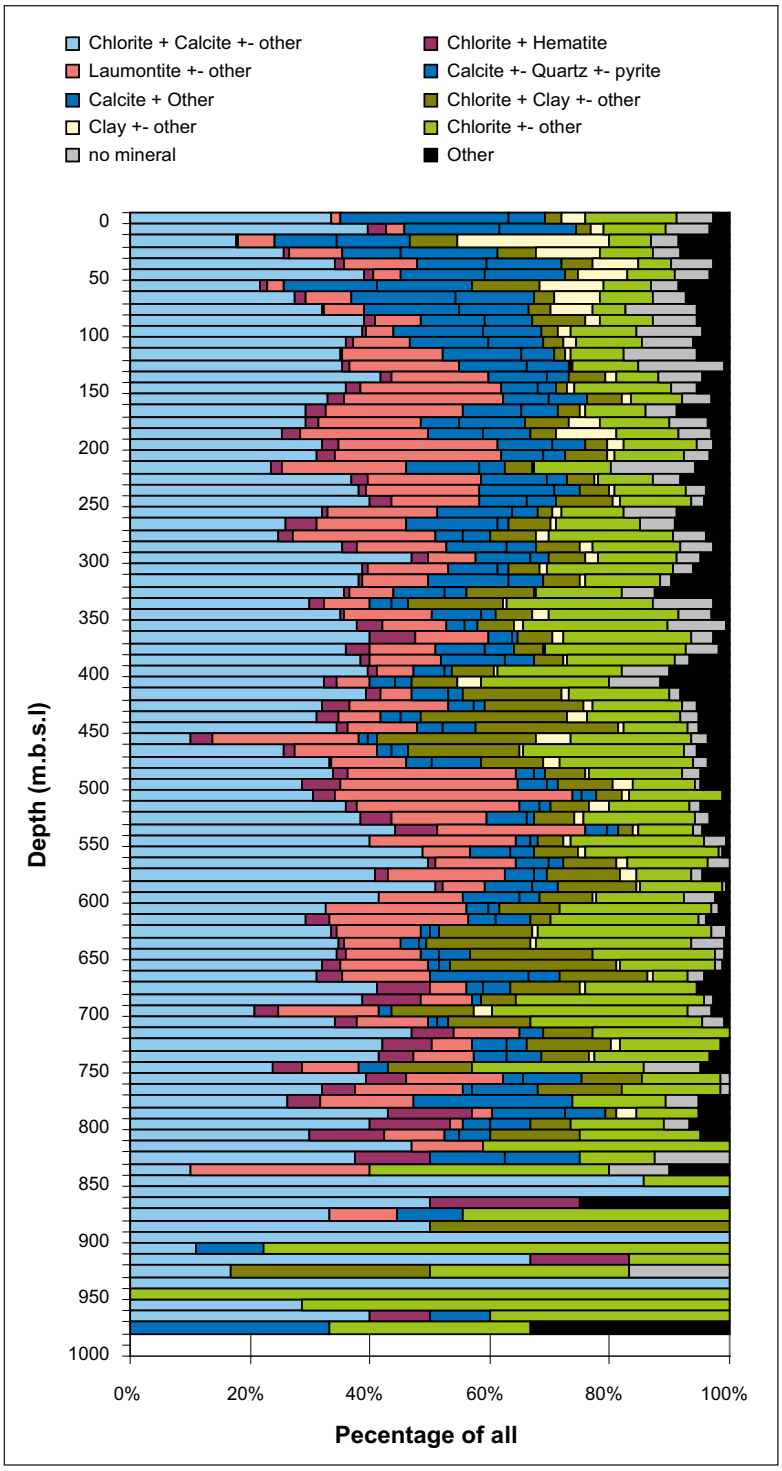

Figure 6-9. *Fracture mineralogy in all open fractures (both in deformation zones and fracture domains) given as percentage of all open fractures. The fracture minerals have been divided into 10 different sets /Byegård et al. 2008/.*

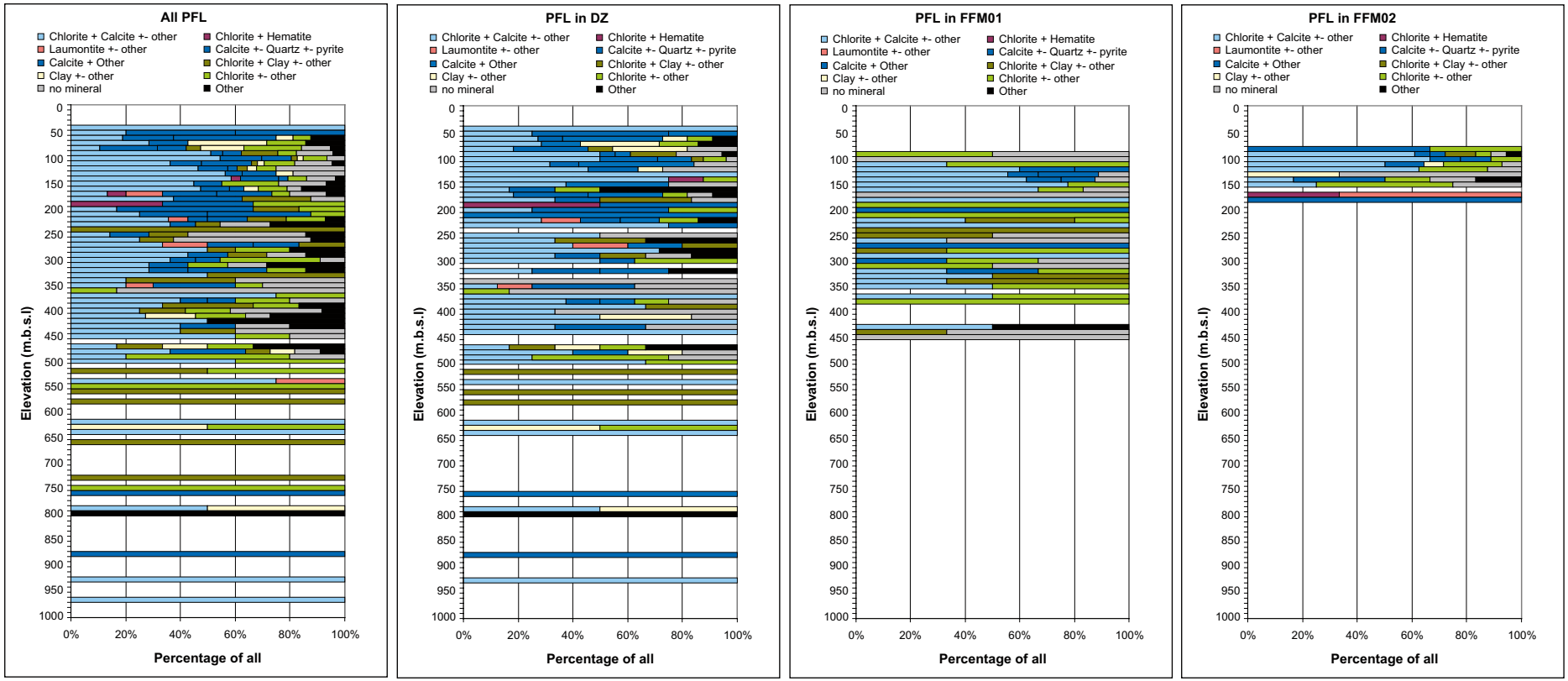

Figure 6-10. *Fracture mineralogy in open fractures with PFL-anomalies given as percentage of total number of fractures with PFL-anomalies. The fracture minerals have been divided into 10 different sets /Byegård et al. 2008/.*

7 Fracture filling geochemistry

The fracture filling chemistry has been determined by:

1) SEM-EDS analyses of specific mineral grains for their major elements.

2) ICP analyses of "bulk fracture fillings". This gives both the major and trace element composition of the fracture coating, although the samples consist of a mixture of minerals. The ICP analyses complement the SEM-EDS analyses but can also be used to identify chemical deviations associated with undetected or overlooked mineral phases and thus assist in the identification of mineral phases in the fracture system.

7.1 Geochemistry of selected fracture minerals.

The geochemistry of selected fracture minerals from the Forsmark site is based on SEM-EDS analyses of pure mineral phases in thin section /Sandström et al. 2004, Sandström and Tullborg 2005/. Because most fracture fillings consist of a mixture of different mineral phases, the geochemical composition of the minerals are "end-members" of the different fracture filling compositions. Trace element analyses of calcite have been carried out by ICP-MS and laser ablation ICP-MS /Sandström et al. 2004, Sandström and Tullborg 2005/.

Asphaltite

Asphaltite consists of a mixture of hydrocarbons and is often associated with sulphides. The S content is therefore high in the samples analysed and varies between 1,220 and 25,600 ppm. No elevated U or Th content have been detected in the two analysed asphaltite samples /Sandström et al. 2006b/.

Calcite

The calcite is relatively pure $CaCO_3$ with low contents of FeO, MgO and MnO; in most calcites the total amounts of trace components are < 1 wt%. The Sr content varies between different generations of calcite, but the most abundant calcite, especially in open fractures, generally has a low content, between ~ 20 and 54 ppm, whereas concentrations between 112 and 334 ppm have been detected in older hydrothermal (generation 2) calcites. Both U and Th contents are low, usually below 0.2 ppm. No carbonates other than calcite have been identified in the fractures at the Forsmark site.

Chlorite/corrensite

Chlorite and corrensite are the most important Fe^{2+} bearing fracture minerals at the Forsmark site. The total Fe content expressed as FeO in chlorite/corrensite is normally between 20 and 30 wt% and the MgO content varies between 3 and 24 wt%. The CaO content is normally between 0.2 and 0.9 wt% due to the corrensite component. The Mn and Ti contents in the chlorites are usually low but a few samples have values between 1 and 1.5 wt%, possibly due to inclusions of titanite or illmenite.

Epidote

Epidote contains almost exclusively Fe^{3+} and the Fe_2O_3 content varies between 9 and 15 wt%. The MnO content varies between 0.1 and 0.8 wt% and the CaO content is ~ 23 wt%.

Laumontite

Laumontite has a CaO content between 10 and 13 wt% and the total Fe content expressed as FeO is below 0.5 wt%. Although laumontite occurs together with small grains of hematite, a bulk sample of such a fracture filling does not exceed 1% wt Fe_2O_3. Elevated Sr contents have been found in bulk fracture filling samples dominated by laumontite with Sr contents between ~ 300–850 ppm.

Prehnite

Fe in prehnite is almost almost exclusively Fe^{3+} and the Fe_2O_3 content varies between 1.1 and 6.1 wt%.

Sulphides

The sulphide minerals in the fractures are totally dominated by pyrite which constitutes more than 99% of all the sulphides. Other sulphides present are galena, sphalerite and chalcopyrite.

7.2 Geochemistry of bulk fracture filling material

K, Cs, Rb, Ba

K^+, Rb^+ and Cs^+ behave similarly due to their similar valence and ionic size; and they are mainly hosted in K-feldspar, micas and clay minerals. Rb^+ and Cs^+ are enriched (in relation to $K^{+)}$, in the fracture coatings compared with the host rock. Ba^{2+} is similar to K^+ in size and is preferentially incorporated into K-feldspar in granitic rocks /de Albuquerque 1975/. XRD analyses show that all samples with Ba > 1,000 ppm contain K-feldspar/adularia, indicating this as the main Ba-containing phase in the fracture filling material. The positive correlation between K and Ba seen in Figure 7-1 also indicates that K-feldspar dominates over mica and clay minerals in the analysed samples.

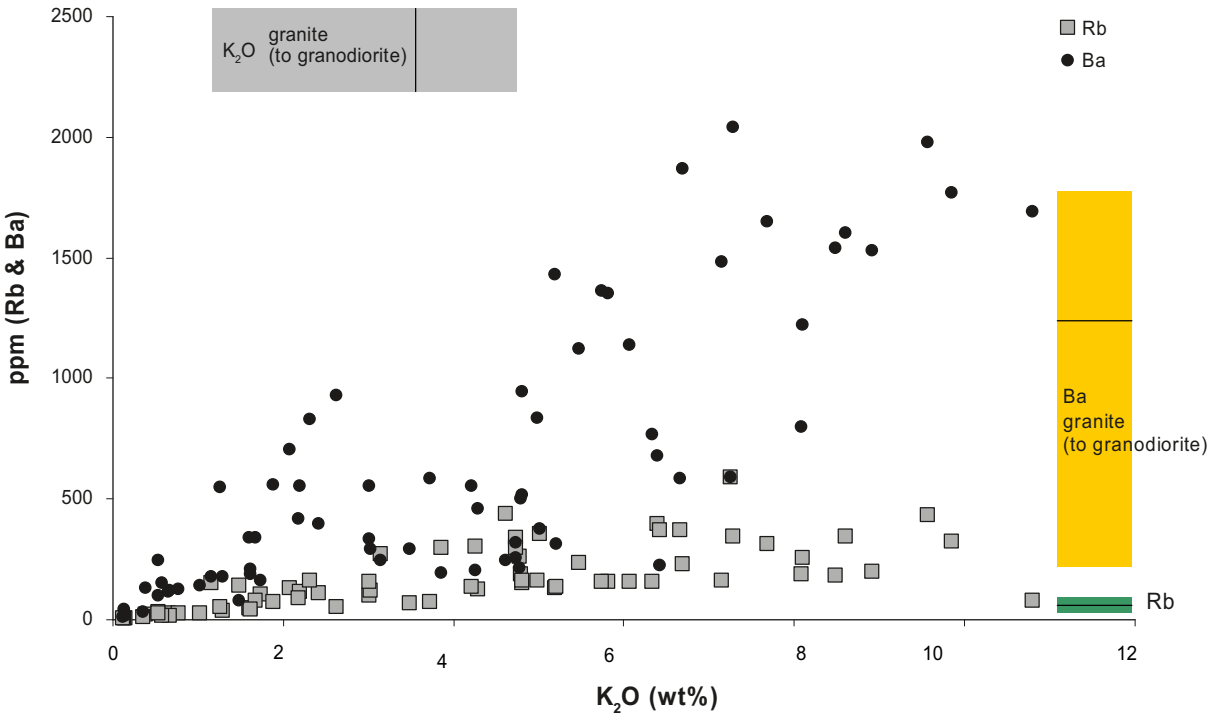

Figure 7-1. *Rb and Ba plotted against K_2O. The coloured fields represent the compositional span in the dominating granite (to granodiorite) of the Forsmark area with the median value outlined.*

Cesium is highly enriched in the two samples consisting dominantly of analcime (Figure 7-2). The high concentrations of Cs in these samples are not surprising since analcime forms a continuous series with pollucite ((Cs, Na)[$AlSi_2O_6$]·nH_2O). However, Cs must be incorporated in the analcime during crystallisation and not by subsequent cation exchange since analcime does not readily exchange Cs /King 2001/. The preferable uptake of Cs by analcime during crystallization is also manifested in the Cs/Rb ratios plotted versus K_2O in Figure 7-3, where all samples containing analcime show high Cs/Rb ratios. However, analcime was not identified by XRD in one of the samples showing an anomalous Cs/Rb ratio; it is however plausible that this sample contains analcime as well, but below the detection limit of the XRD analysis (~ 1–5 vol%).

Potassium-bearing clay minerals such as illite and mixed layer clays are generally the most likely minerals to act as sinks for the large Rb^+ and especially Cs^+ ion in the fracture systems during present conditions. The latter is supported by the fact that samples with Cs concentrations > 10 ppm (analcime samples excluded) all contain either illite or mixed layer clays (or both) (Figure 7-4). The most Cs rich (i.e. analcime rich) samples are concentrated at shallow levels in the bedrock as seen in Figure 7-5. No other significant trends can be seen when Cs is plotted against elevation; any variation seen is probably due to variations in the abundance of clay minerals. However, it is evident that Cs (possibly from the rock) has been mobilised, for example as a result of biotite/chlorite alteration, and retained in the fracture minerals since most of the fracture coatings have Cs contents much higher than the host rock (~ 1 ppm). Redistribution of Cs by groundwater-fracture mineral interaction is most probably an ongoing process.

All samples with Rb^+ concentrations above 200 ppm contain one or more of the K-bearing minerals illite, mixed layer clays (smectite/illite or vermiculite/illite) or apophyllite (Figure 7-4). These three minerals are therefore interpreted as the main Rb bearing minerals in the fracture filling material. Apophyllite has only been identified in a few fractures and its significance as a Rb bearing mineral in the fractures is probably minor. No significant trend can be seen when Rb is plotted against depth (Figure 7-6). The absence of fracture fillings with Rb concentrations below 100 ppm at depths under ~ 500 m is most likely due to that the selected fractures contain a large fraction of clay minerals.

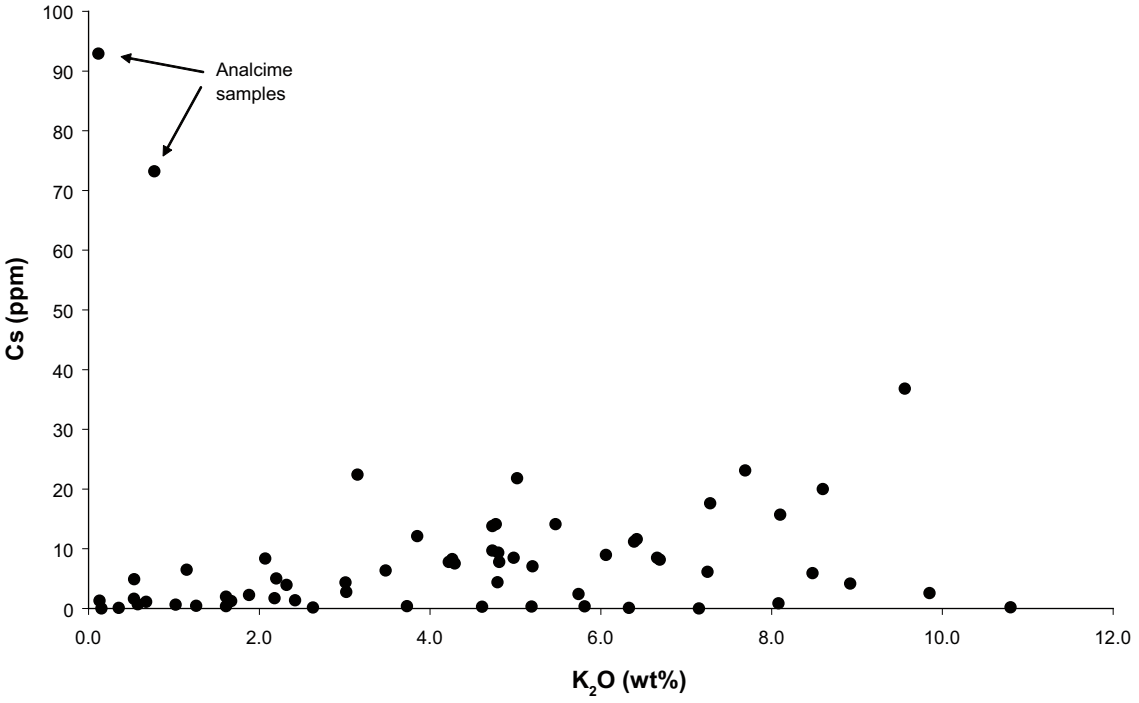

Figure 7-2. *Cs plotted against K_2O. The Cs content in the dominating granite (to granodiorite) of the Forsmark area varies between 0.2 and 1.5 ppm (median 0.65).*

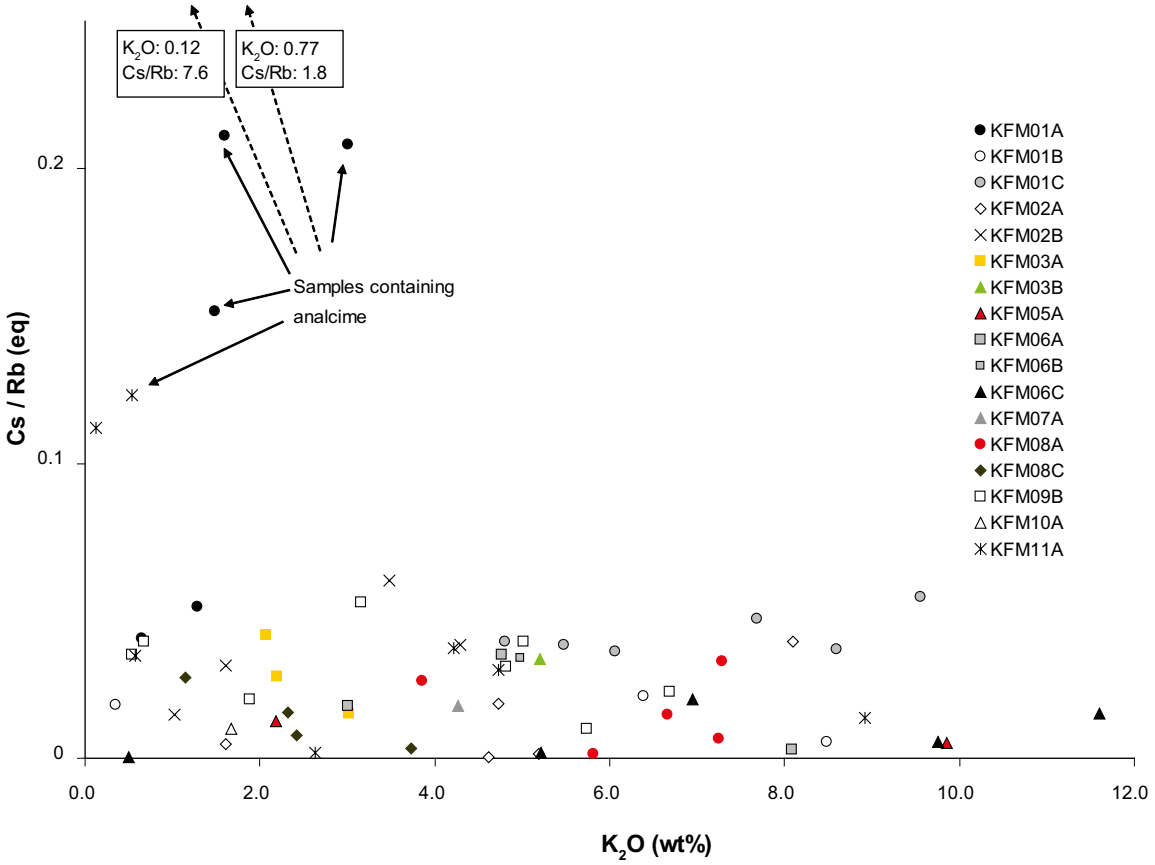

Figure 7-3. *K_2O (wt%) versus Cs/Rb ratio (from equivalents) in bulk fracture filling material. Observe that two analcime rich samples fall outside the scale of the plot (dashed arrows).*

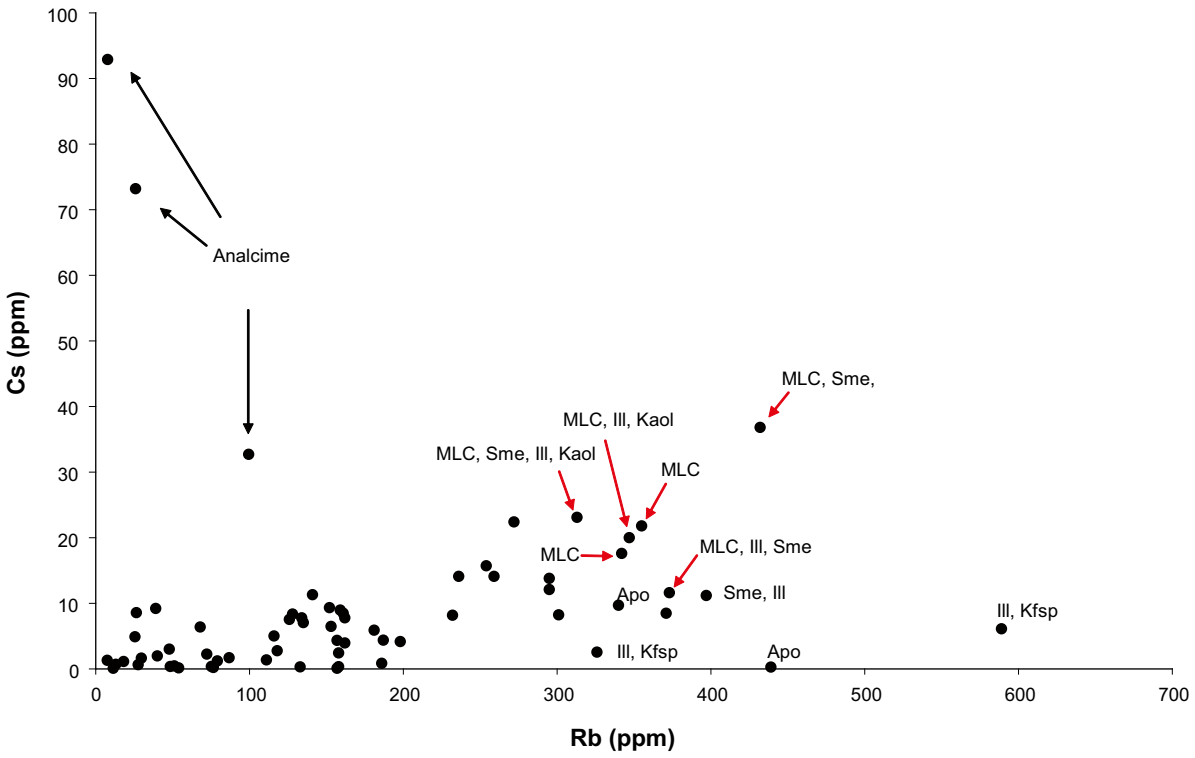

Figure 7-4. *Rb (ppm) versus Cs (ppm) in bulk fracture filling material. Relevant fracture minerals (identified by XRD) are indicated on samples with elevated values. Apo = apophyllite, Ill = illite, Kaol = kaolinite, MLC = mixed layer clay, Sme = smectite.*

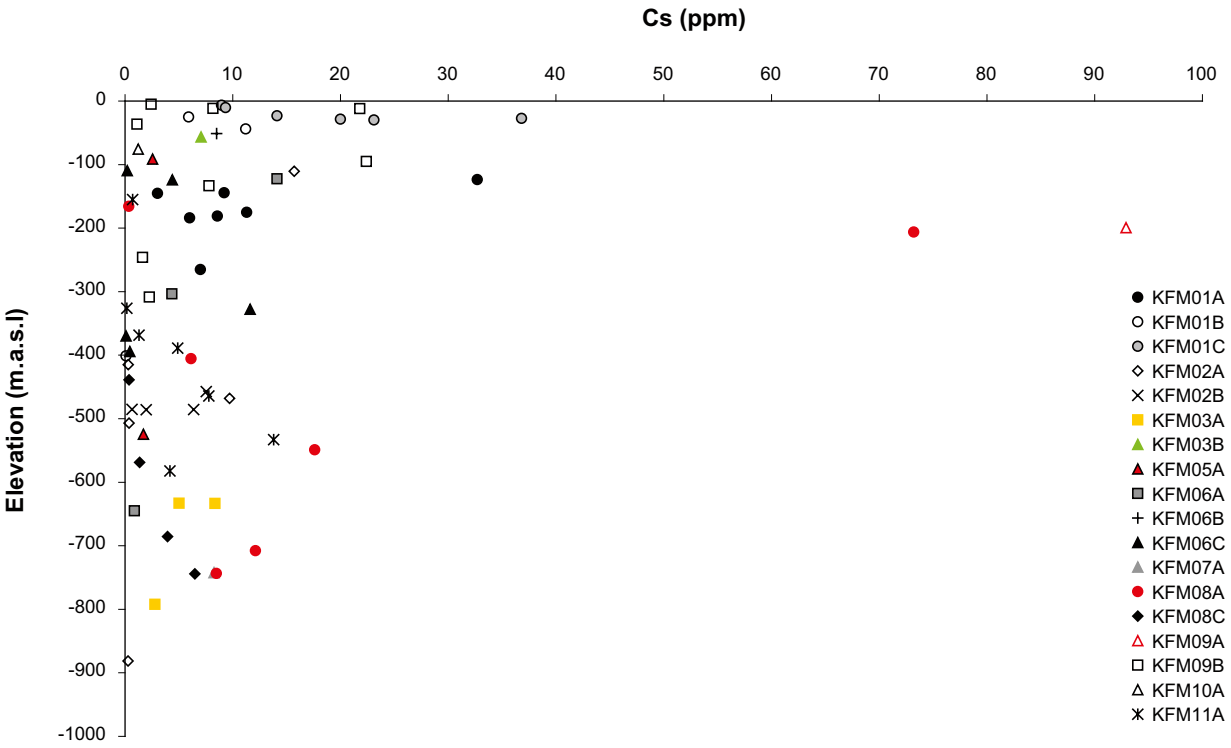

Figure 7-5. *Cs (ppm) variation versus depth (elevation) in bulk fracture fillings. The extreme values (> 70 ppm) consist of almost pure analcime.*

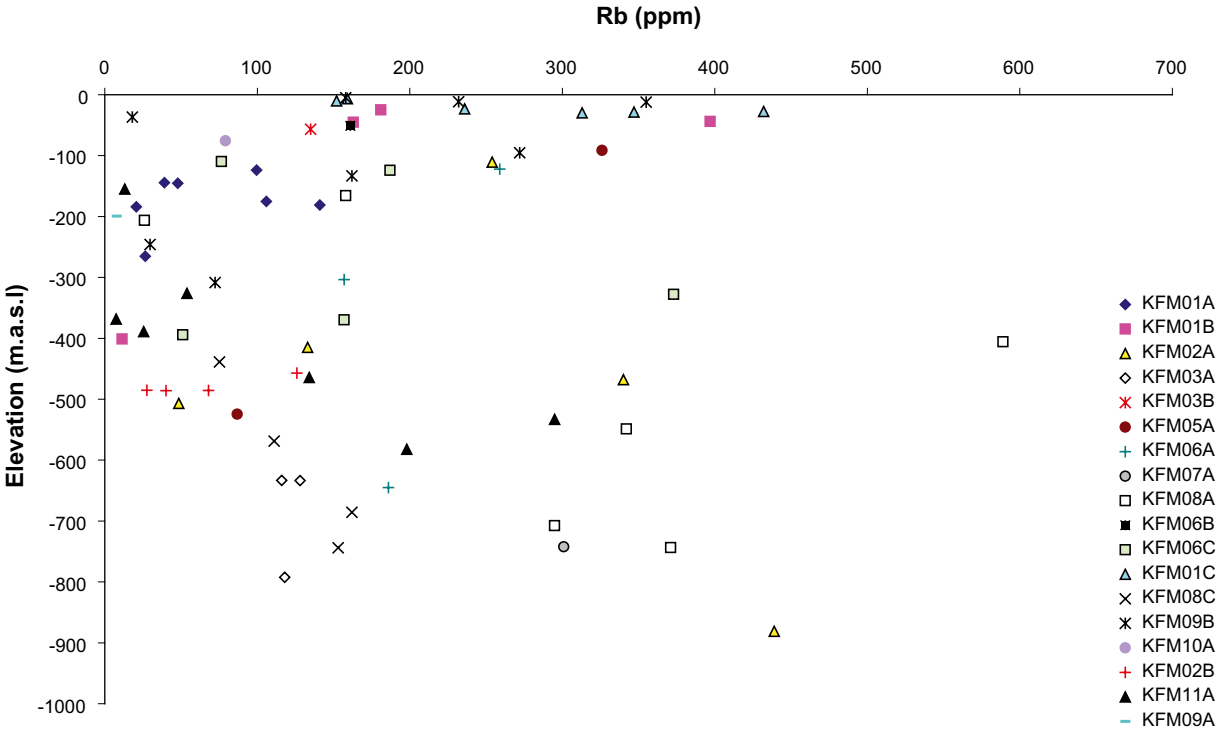

Figure 7-6. *Rb (ppm) variation versus depth (elevation) in bulk fracture fillings.*

Na, Ca, Sr

Albite and in a few fractures, analcime, are the main Na-bearing fracture minerals at Forsmark. Small amounts of Na^+ are also incorporated in smectite which occurs as layers in corrensite but also in other mixed layer clays and as a pure clay mineral. The major Ca mineral is calcite but Ca-Al-silicates also occur abundantly (laumontite > epidote > prehnite). Small amounts of Ca^{2+} are also incorporated in smectite and vermiculite. The correlation between Ca and Sr differs between different minerals; samples rich in calcite (high CaO content) show no correlation between Ca and Sr whereas samples with low concentrations of CaO show a positive correlation between CaO and Sr (Figure 7-7). The lack of correlation between CaO and Sr in calcite rich samples is confirmed by ICP-MS analyses of calcite leached with weak HCl acid, which shows no correlation between Ca and Sr. Most calcites have a low Sr content; often close to 50 ppm or below (although a few samples show up to 333 ppm) /Sandström and Tullborg 2005/. The fracture fillings with low CaO content are dominated by Ca-Al-silicates and chlorite/corrensite. The samples with highest Sr values (> 300 ppm) contain laumontite and/or corrensite indicating that these minerals have a high affinity for Sr^{2+}. Also samples rich in epidote show elevated Sr content.

The Ca/Sr ratio in fracture fillings indicates where Sr has been enriched or depleted compared to the wall rock and groundwater. It is evident from Figure 7-8 that there is a large overlap between the Ca/Sr ratio in fracture fillings and in the major rock types and groundwaters. However, a large number of fracture fillings (especially above 500 m elevation) show elevated Ca/Sr ratios compared to both wall rock and the groundwater. This could reflect that Palaeozoic calcite, which has low Sr content (Palaeozoic; section 5.4), is more abundant in the upper part of the bedrock.

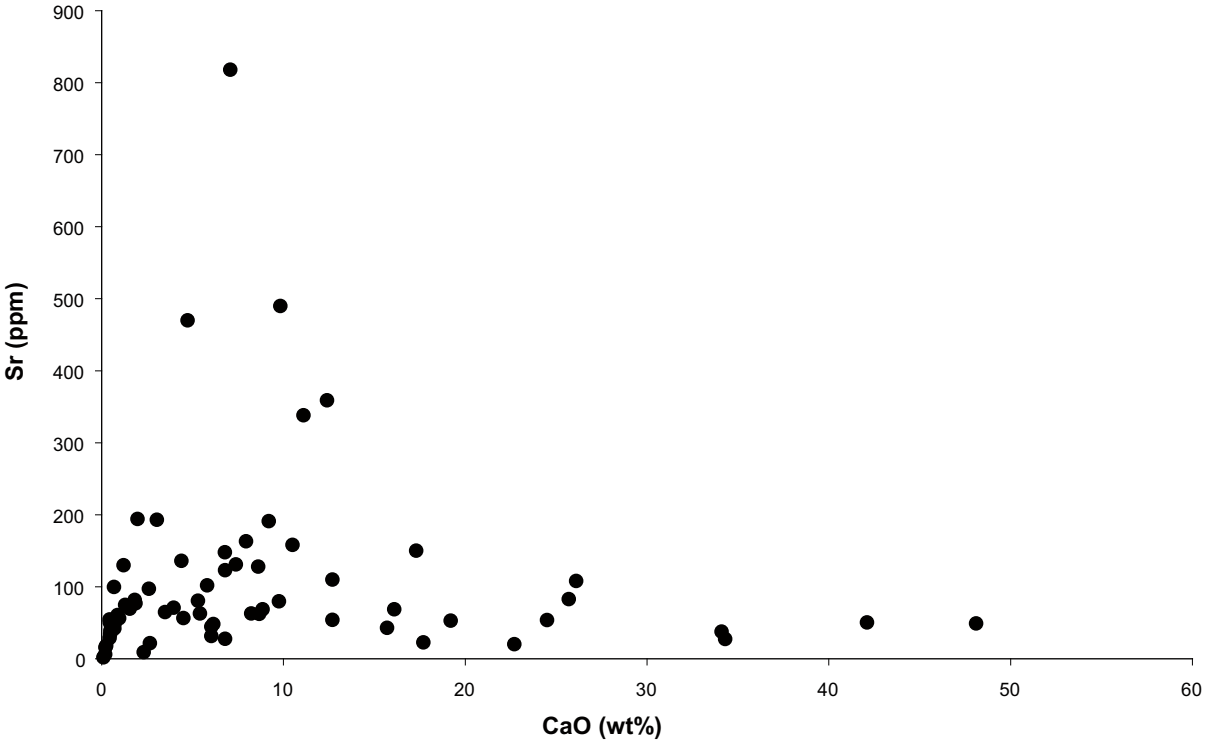

Figure 7-7. *CaO (wt%) plotted against the Sr content (ppm) in bulk fracture fillings.*

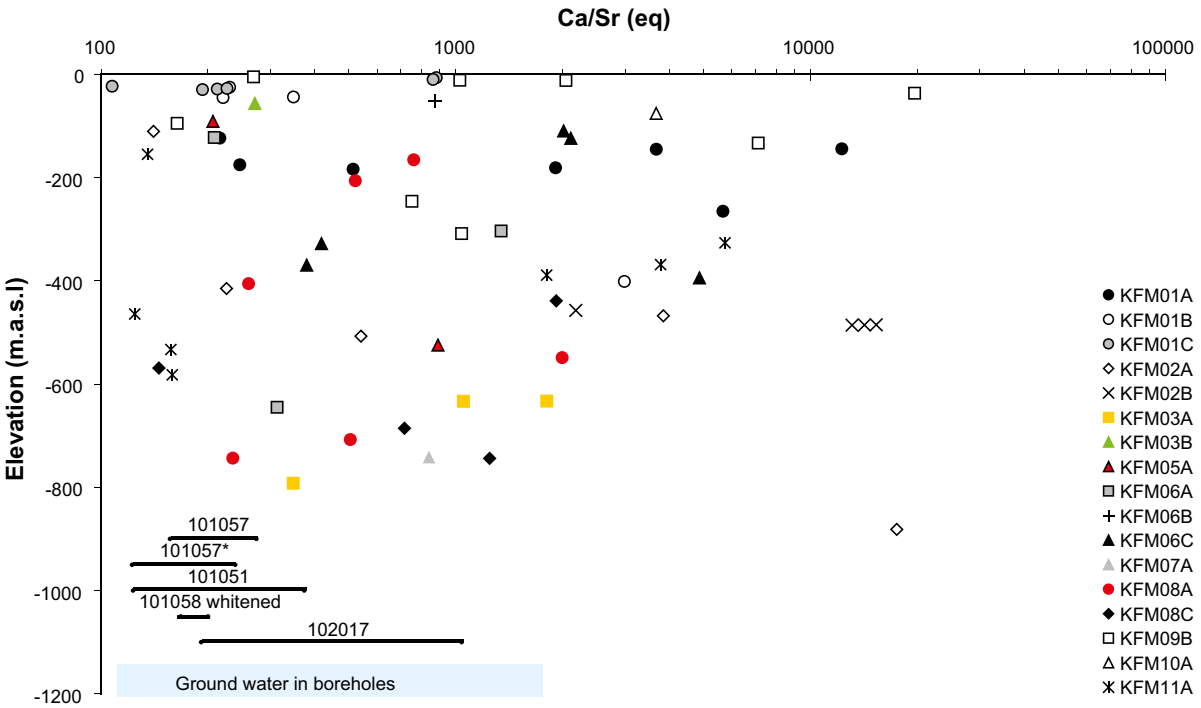

Figure 7-8. *The Ca/Sr ratio (based in equivalents) in bulk fracture fillings plotted against depth (elevation). The lines represent the ranges in Ca/Sr ratios in the most abundant rock types within the target area. A field for pegmatite has not been included in the figure since only a single data point exists. 101057: granite (to granodioritic rock), 101057*: granite (to granodioritic rock), metamorphic, altered with red staining, 101051: granodiorite, tonalite and granite, metamorphic, 101058: granite, metamorphic, aplitic (altered bleach), 102017: amphibolite. The blue field represents the Ca/Sr ratio in groundwater samples from cored boreholes.*

The near surface groundwaters from the overburden show higher Ca/Sr ratios (around 1,200) whereas the ratios for groundwaters in the percussion boreholes show ratios around 300, and the deeper, more saline waters show even lower ratios (around 200) /Tröjbom et al. 2007/. This is interpreted as a major influence from calcite dissolution in the upper near surface waters in the Quaternary overburden, whereas the Ca/Sr ratio in the deeper waters is probably more controlled by water-rock interaction. Ion exchange together with silicate alteration are possible mechanisms for controlling the Ca/Sr ratios in the bedrock aquifer.

Fe, Mg, Mn

Iron is mainly hosted by chlorite and corrensite in the fracture system as indicated by the correlation between Fe and Mg in Figure 7-9 (chlorite and corrensite are the only two major Mg bearing fracture minerals in Forsmark). The variation in Mg/Fe ratio in the bulk fracture fillings is due to the variation of the Mg/Fe ratio in fracture filling chlorite and corrensite. Hematite is commonly present only in trace amounts and seldom constitutes more than 1 vol% of the fracture minerals. No significant trends can be seen when total Fe content expressed as Fe_2O_3 is plotted against depth (Figure 7-10). Fe and Mg are highly enriched in most fracture fillings compared to the dominating granite (to granodiorite) in the area (Figure 7-9).

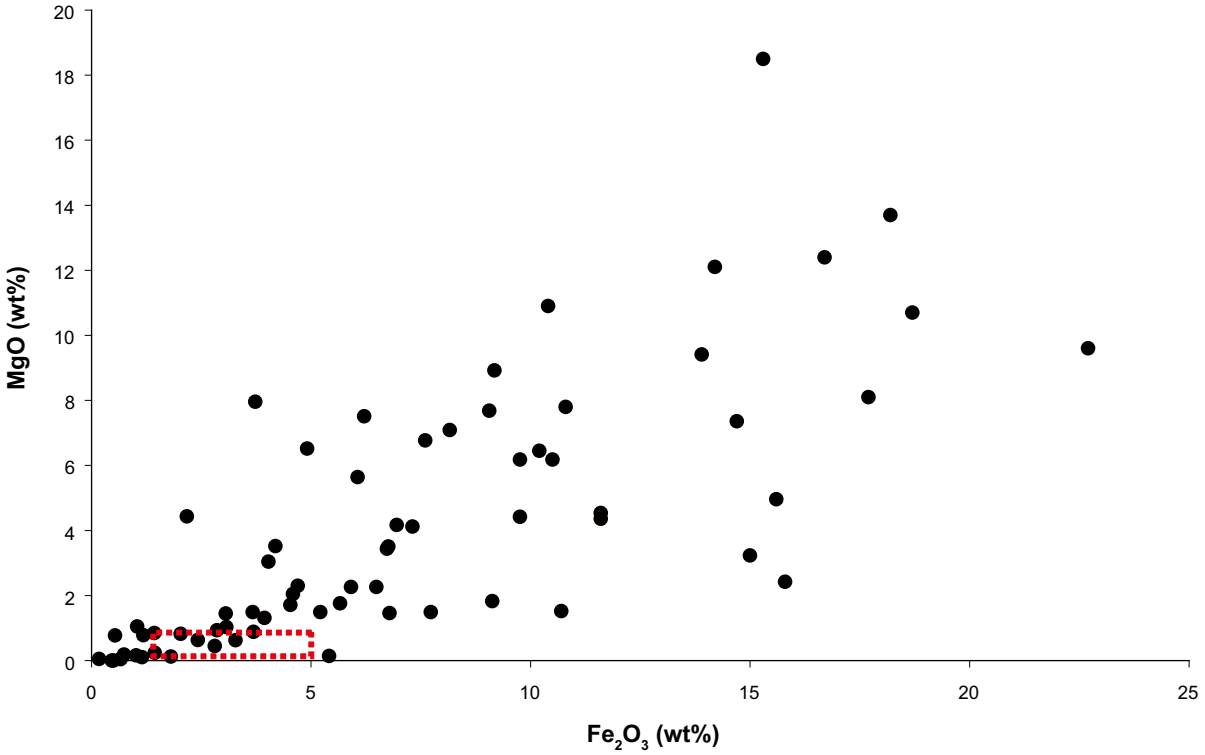

Figure 7-9. *Fe_2O_3(total) versus MgO for bulk samples of fracture fillings. The red dashed square represents the compositional span in the dominating granite (to granodiorite) of the area.*

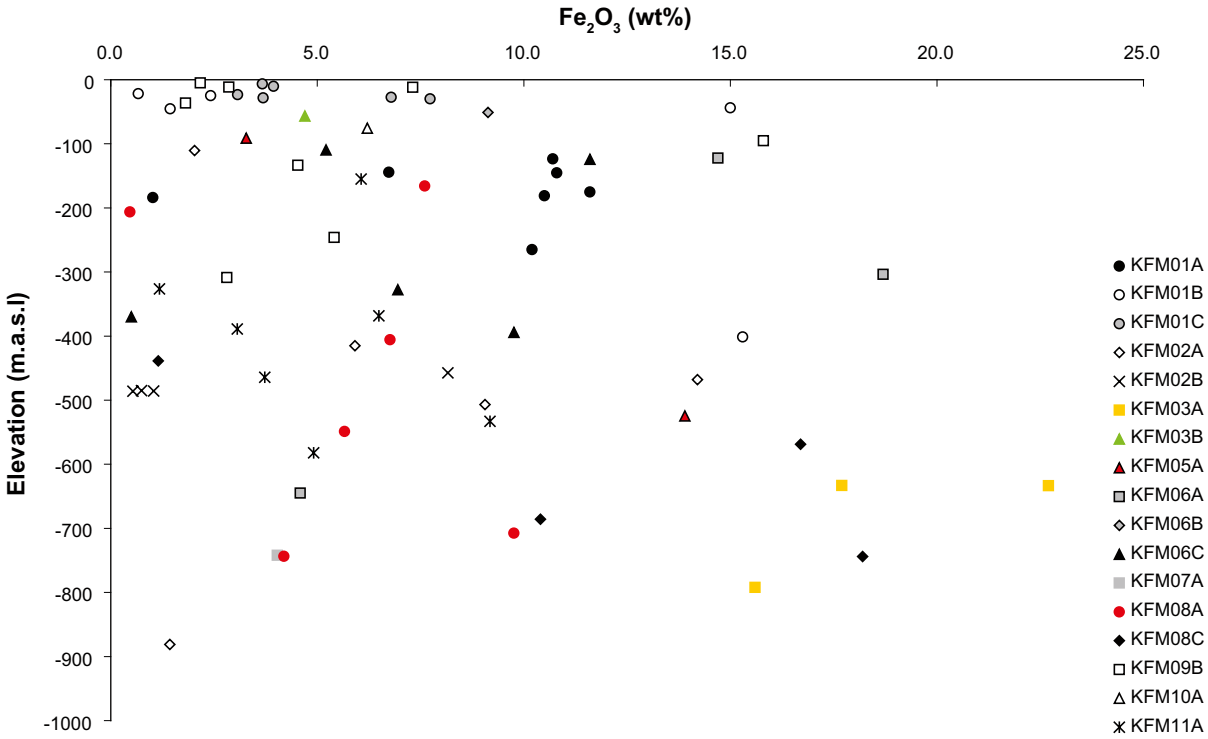

Figure 7-10. *Fe_2O_3(total) in bulk fracture fillings versus elevation.*

Manganese (given as MnO) shows a significant positive correlation with Fe indicating its presence in chlorite and clay minerals. MnO is also highly enriched in most fracture fillings compared to the dominating granite (to granodiorite) of the area. The highest MnO values are found below ~ 300 m (Figure 7-11) and since Mn is a redox sensitive element, this could be due to different redox conditions at present or at earlier periods during the hydrogeological evolution at the site. The reduced Mn^{2+} ion is highly soluble in contrast to oxidised Mn^{3+} and Mn^{4+}. Mn reducing bacteria produces Mn^{2+} during the oxidation of organic material. At Forsmark, Mn reducers are more frequent in the groundwater samples from the upper 500 m, which also largely corresponds to higher Mn^{2+} content in the groundwaters down to approximately this depth /Laaksoharju et al. 2008/. This behaviour is also valid for the Fe system.

Iron, magnesium and manganese in their divalent states can form carbonates during favourable conditions. However, no carbonates other than calcite ($CaCO_3$) have been identified in the fracture coatings at Forsmark and the Mn, Fe and Mg contents in the analysed calcites are generally low (together < 1 wt%; cf section 7.1).

U, Th

The U content in bulk fracture fillings varies between 0.1 and 164 ppm except in two samples from KFM03A 643.80–643.12 m and KFM03A 644.17 m which have U contents of 2,200 and 2,310 ppm, respectively (Figure 7-12). Most fracture fillings have lower Th/U ratios than the main rock type (Figure 7-13). This is mostly due to lower Th contents in the fracture fillings compared to the wall rock as seen in Figure 7-12, but compared to the median U content in the main rock type, most of the fracture fillings are also enriched in U. Fracture fillings with high U content correlate with groundwater samples taken from the same depths and suggest that at least part of the uranium is found at easily accessible sites (Figure 7-14). Uranium and its variability in groundwaters are discussed in more detail in Chapter 8.

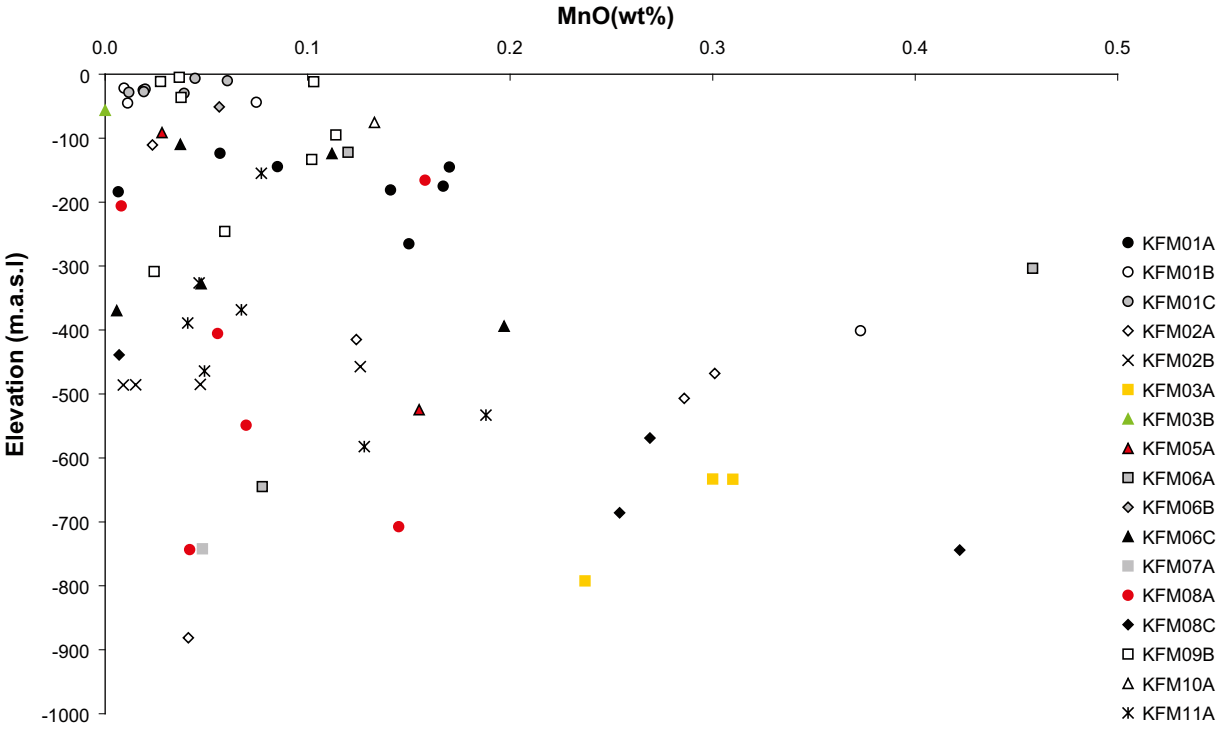

Figure 7-11. *MnO in bulk fracture fillings versus elevation. The dominating granite (to granodiorite) in the area shows MnO contents between 0.02 and 0.05 wt%.*

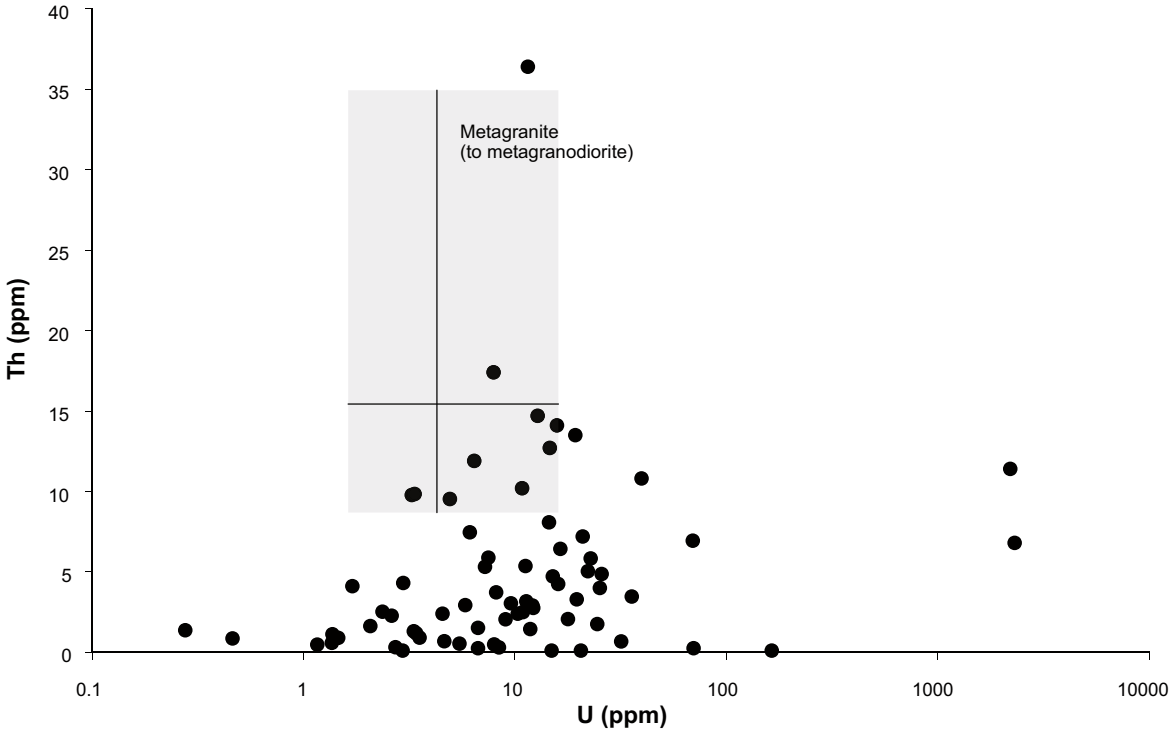

Figure 7-12. *U versus Th in bulk fracture filling. The shaded field represents the compositional range of the metagranitic (to metagranodioritic) rock type that dominates the area (rock code 101057). The lines represent median values.*

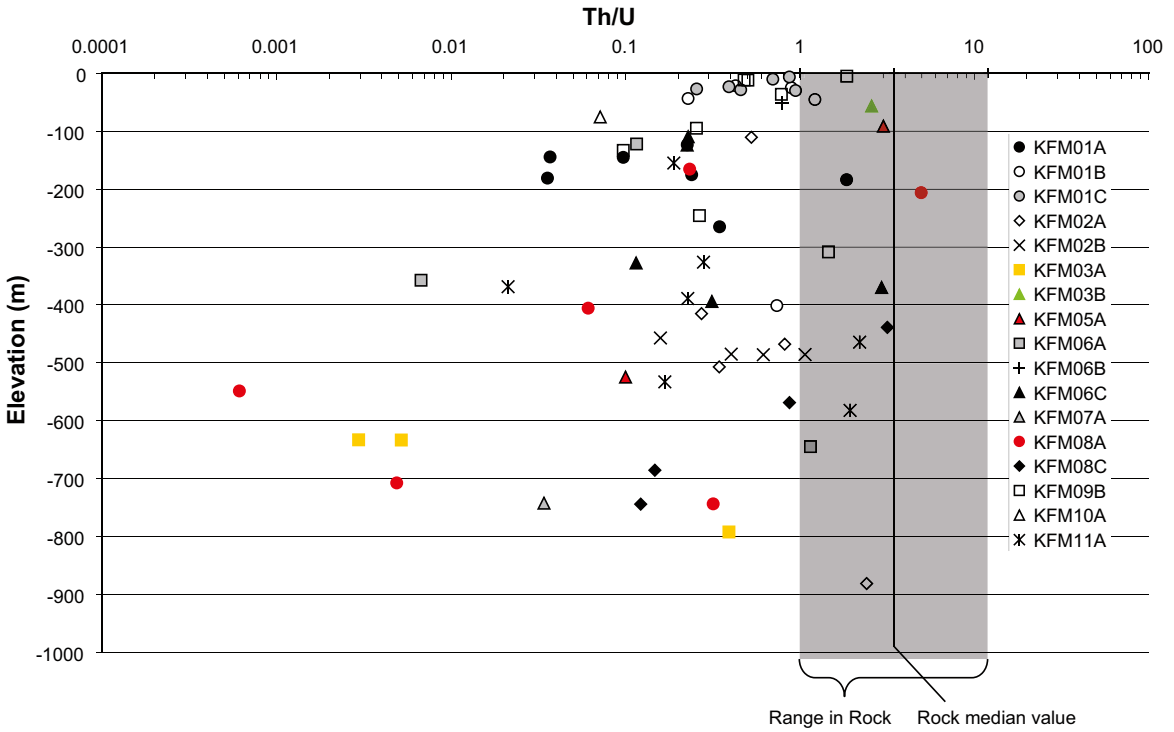

Figure 7-13. *Th/U weight ratio versus vertical elevation. The shaded area represents the range of ratios in the metagranitic (to metagranodioritic) rock type that dominates the area (rock code 101057).*

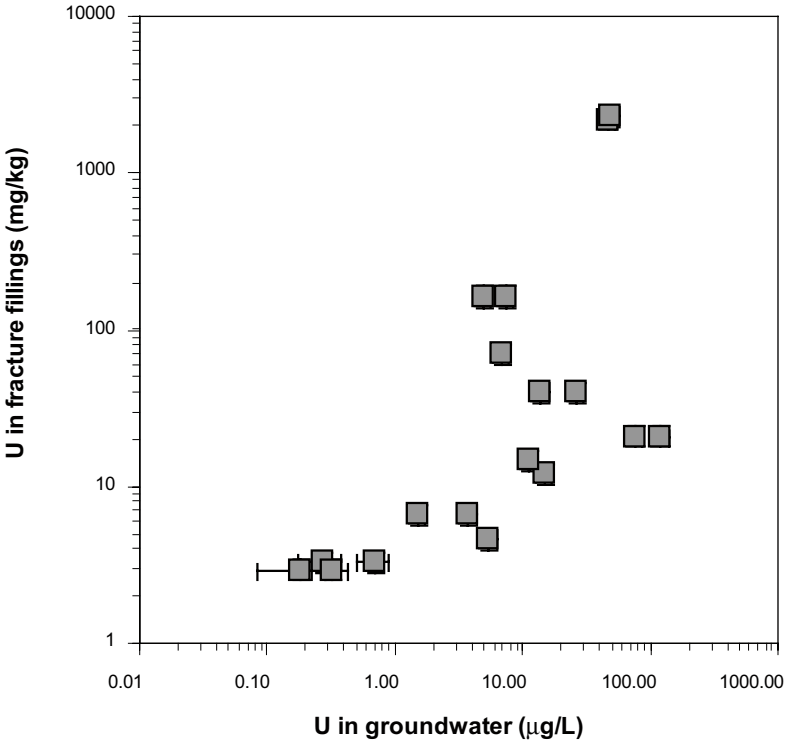

Figure 7-14. *Uranium content in fracture fillings (ppm) versus uranium in groundwater samples (µg/L). The fracture filling samples are from the corresponding drill core length. The precision of both water and fracture analyses is ~ 15%.*

REEs

Chondrite normalised REE-patterns for all analysed bulk fracture fillings are shown in Figure 7-15. The La/Yb ratio varies between 0.1 and 40 except for six samples with ratios 59, 63, 91, 128, 220 and 324 (Figure 7-16). The LREE are both enriched and depleted in the fracture fillings compared to the metagranitic (to metagranodioritic) rock type which dominates the candidate area. Most fracture fillings have a HREE content overlapping with the concentrations in the main rock type, the samples that deviate show an enrichment in HREE. Overall, the REE content in fracture fillings show a larger span than the dominating rock type. All fracture filling samples except one show negative Eu-anomalies, probably inherited from the wall rock. The La/Yb ratio is generally lower in the fracture fillings than in the rock.

A few samples show significantly positive Ce anomalies (Figure 7-17), indicating oxidation of Ce^{3+} to Ce^{4+} and subsequent preferred precipitation of the less mobile Ce^{4+} ion on the fracture surfaces. Negative Ce anomalies are more common in the fracture fillings and are interpreted as a result of precipitation from a fluid depleted in Ce. This could, for example, be due to that the less soluble Ce^{4+} has precipitated in another part of the fracture system or in the Quaternary overburden during oxidising conditions and left the fluid Ce-depleted. Most of the Ce anomalies detected belong to fracture coatings with hydrothermal minerals and give no information about the present redox conditions in the fracture/groundwater system. The Pr anomalies seen in a few samples are due to analytical errors/uncertainties explained by small sample sizes and low concentrations. A few REE-patterns show deviating patterns which could be due to the presence of minor mineral phases with distinctive REE-signatures.

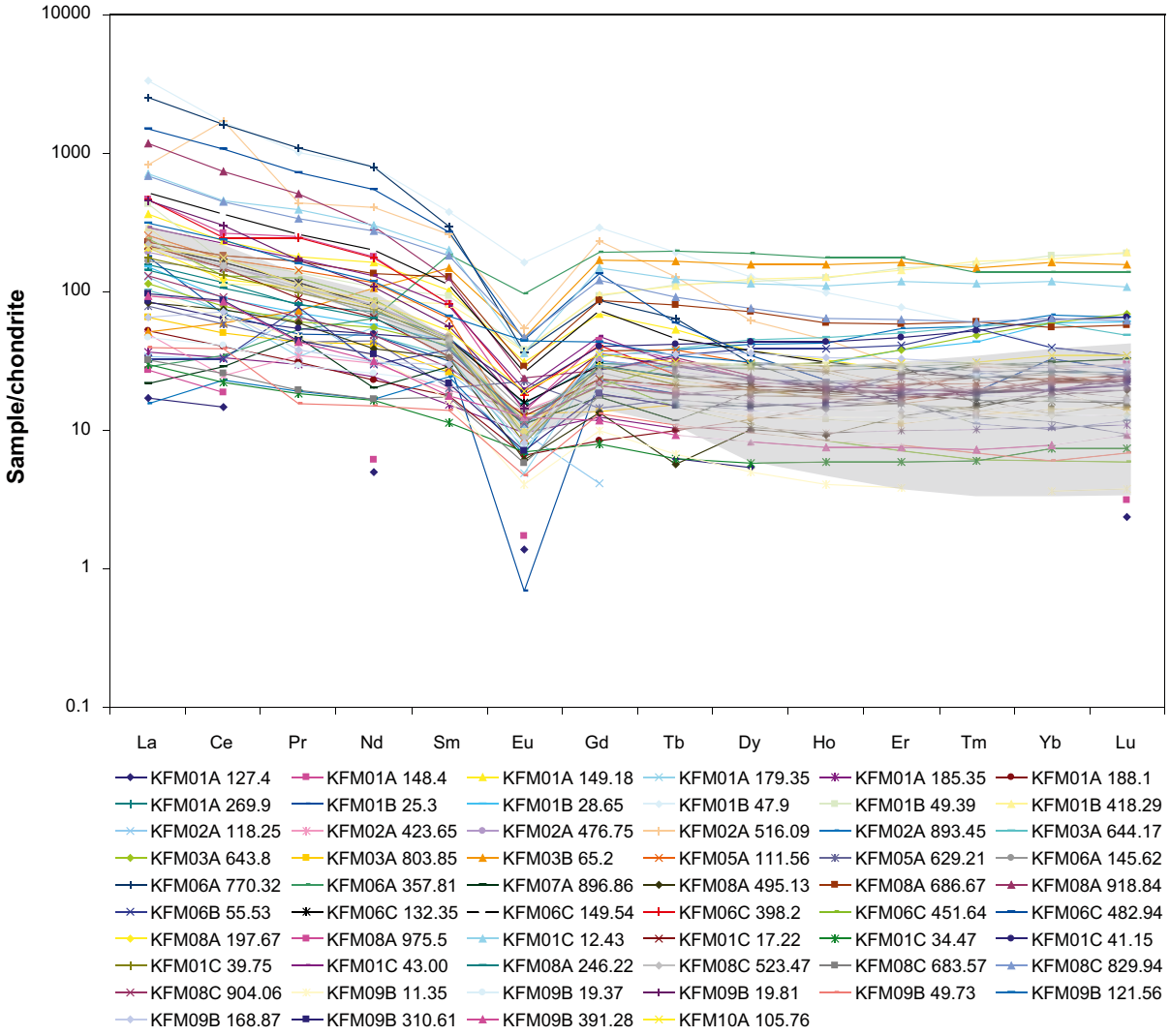

Figure 7-15. *Chondrite normalised REE patterns for all analysed bulk fracture fillings. The shaded area represents the composition of the main rock type in Forsmark (granite to granodiorite; rock code 101057). Chondrite values from /Evansen et al. 1978/.*

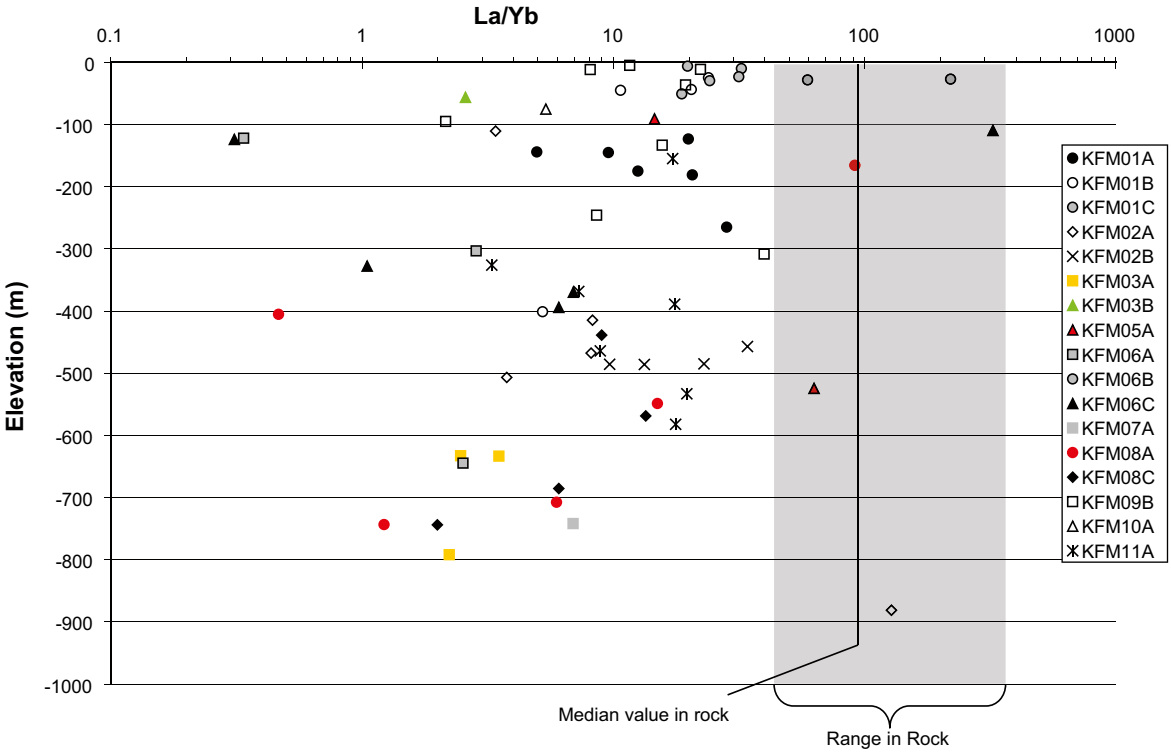

Figure 7-16. *La/Yb ratio versus elevation in bulk fracture fillings. The shaded area represents the compositional range of the main rock type in Forsmark (granite to granodiorite; rock code 101057) and the line the median value.*

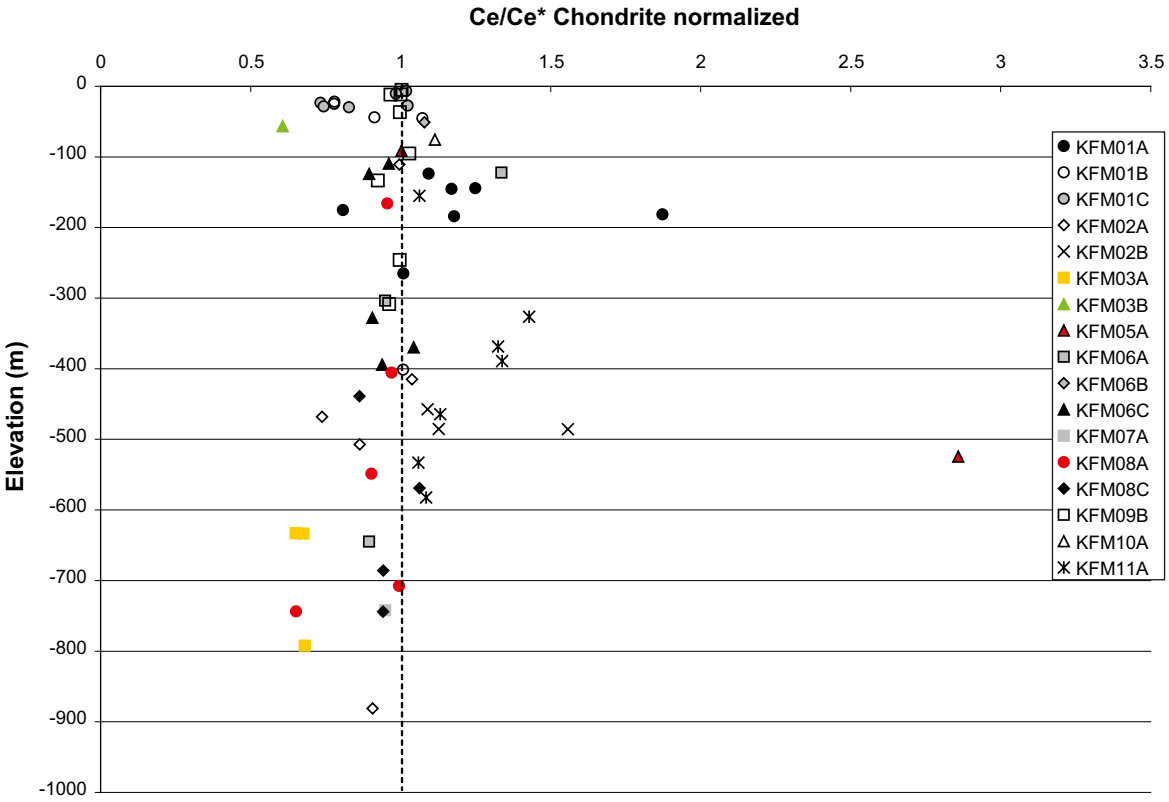

Figure 7-17. *Ce anomalies versus elevation given as Chondrite normalised Ce/Ce* in bulk fracture fillings.* $Ce^{*}=(La \cdot Pr)^{0.5}$.

7.3 Concluding remarks

The ICP analyses largely confirm the mineralogy determined from the drill core mapping, XRD and microscopy, but have also added useful information on the behaviour of trace elements such as Cs and U which show a significant enrichment in fracture coatings compared with the host rock.

Selected elements and the major fracture mineral phases within which they are incorporated are shown below:

K	Adularia, illite, apophyllite
Cs	Analcime, clay minerals (illite and mixed layer clays)
Rb	Clay minerals (illite and mixed layer clays), apophyllite
Ba	Adularia
Na	Albite, analcime
Ca	Calcite, Ca-Al silicates (epidote, prehnite, laumontite) + corrensite
Sr	Ca-Al silicates (laumontite, epidote) + corrensite
Fe	Chlorite/corrensite, pyrite, hematite, epidote, prehnite
Mg	Chlorite
U	U-oxide (pitchblende) but also amorphous phases and minerals such as apatite and zircon (from the wall rock)
REEs	Calcite, allanite, titanite and zircon (the latter three from the wall rock)

8 Uranium and its variability in groundwaters and fracture coatings

8.1 Background

The distribution of uranium in the Forsmark groundwaters has been the focus of discussion and conjecture since the initial observation of elevated uranium concentrations corresponding to a narrow range of chlorinity coinciding mostly, but not always, with the brackish marine (Littorina Sea) groundwaters (Figure 8-1). As an integral part of the hydrogeochemical studies, but also from a safety assessment viewpoint, the importance of explaining these elevated uranium concentrations therefore became prioritised. Several differing hypotheses have emerged which have been individually addressed.

Like many other groundwater trace element constituents, but more so for uranium, sampling under controlled conditions is of paramount importance, for example, the initial removal of contamination from pre-sampling borehole activities, sampling using optimum pump flow rates (e.g. minimising changes in groundwater chemistry and redox conditions), adequate period of pre-sampling monitoring to ensure stabilisation etc. Care is also required when sampling from low transmissive fractures to avoid removing loosely bound trace constituents from the fracture surfaces. There are numerous examples were trace elements in the groundwater finally selected for analyses are anomalously high, even though the major constituents indicate stability. The uranium data have been carefully scrutinised to evaluate such possible negative effects (e.g. repeated sampling and double analyses have been performed) and, while anthropogenic effects undoubtedly have influenced many of the uranium contents to a degree, the overall elevation of uranium in the measured groundwaters is a hydrogeochemical anomaly in the Forsmark bedrock that needs to be explained.

Given that there may be uncertainties with respect to the quality of some of the groundwater samples analysed, fracture coating material, if possible selected from the same open fracture sampled for groundwater, has been analysed for the uranium decay series isotopes together with the groundwater suite of samples. Can the fracture coatings help explain the observed uranium anomaly?

8.2 Distribution of uranium in the bedrock and possible sources

From bulk fracture coating analyses (cf section 7.2) it is obvious that enhanced uranium concentrations occur in some of the fracture systems within the Forsmark candidate site /cf Laaksoharju et al. 2008/. Most of the fracture samples analysed have uranium concentrations in the range 0.1 to 164 ppm, except for two samples from KFM03A 643.80–643.12 m and KFM03A 644.17 m, which show contents of 2,200 and 2,310 ppm U respectively. Out of the 70 fracture samples analysed, nine show uranium concentrations higher than 24 ppm in combination with a U/Th ratio greater than 10, which strongly indicates deposition of the uranium in the fractures. Of these nine samples taken from depths ranging from 133–633 m, seven belong to the gently-dipping deformation zones which characterise FFM03 and one is sampled from KFM11A, to the west of the large NW-trending Singö deformation zone. It has only been possible to identify one uranium-bearing phase and that is from sample KFM03A 644.17 m; this comprised one small grain of pitchblende from the fracture coating material which also recorded the highest uranium concentration (Figure 8-2). Although not demonstrated, part of the uranium is assumed to be sorbed onto clay minerals or Fe-oxides in the fracture coatings.

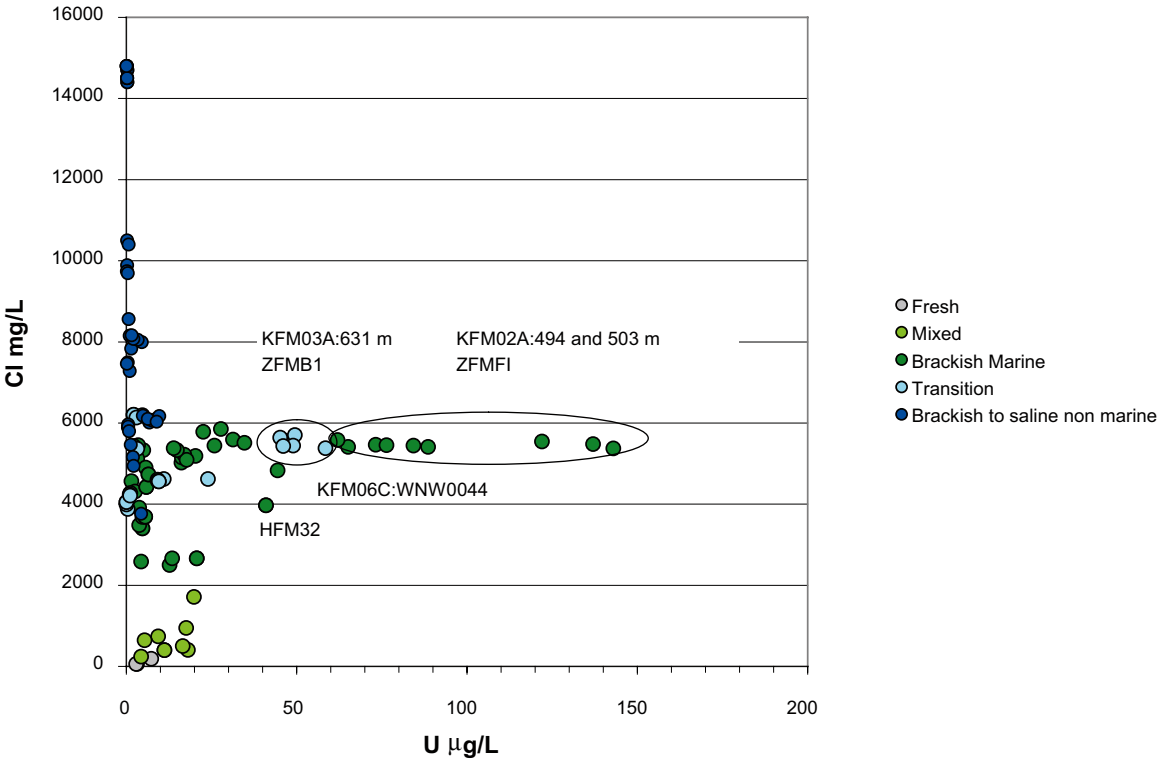

Figure 8-1. *Cl versus U for groundwaters from Forsmark. A large number of data are plotted for KFM02A around 500 m depth representing groundwaters from the gently dipping deformation zone ZFMF1. For further information on the water classification, see /Laakshoharju et al. 2008/.*

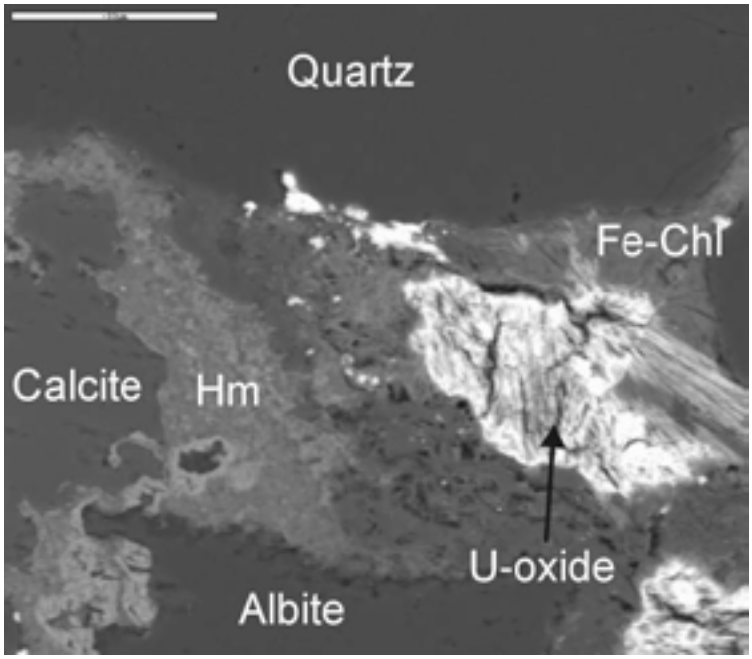

Figure 8-2. *Altered U-oxide (Pitchblende) together with chlorite (Fe-Chl), hematite (Hm) and calcite (KFM03A 644.17 m). Back scattered electron image. Scale bar is 50 µm.*

The bedrock within the candidate site is generally low in U (< 10 ppm), but some of the pegmatites show slightly enriched uranium values. A maximum value of 62 ppm is indicated by gamma spectrometric data /Stephens et al. 2007/. However, uranium mineralisations are not unknown in the region and several are found associated with iron ores in the northern Uppland area (Figure 8-3) /Welin 1964/. Three types of mineralisations have been identified: 1) The oldest (c. 1,785 Ma) is related to the late Svecokarelian epoch consisting of disseminated uraninite precipitated from oxidation-reduction reactions in the iron-bearing skarn ores. 2) The second type of mineralisation (c. 1,585 Ma) occurs in the fissured bedrock, resulting in the formation of pitchblende, hematite and some sulphides related to mineralised fractures or veins of chlorite, calcite and quartz. 3) A younger, less well-constrained period of uranium mineralisation was distinguished, consisting of pitchblende precipitation in a chemically reactive 'ferriferous rock' /Welin 1964/. Asphaltite has, as mentioned in previous sections, been identified in fractures in the upper 150 m in Forsmark and based on analyses of stable carbon isotopes and biomarkers, the asphaltite found in fractures in the crystalline basement at Forsmark has been shown to be of biogenic origin /Sandström et al. 2006b/. The most plausible source rock is the late Cambrian to early Ordovician Alum Shale that covered most of southern Sweden during the Palaeozoic. Alum shales can be enriched in uranium and some of the asphaltite occurrences in south central Sweden are high in uranium and thorium (i.e. termed thucholite; an acronym for Thorium, Uranium, Carbon and Hydrogen (Th, U, C, H)) /Welin 1966/. However, the fracture asphaltites analysed from the Forsmark site show low uranium and thorium and probably do not contribute significantly to the elevated uranium contents in the groundwaters.

Based on the information above, it is not surprising that fracture coatings with large variations in uranium content occur in the fractures at Forsmark and that in the fracture coatings, both U(IV) and U(VI) may be hosted in different phases and some may also be sorbed onto mineral phases such as hematite and clay minerals.

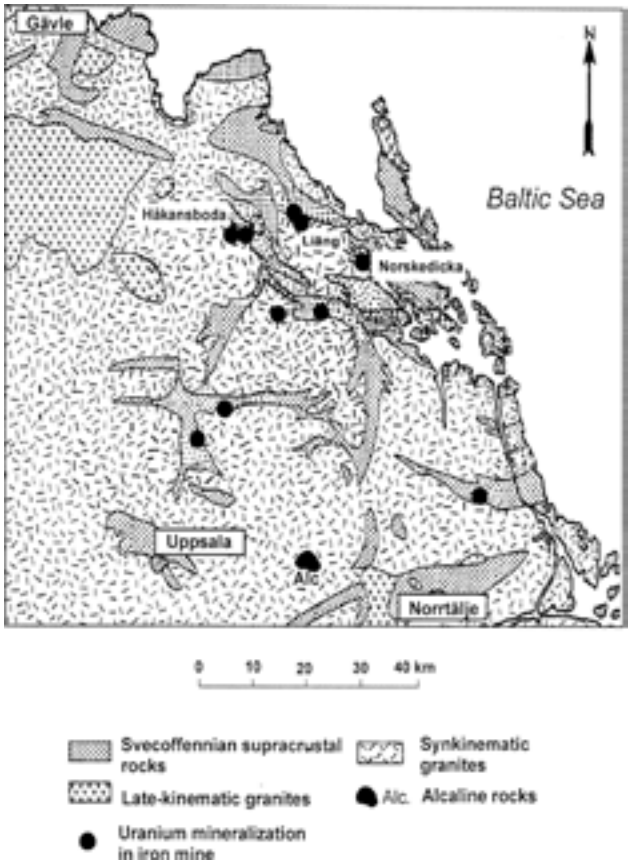

Figure 8-3. *Localised uranium mineralisations in northern Uppland, near Forsmark /Welin 1964/.*

8.3 Distribution of uranium in groundwaters

From analyses of groundwaters sampled in the cored boreholes at Forsmark it is known that part of the uranium found in the fractures is easily mobilised during certain conditions, especially with respect to redox and bicarbonate content (SKB 2007; Appendix 3). Figure 8-4 shows uranium content versus elevation for representative groundwater samples. To facilitate discussion of these results, a brief presentation of the groundwater system at Forsmark is given below based on /Laaksoharju et al. 2008/.

The upper highly transmissive part of the rock (upper 150 m) is characterised by an abrupt change from fresh water (dominantly modern meteoric waters; grey symbols in the plots) in the upper 30 to 100 m, to brackish marine water (green symbols in the plots). This brackish water is dominated by components from the former Littorina Sea transgression some 4,500–3,000 BC, and also mixed portions of glacial melt water from the last deglaciation. Towards depth the marine component diminishes and a brackish to saline non-marine water dominates (blue symbols in the plots). Along the gently dipping fracture zones which characterise FFM03, the marine brackish water reaches depths of 500 to 600 m, but in less transmissive parts of the rock (as shallow as 200 m), which appear to have escaped the influence of the post-glacial marine waters, older, non marine brackish to saline groundwaters still reside (cf Smellie et al. 2008).

Elevated uranium contents (up to ~ 150 µg/L) have been detected in some of the brackish marine groundwaters (compared with about 3 µg/L uranium concentration in seawater) from depths of 50–650 m (Figure 8-4). The two sections showing the highest values belong to the gently dipping deformation zones ZFMF1 at 497 m in borehole KFM02A, and ZFMB1 in borehole KFM03A at 631m. The brackish to saline non-marine groundwaters show generally low uranium contents (usually < 2 µg/L) despite depth; only one section in KFM08A shows increased values (4–10 µg/L U).

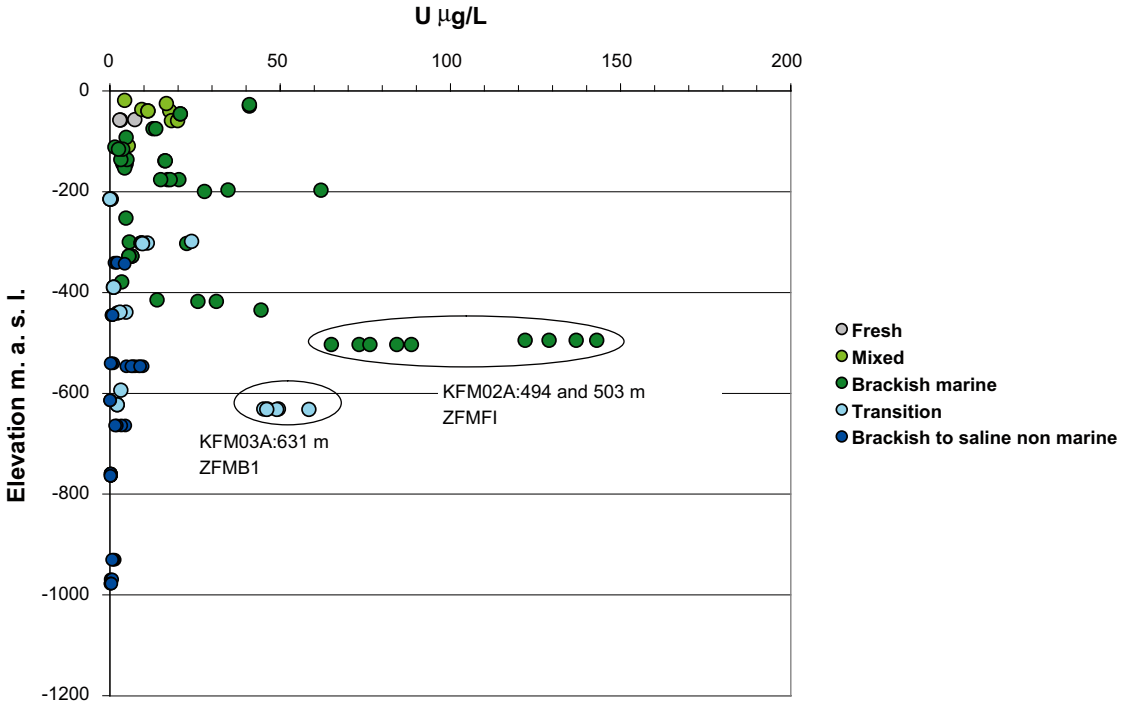

Figure 8-4. *Uranium in groundwaters from percussion and cored boreholes versus elevation. Only representative samples are included and ringed samples denote time series measurements for KFM03A 631 m and KFM02A 494 m and 503 m, /cf Laaksoharju et al. 2008).*

Large variations in uranium are measured in surface and near surface waters (from 0.05 to 40 µg/L; not shown in Figure 8-4). This is common and usually ascribed to variations in redox conditions and in concentrations of complexing agents, notably bicarbonate, the presence of which enhances solubility and hence mobility of uranium.

The reason for the elevated uranium contents in the groundwaters at intermediate depth has been discussed in, for example /SKB 2007/, where it was concluded that:

1. Despite negative Eh-values, elevated uranium contents in the groundwaters are restricted to samples showing mildly reducing conditions (Eh between –140 to –200 mV), whereas the more reducing groundwaters are low in uranium /SKB 2007; Appendix 3/. Furthermore, the amounts of dissolved bicarbonate in these waters allow uranium-carbonate complexation.
2. A study of uranium oxidation states in groundwater by /Suksi and Salminen 2007/ from the section showing the highest uranium content (~ 120 µg/L), showed a total dominance of U(VI) in the groundwater.
3. Even though elevated uranium contents seem to be related to present fresh meteoric water and brackish marine waters of post-deglaciation origin, it seems unlikely that uranium has been mobilised and transported into the bedrock by these waters, based on the wide range in uranium contents and the spatial distribution of elevated uranium groundwaters,
4. Disturbances caused by the drilling may have enhanced the mobility of the uranium especially in fractures potentially opened for groundwater flow by the drilling.
5. Microbial activity (possibly enhanced by perturbation in connection with the drilling) may have increased the uranium mobility /SKB 2007; Appendix 2/.
6. Colloid uptake plays a minor role in the mobilisation and transport of the uranium /Nilsson et al. 2006, Bergelin et al. 2007, Hallbeck and Pedersen 2008/.
7. Changes in redox conditions associated with the nearness to the high voltage cable passing trough the area may possibly have had local effects on the U mobility /cf SKB 2007/.

Additional Forsmark 2.2/2.3 data comprising uranium contents from sections selected for groundwater monitoring indicate that most of the sections originally showing low uranium remain low and sections with high uranium remain high (and in several cases even higher during the monitoring phase as discussed in section 8.1). Recent speciation-solubility calculations indicate possible equilibrium with amorphous uranium phases such as $UO_{2.66}$, $UO_{2\,(am)}$ and $USiO_{4\,(am)}$ for groundwaters with the highest uranium contents /Gimeno et al. 2008/. The best fit was found for $UO_{2.66}$ whereas oversaturation was indicated in respect of $UO_{2\,(am)}$ and $USiO_{4\,(am)}$) but the calculations was uncertain due to lack of corresponding measurements of Eh, pH and U(IV)/U(VI) (measurements of sample from the same section at the same time).

Not only dissolution of uranium phases but also sorption/desorption of uranium need to be considered when discussing U mobility. Sorption coefficients (K_d) for U(VI) measured on fracture fillings from deformation zone ZFMA2 at ~ 50 m depth (KFM01B) show values of around 2×10^{-2} (m^3/kg) /Byegård et al. 2008/.

As described above, there is a close association of elevated uranium contents with many of the brackish marine (Littorina) groundwaters, and since these groundwaters have been mostly collected from the highly transmissive, gently dipping fracture zones, it is a secondary relationship between U and transmissivity, which suggests that when groundwaters with elevated uranium contents entered the bedrock, they followed the most transmissive pathways.

8.4 Uranium decay series measurements

Analyses of isotopes in the uranium decay series can be used to infer redox conditions. Not only contemporary conditions can be characterised, but also evidence of past changes (e.g. during the last deglaciation some 10 ka ago) can be preserved in minerals which coat the fracture walls along groundwater pathways. Uranium decay series data (USD) for groundwaters and solid fracture phases from the Forsmark site have been analysed and are discussed below.

It is the first part of the uranium decay chain that is usually used for the USD series analyses and in this case mainly ^{234}U and ^{238}U for the water samples and ^{234}U–^{238}U–^{230}Th in the solid samples (fracture coatings).

Isotope	**^{238}U** →	^{234}Th →	^{234}Pa →	**^{234}U** →	**^{230}Th** →	^{226}Ra
Half-life	4.5×10^{9}a	24.1d	1.2min	2.5×10^{5}a	7.6×10^{4}a	1.6×10^{3}a

8.4.1 USD on groundwaters

A summary of the contents of chloride, bicarbonate, uranium and measured $^{234}U/^{238}U$ activity ratios for the different groundwater types are shown in Table 8-1.

For groundwater samples, the ^{238}U and ^{234}U activities (Figure 8-5) show that most of the waters with elevated uranium concentrations (higher than 5 μg/L ~ 60 mBq/kg) have $^{234}U/^{238}U$ activity ratios between 2 and 3. The sample showing the highest uranium concentration (KFM02A 497 m; deformation zone ZFMF1) has a ratio around 2 and the sample from KFM03A 631 m (deformation zone ZFMB1) has an activity ratio of around 1.5 (Figure 8-6).

There is no correlation between $^{234}U/^{238}U$ activity ratio and uranium content (Figure 8-6), or $^{234}U/^{238}U$ activity ratio and depth (Figure 8-7), which is quite expected considering that the samples represent fractures with different transmissivities and geological history. Both low (1.5) and relatively high activity ratios occur from 150–700 m (Figure 8-7). However, a majority of the samples show activity ratios < 2.8. In reducing groundwater conditions from intermediate to great depth from, for example, Olkiluoto and Äspö, activity ratios ≥ 3 are much more common and the uranium contents are usually lower /Pitkänen et al. 1999, Tullborg et al. 2003/. Ratios close to one in conjunction with high uranium concentrations can be interpreted as being indicative of dissolution under oxidising conditions.

Table 8-1. Cl, HCO_3^-, U and $^{234}U/^{238}U$ activity ratios (AR) for different groundwater types at Forsmark.

Water-type	Cl mg/L	HCO_3^- mg/L	U μg/L	$^{234}U/^{238}U$ AR
Dominantly Fresh	0–2000	317–450	2–20	2–3.1
Brackish Marine	2,000–6,000	45–260	1.5–143	2–4
Transition zone sample (Marine/Non-marine	5,500–6,000	23–34	45–59	1.5
Brackish/Saline	4,000–15,000	7–35	> 0.1–2	2–3.6
Non-marine			One sample 6–8	

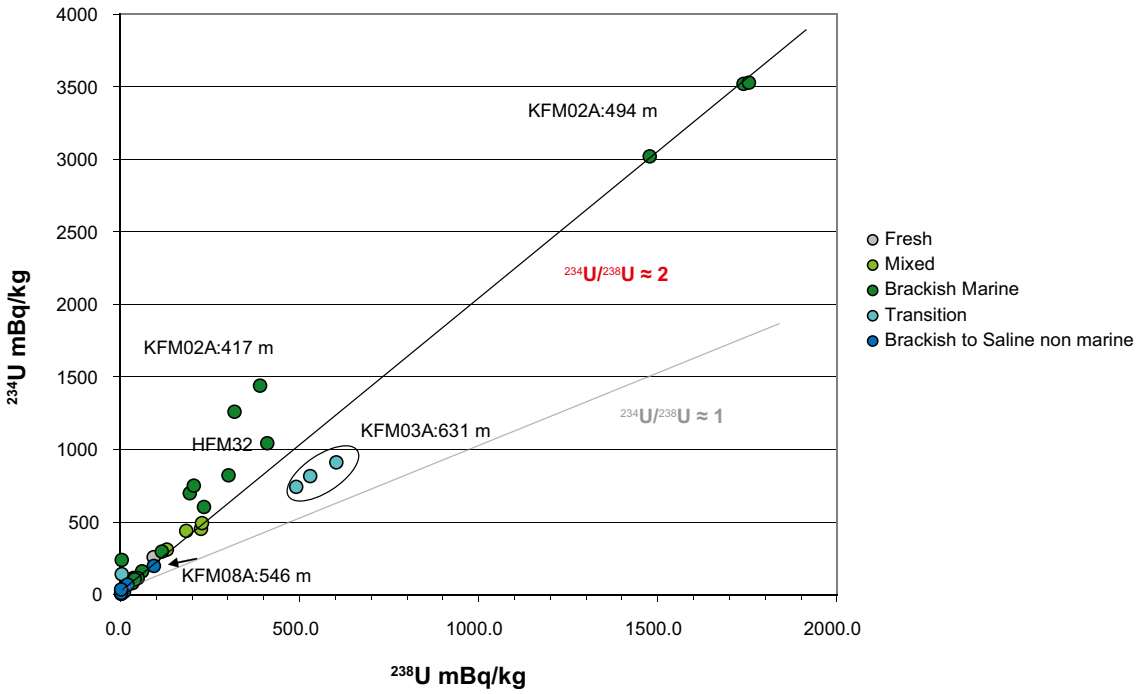

Figure 8-5. *Plot of ^{238}U versus ^{234}U activity for groundwaters from percussion and cored drilled boreholes at Forsmark;some of the boreholes with elevated uranium contents are labelled. The black line connects samples with lowest $^{234}U/^{238}U$ ratios and all samples are clearly above unity. KFM03A and KFM08A are of special interest and are discussed separately in the text.*

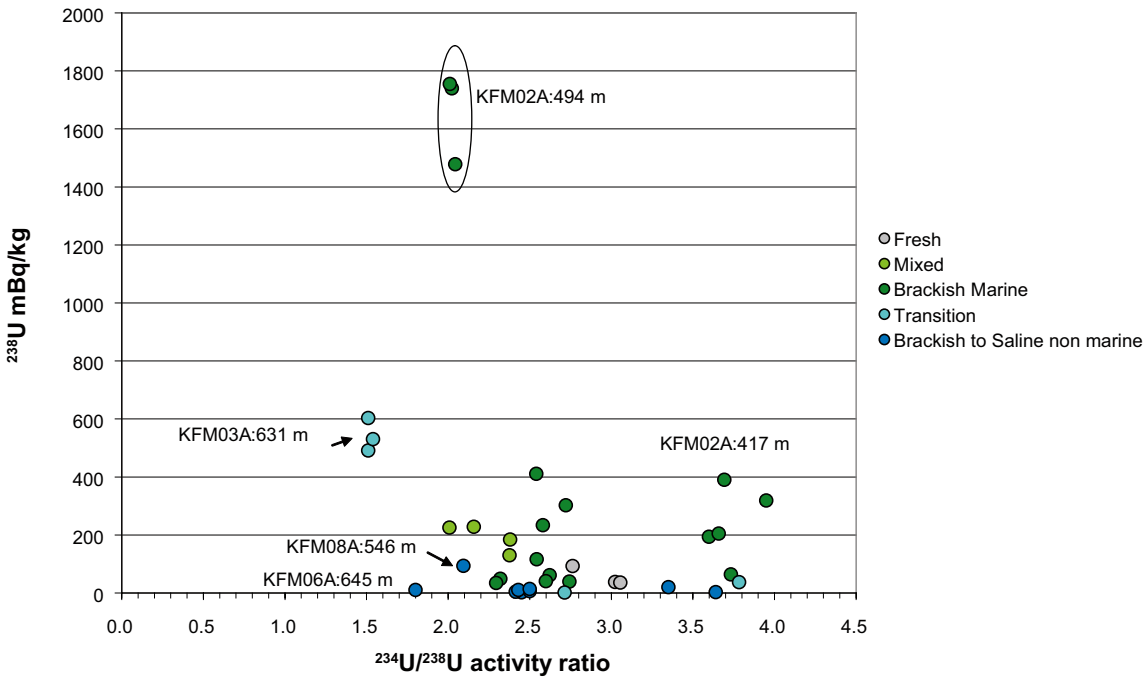

Figure 8-6. *$^{234}U/^{238}U$ activity ratio versus ^{238}U activity (mBq/L) for groundwaters from percussion and cored drilled boreholes at Forsmark; only boreholes with elevated uranium contents are indicated.*

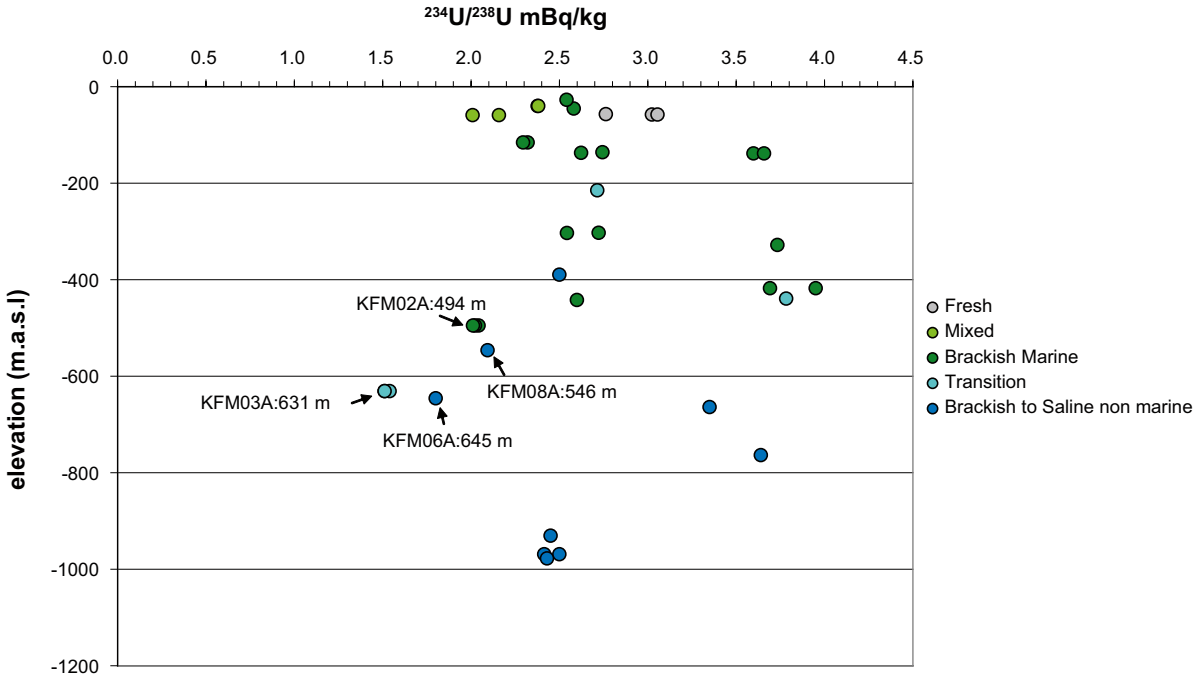

Figure 8-7. *$^{234}U/^{238}U$ activity ratio versus elevation.*

From the measured uranium contents and $^{234}U/^{238}U$ activity ratios available in the extended 2.3 data set for the different groundwater types, it can be concluded that:

- The highest uranium contents are associated with some of the brackish marine waters and appear to have accumulated in the transition zone between brackish marine and brackish non-marine waters (e.g. KFM03A:631 m).
- The brackish marine waters all have $^{234}U/^{238}U$ activity ratios much greater than that of Baltic Sea water (1.158 ± 0.008 at a salinity of 24‰ /Andersson et al. 1995/).
- There are several samples of brackish marine groundwater that show low uranium contents, so elevated uranium is not typical for this groundwater type.
- One of the brackish/saline non-marine waters, representing a depth of ~ 550 m in a possible deformation zone, showed a small increase in uranium content to 4–10 µg/L.
- All of the $^{234}U/^{238}U$ activity ratios are significantly greater than unity which theoretically can indicate an absence of rapid oxidative dissolution of uranium (which in such case would have resulted in activity ratios close to one). However, in a heterogeneous and complex system such as Forsmark, this may not be so clear cut as it is not possible to exclude the dissolution and contribution from a partly oxidised uranium mineral phase that could lower the activity ratios because of equal dissolution rates for both isotopes in the oxidised state.

8.4.2 USD on fracture coatings

Fracture coatings analysed for uranium series isotopes are all selected to represent open conductive fractures and are, with only a few exceptions, hosted in deformation zones; the results are shown in Table 8-2. However, it can never be assured that the actual sampled part of the fracture coating is in contact with the present-day flowing groundwater, for example, due to channelling. Furthermore, drilling (e.g. high flushing water under high pressures), subsequent handling of the drill cores (e.g. during mapping and routine testing for calcite in fracture coatings using HCl acid), perhaps intermediate storage in humid conditions, and ultimately sample preparation, always leads to a degree of uncertainty when interpreting uranium decay series data because of their potential sensitivity to such conditions. At present, there is no clear cut evidence that can ensure that one or several of such disturbances have not affected the samples to some degree.

Table 8-2. Thorium, uranium and uranium series data of fracture coating material.

Elevation (m.a.s.l.)	Sample	Th (ppm)	U (ppm)	^{238}U (Bq/kg)	± 1σ	^{234}U (Bq/kg)	± 1σ	^{230}Th (Bq/kg)	± 1σ	^{232}Th (Bq/kg)	± 1σ	^{234}U/^{238}U	± 1σ	^{230}Th/^{234}U	± 1σ
–25.00	KFM01B 28.65–28.70 m	14.1	15.8	201	2.3	319	3	331	6.7	66	2.1	1.59	0.022	1.04	0.023
–43.86	KFM01B 47.90–48.00 m	5.04	22.1	237	2.5	367	3.2	382	8.1	24.2	1.2	1.55	0.019	1.04	0.024
–401.27	KFM01B 418.29–418.43 m	5.31	7.21	72.0	0.68	70	0.67	80	1.6	3.2	0.18	0.97	0.013	1.14	0.025
–56.49	KFM03B 65.20–65.25 m	8.07	14.5	174	1.3	181	1.3	531	11	47	1.8	1.04	0.011	2.93	0.062
–633.14	KFM03 643.80–644.17 m	6.80	2,310	25,300	374	25,700	380	31,300	656	69	3.8	1.02	0.005	1.22	0.031
–792.25	KFM03A 803.85–804.05 m	1.30	3.32	134	1.2	129	1.2	173	3.5	26	0.9	0.96	0.012	1.34	0.03
–91.21	KFM05A 111.56–111.60 m	9.77	3.25	34.8	0.47	33	0.47	46.5	1	19	0.5	0.95	0.018	1.41	0.036
–122.29	KFM06A 145.62 m	2.06	17.8	169.8	1.6	333	2.3	275.1	4.6	112	5	1.96	0.02	0.83	0.01
–453.80	KFM06A 622.31 m	n.a.	n.a.	60.5	0.8	55	0.8	61.6	2.4	23.5	1.3	0.91	0.02	1.12	0.05
–644.95	KFM06A 770.32 m	14.7	12.8	241.9	1.9	239.1	1.9	268	5.5	926	24	0.99	0.01	1.12	0.02
–742.18	KFM07A 896.68 m	< 0.1	2.94	34.9	0.4	35.1	0.4	35	1.2	48.6	1.4	1	0.02	1	0.03
–795.00	KFM07A 968.68 m	n.a.	n.a.	350.3	2.7	354.4	2.7	364.1	6.5	151.6	32	1.01	0.01	1.03	0.02
–405.66	KFM08A 495.15 m	0.49	7.97	92.0	1.4	92	1.4	91	1.9	39	0.9	1	0.019	1	0.025
–548.81	KFM08A 686.67 m	< 0.1	164	1,450	24	1,844	27	1,778	38	22	2.3	1.27	0.025	0.96	0.025
–707.64	KFM08A 918.84 m	5.88	7.48	283	3.3	281	3.3	262	2.5	34	6.6	0.99	0.014	0.93	0.088
–29.84	KFM01C 43.0 m	10.2	10.8	83.0	1	111	1	125	2	60	1	1.33	0.02	1.12	0.02
–303.61	KFM06A 357.81 m	0.10	14.9	65.0	1	70	1	89	4	31	2	1.07	0.02	1.27	0.06
–568.89	KFM08C 683.57 m	2.27	2.61	78.0	1	101	1	118	6	55	4	1.29	0.02	1.16	0.06
–685.63	KFM08C 829.94 m	0.68	4.63	69.0	1	71	1	121	2	14	1	1.02	< 0.02	1.71	0.04
–744.06	KFM08C 904.06 m	1.44	11.8	109	1	116	1	117	4	21	2	1.07	0.02	1.01	0.04
–11.97	KFM09B 19.81 m	2.93	5.82	111	1	117	1	119	6	20	2	1.05	< 0.01	1.02	0.05
–75.53	KFM10A 105.79	24.5	24.5	355	2	450	2	450	9	16	1	1.27	0.01	1	0.02

However, if the disturbances would have had a major and consistent effect on uranium, this would have levelled out the original uranium series disequilibria and such different and versatile characteristics as obtained here would not have been observed.

Almost all samples collected from the upper 150 metres show disequilibria in one or both of the $^{234}U/^{238}U$ and $^{230}Th/^{234}U$ activity ratios when they are plotted against depth (Figure 8-8). Most of the samples show $^{234}U/^{238}U > 1$ in combination with $^{230}Th/^{234}U$ close to 1, indicating deposition of uranium during the past 1 Ma, or several processes (deposition and removal of uranium) overprinting each other. One sample indicates a possible late (post glacial) deposition of uranium (KFM06A 122 m) and two samples (KFM05A 91 m and KFM03B 56 m) indicate uranium removal possibly during the same period. One sample at only 20 metres depth sampled in an ENE trending deformation zone in KFM09B, shows activity ratios close to secular equilibrium indicating, most probably, that the sampled part of the fracture has not been conducting water during the last 1 Ma (i.e. an absence of water/rock interaction).

14 samples from greater depths (300 m and downwards) have been analysed and most of these show values closer to secular equilibrium than the near surface samples; six samples show secular equilibrium within ± 0.1 and these represent depths from 400 m to 745 m. Eight samples show $^{230}Th/^{234}U$ activity ratios between 1.1 and 1.7 and $^{234}U/^{238}U$ activity ratios close to secular equilibrium. Two samples below 300 m show $^{234}U/^{238}U$ activity ratios ~ 1.3 indicating possible uranium deposition. These samples are from KFM08A at ~ 550 m and KFM8C at ~ 570 m.

In Figure 8-9, the same activity ratios are plotted against uranium contents (^{238}U) showing that $^{230}Th/^{234}U$ is greater than one and indicating that leaching is possibly more common in samples with low uranium contents, up to 180 Bq/kg ^{238}U (i.e. ~ 15 ppm U). However, one exception is the fracture coating with the highest uranium content (2,310 ppm) which also shows $^{230}Th/^{234}U > 1$. $^{234}U/^{238}U$ activity ratios > 1 indicating uranium deposition are usually associated with uranium contents higher than 300 Bq/kg (i.e. ~ 25 ppm U) in the Forsmark samples.

Plots of the activity ratios $^{234}U/^{238}U$ and $^{230}Th/^{238}U$ are presented in a standard Thiels diagram in Figure 8-10 /cf Thiel et al. 1983/. This shows that samples from the upper 150 m (labelled red in the figure) plot either in the uranium deposition field or in (or close to) the uranium leaching sector. Samples from greater depths plot closer to secular equilibrium but a number of samples show increased $^{230}Th/^{238}U$ ratios but with the $^{234}U/^{238}U$ activity ratios close to one. This is interpreted as the result of a late and rapid single process of uranium mobilisation of (partly?) oxidised uranium present in some of the fractures. Two of the deep samples show, as mentioned above, deposition of uranium during the past 1 Ma (cf Figure 8-10).

8.5 Concluding remarks

Probable deposition of oxidised uranium at repository depth in some of the deformation zones at Forsmark has to be considered. Present studies of the uranium contents and uranium decay series isotopes in both groundwaters and fracture coatings, indicate that part of the uranium has been mobilised during the last 1 Ma, but the uranium enrichment in the fractures is generally older; for example uranium contents up to 30 ppm are detected in fractures showing uranium isotope secular equilibrium. Significant recent (postglacial) deposition of uranium should have yielded samples with $^{230}Th/^{238}U << 1$ which has not been observed in the studied fractures. However, one problem is that only bulk samples have been analysed and small portions of recent (postglacial) deposited U can not be distinguished accurately.

The elevated uranium contents commonly (but not always) associated with the Brackish-marine groundwaters, have remained dissolved and have not been deposited in the fractures.

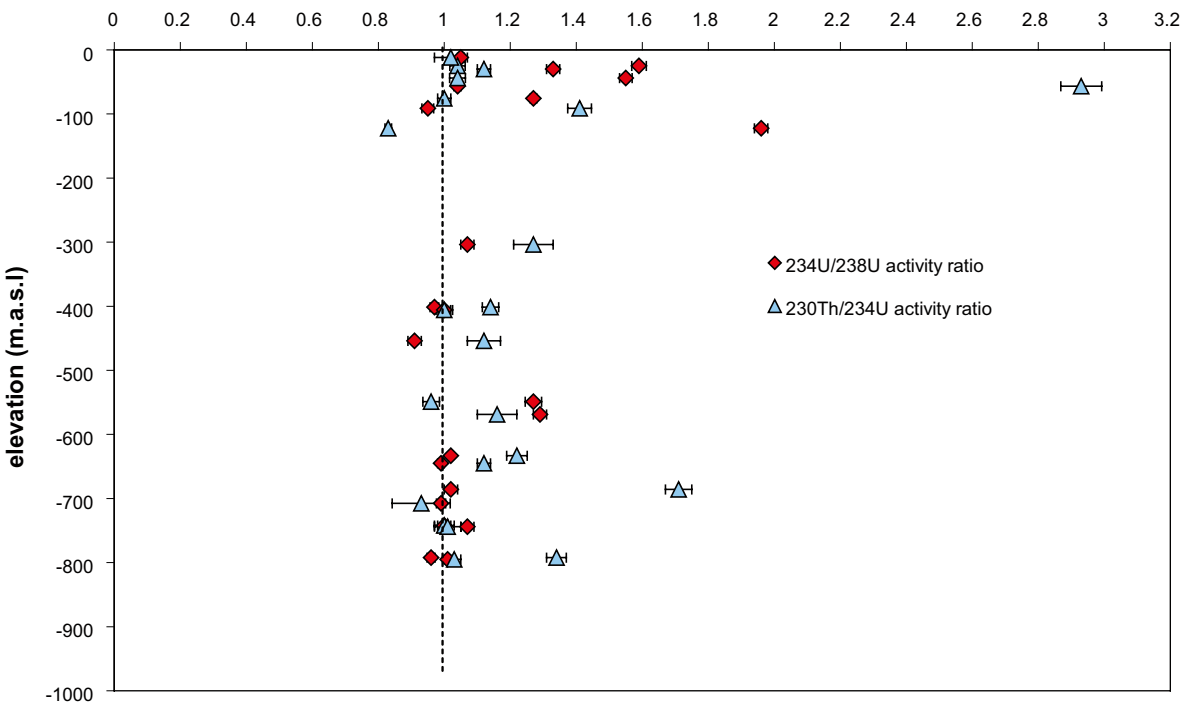

Figure 8-8. *Plots of fracture coating $^{234}U/^{238}U$ and $^{230}Th/^{234}U$ activity ratios versus elevation.*

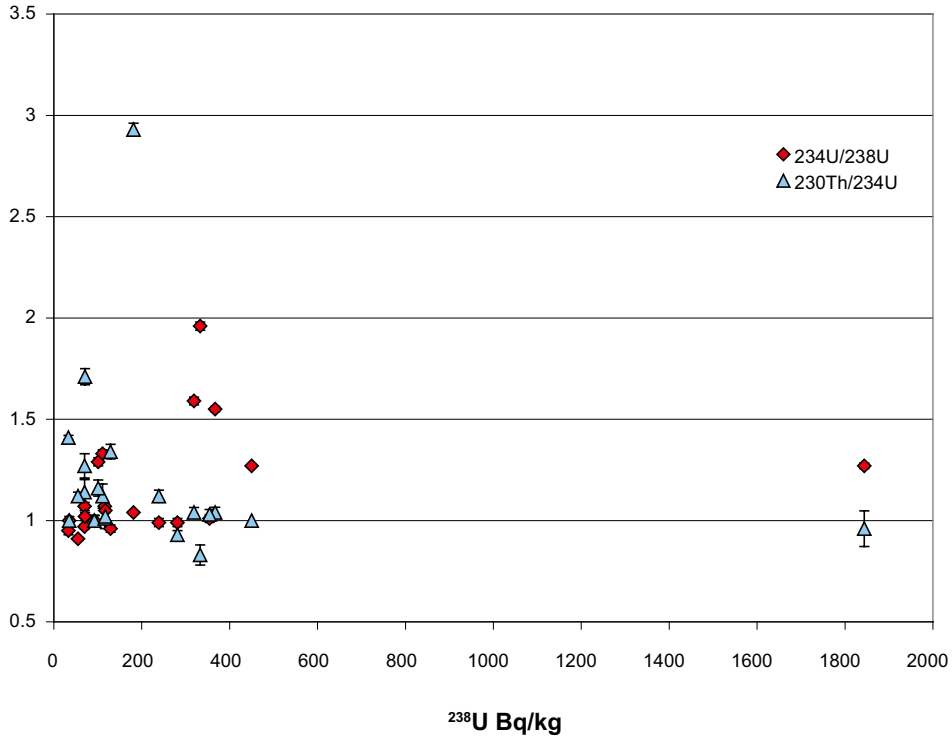

Figure 8-9. *Plots of fracture coating $^{234}U/^{238}U$ and $^{230}Th/^{234}U$ activity ratios versus ^{238}U activity (similar to U content). Note that sample KFM03A 643.8 m is not included in the plot because of a much higher uranium content in this sample (see comments in text).*

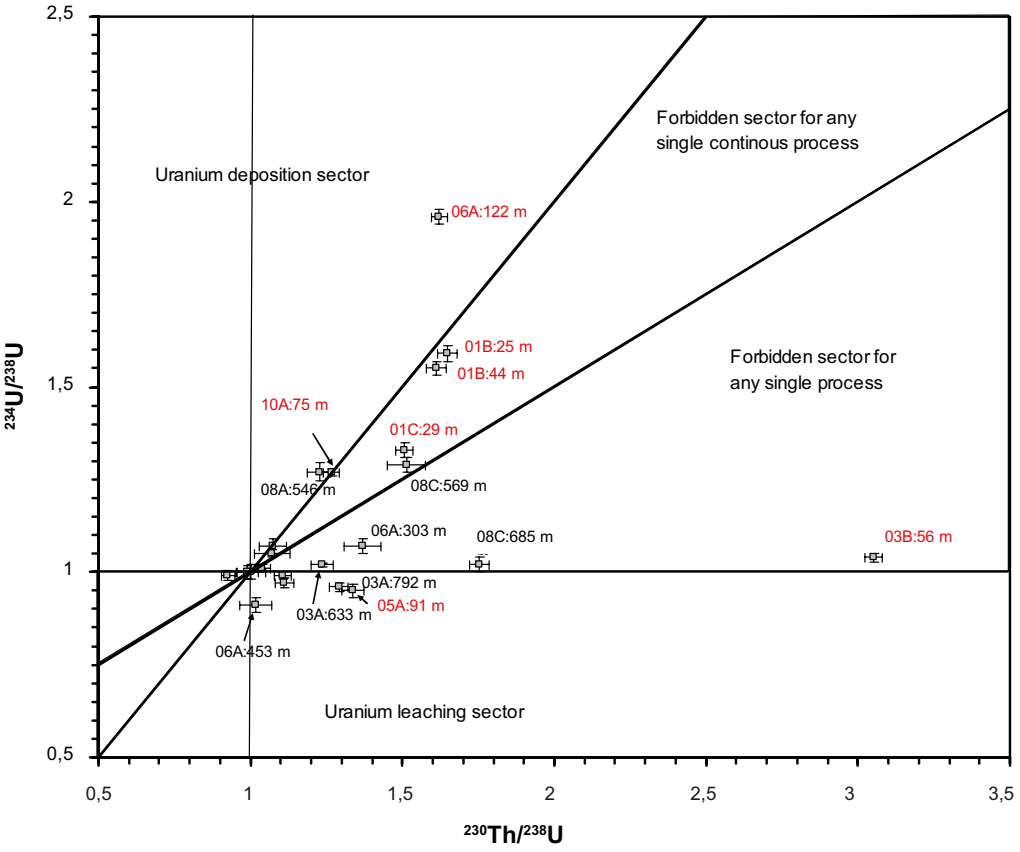

Figure 8-10. *$^{234}U/^{238}U$ activity ratio versus $^{230}Th/^{238}U$ activity ratio plot (Thiels diagram /cf Thiel et al. 1983/) for fracture coating samples from Forsmark. Samples showing disequilibrium (deposition or leaching of U) during the last 1 Ma are labelled. Samples from the upper transmissive 150 m of the bedrock are labelled in red. Sample names should all be preceded by KFM.*

The main conclusions are:

- Deformation zones in the upper transmissive 150 metres of the bedrock show more pronounced deposition and leaching of uranium compatible with a dynamic and heterogeneous groundwater flow system.
- The highest uranium contents in both fracture coatings and groundwaters are found in fractures (all belonging to deformation zones) at depths between 400 and 700 m. Not only fractures in the most common ESE-WNW orientated gently-dipping zones, but also steeply dipping zones orientated ENE and WNW are represented. It is important to note that at the same depth interval, low uranium contents are found in both fracture coatings and groundwater samples indicating a spot wise appearance of the uranium.
- The uranium present in groundwaters associated with fracture coatings is dominantly enriched in the oxidised U(VI) state. This may have been introduced into the sampling section (drilling source) or formed in situ by dissolution of a mainly U(VI)-bearing mineral phase(s). From the present understanding of the groundwater system at site, the latter explanation is favoured. The earlier indicated possible correspondence between drilling fluid and uranium content /SKB 2007/ is not supported in the F2.3 groundwater data set.
- The accumulation of oxidised uranium at around 500 m depth does not necessarily mean that oxygenated water has penetrated to this depth. Instead it is shown that that mildly reducing groundwaters with sufficient HCO_3^- (> 30 mg/L) are capable of keeping U(VI) mobile and this has resulted in variable accumulations occurring within the fracture zones to maximum depths of around 500 m depth.

- There is no evidence that colloid uptake has played a major role for the mobilisation and transport of the uranium /cf Hallbeck and Pedersen 2008/.
- Microbial activity (possibly enhanced by perturbation in connection with the drilling) may have increased the uranium mobility. It is e.g. known that siderophore producing bacteria may affect the mobilisation of radionuclides such as uranium /Johansson et al. 2006/ and such bacteria has been identified in borehole KFM08D /L. Hallbeck pers. comm. ongoing research/.
- Dissolved uranium has become concentrated where there is a transition from high to low transmissivity, corresponding to the present day transition from brackish marine (Littorina) to brackish non-marine groundwters.
- Generally, the deposition of uranium at depth below 150 m seems not to have occurred primarily during the last deglaciation or postglacial groundwater circulation, but partly (documented in five samples) related to groundwater activity during the last 1 Ma.

9 Redox conditions

9.1 Mössbauer analyses

Mössbauer analyses on fracture filling material from hydraulically conductive fractures and crushed zones have been carried out and the data have been presented in /Sandström and Tullborg 2005, Sandström et al. 2008/; the results are presented in Table 9-1.

The dominating silicates in the analysed samples are chlorite and/or clay minerals. The oxides in the samples are mainly hematite, although traces of magnetite and goethite (FeOOH) have also been found. The total oxidation factor ($Fe^{3+}/(Fe_{total})$) varies between 0.07 and 0.72 with a median value of 0.29 indicating that most Fe is present as reduced Fe^{2+} in the fracture filling material. The more oxidised samples (total oxidation factor > 0.4) are all found at depths shallower than 200 m (Figure 9-1), possibly indicating downward penetration of oxidised fluids during different periods in the past.

The silicate oxidation factor varies between 0.07 and 0.43 (median value 0.29). Due to small amounts of oxides present in the samples, oxide oxidation factors have only been obtained from two samples.

9.2 Concluding remarks

Different mineralogical and geochemical indicators of past and present redox conditions are presented in this report. Schematic figures of how some of these indicators are used to locate redox zone environments are presented in Figure 9-2 and Figure 9-3 /cf Tullborg et al. 2008/. A major problem encountered at the Forsmark site is that most of the drill cores do not start at the bedrock surface (no data are available from the upper five metres). The amount of data from the uppermost part of the bedrock is therefore insufficient (cf section 6.2). Furthermore, the uppermost hundred metres of the bedrock at Forsmark is characterised by sub-horizontal to gently dipping highly transmissive deformation zones, which creates a strong horizontal component in the groundwater flow and therefore the downward propagation of a typical vertical redox front is not likely under present conditions. However, if an individual gently dipping fracture zones could be sufficiently sampled, a redox front could probably be detected.

Table 9-1. Results from Mössbauer analyses of bulk fracture filling material. tr = trace amounts Oxidation factor = Fe^{3+}/Fe_{total}.

Sample (Secup)	Elevation (m.a.s.l.)	Fe minerals	Silicate oxidation factor	Oxide oxidation factor	Total oxidation factor
KFM02A 118.25 m	–117.80	chlorite, tr. hematite	0.33	1	0.35
KFM02A 903.65 m	–872.86	chlorite, tr. magnetite	0.28		
KFM03A 451.85 m	–450.76	chlorite, epidote, tr magnetite	0.30		
KFM03A 803.85 m	–801.92	chlorite, tr FeOOH	0.12		
KFM04A 192.00 m	–166.28	chlorite, epidote, hematite	0.42	1	0.67
KFM01C 12.43 m	–9.47	chlorite	0.37		0.37
KFM01C 39.75 m	–30.27	chlorite, hematite, tr. magnetite	0.43		0.57
KFM01C 41.15 m	–31.34	chlorite, hematite	0.37		0.72
KFM08C 683.57 m	–591.99	chlorite	0.15		0.15
KFM08C 829.94 m	–718.75	chlorite. tr. magnetite	0.21		0.27
KFM08C 904.06	–782.94	chlorite	0.07		0.07
KFM09B 121.56 m	–105.27	chlorite	0.12		0.12
KFM10A 105.79 m	–81.02	chlorite, epidote	0.29		0.29

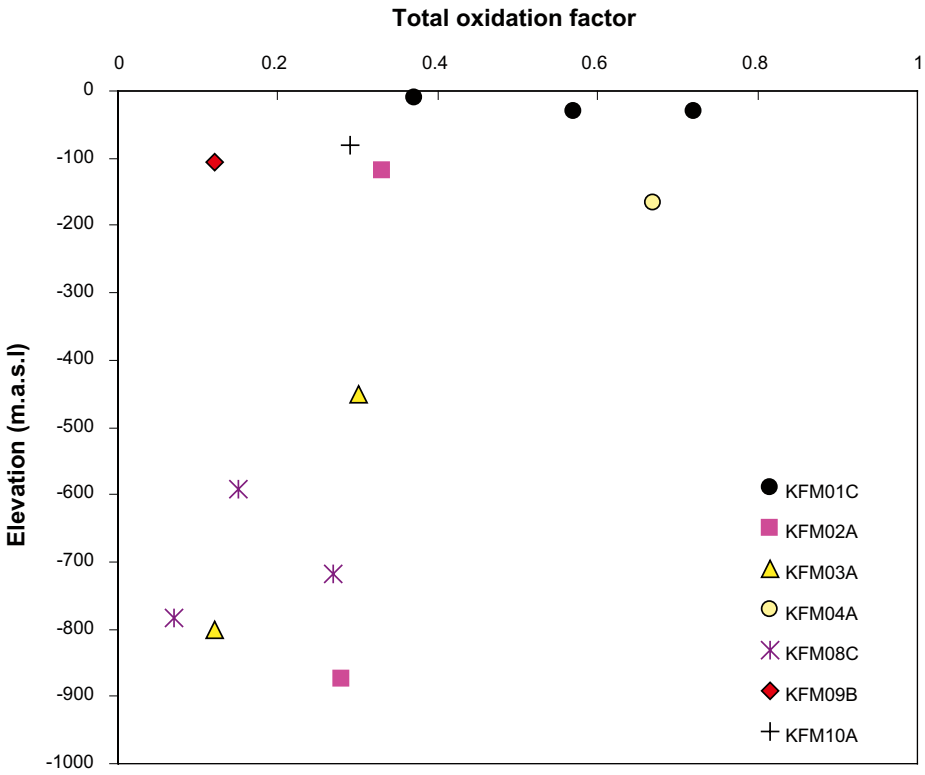

Figure 9-1. *Total oxidation factor ($Fe^{3+}/(Fe_{total})$) of bulk fracture filling material. Where the total oxidation factor has not been possible to determine due to small amount of oxides, the silicate oxidation factor has been used in the plot.*

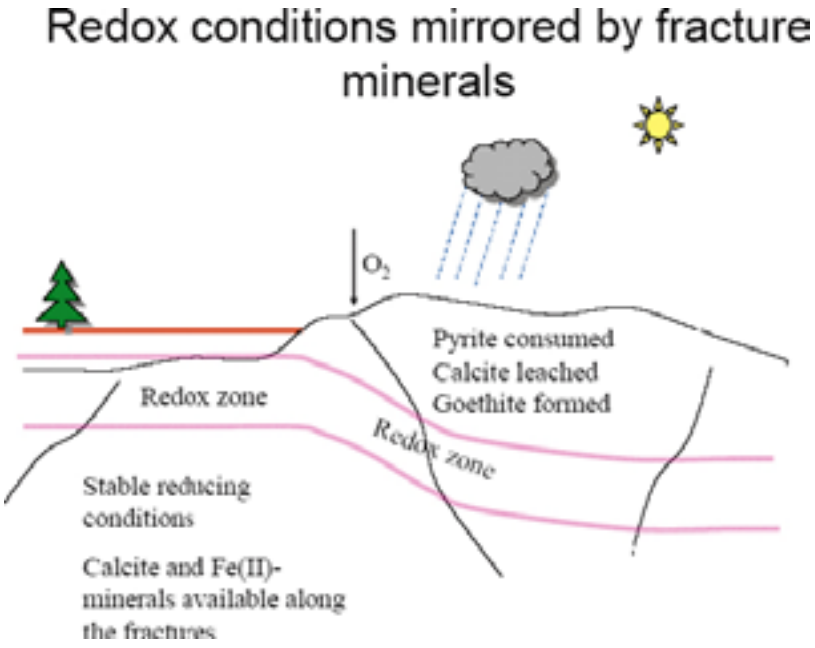

Figure 9-2. *Schematic figure of variations in fracture mineralogy used to locate the position of potential redox zones. The figure is based on indicators summarised in /Tullborg et al. 2008/.*

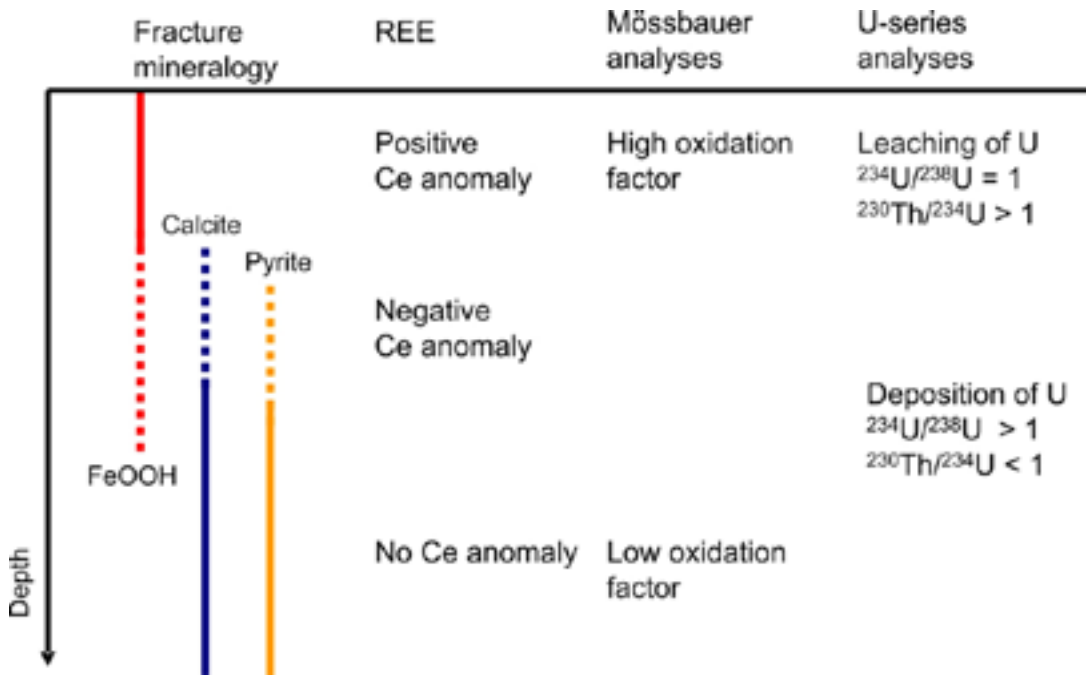

Figure 9-3. *Schematic depth profile with some of the indicators used for identifying potential redox zones. FeOOH = goethite. The figure is based on indicators summarised in /Tullborg et al. 2008/.*

However, based on a combination of different redox indicators, the following conclusions of the redox conditions can be made:

- During the two Proterozoic events of fracture mineralisation (generation 1 and 2), the presence of oxidised Fe^{3+} in hematite associated with these fracture mineral parageneses, together with a number of Ce-anomalies in fracture coatings of these generations, generally support oxidising conditions. On the other hand, chlorite with a significant Fe^{2+} content is also part of the generation 1 and 2 parageneses, suggesting variable redox conditions, both temporally and spatially. These two generations represent hydrothermal conditions, which in this case mean temperatures higher than 150°C. Related to these two fracture generations are also hydrothermal alteration/oxidation of the wall rock adjacent to the fractures. This alteration extends a few centimetres into the wall rock adjacent to discrete fractures but results in more extensive alteration zones within deformation zones. The major mineralogical changes in these altered rims are almost complete saussuritisation of plagioclase, chloritisation of biotite and to some extent hematisation of magnetite. The overall increase in $Fe^{3+}/Fe(tot)$ is small (~ 10%).
- Generation 3 (Palaeozoic) is characterised by reducing conditions as indicated by pyrite precipitation and also supported by the organic influence associated with this period of mineralisation. Well preserved pyrite crystals of Palaeozoic origin suggest that the reducing conditions have prevailed in large parts of the fracture system since this period.
- The presence of goethite (FeOOH) in some hydraulically conductive fractures and deformation zones (mainly in the gently dipping zone ZFMA2) in the upper part of the bedrock, indicate circulation of oxidising fluids during some period. This is also supported by the high oxidation factor (Mössbauer analyses) seen in a few superficial samples. However, the presence of pyrite in the same structural zones does suggest that the redox conditions have been complex. It is plausible that the circulation of oxidising fluids has been concentrated along channels within the uppermost fractures and zones and different redox micro-environments may therefore have been formed.
- The detected Ce anomalies in many samples are difficult to evaluate since most are found in fracture coatings composed of hydrothermal minerals (generation 1 and 2), and thus reveal no information about present redox conditions in the fracture/groundwater system.

- No significant decrease in the frequency of calcite coated fractures in the uppermost part of the bedrock can be seen in the Boremap data. This indicates that major events of groundwater penetration, unsaturated in respect of calcite (e.g. very diluted waters with low pH), have not occurred. Although calcite, *senso stricto*, is not a redox sensitive mineral, a close relation between the redox front and dissolution of calcite has been shown in fractures in similar crystalline bedrock in Sweden due to the often higher acidity of penetrating oxidised waters /Tullborg 1989/. Thus, calcite is here used as a secondary indicator of the redox front. However, no boremap data are availble from the uppermost five metres and it can not be excluded that a narrow surface related zone of oxidation of pyrite and dissolution of calcite is present there.
- Uranium-rich phases are present in some of the fracture coatings although, to date, only one small grain of pitchblende has been identified. The origin of these phases is largely unknown but it can be concluded that uranium has been circulating throughout the geological history of the site. For example, some of the pegmatites show slightly enriched uranium values (a maximum value of 62 ppm is indicated by gamma spectrometric data /Stephens et al. 2007/). Even more importantly, there is evidence of redistribution and deposition of uranium irregularly along permeable structures during the Proterozoic /cf Welin, 1964/. Moreover, during the Palaeozoic, potentially U-rich alum shales covered the area and these may have made a contribution of uranium to the system. Of special interest for understanding the present groundwater/mineral systems is the potentially late (Quaternary) redistribution of uranium. The use of U-series decay isotope analyses (USD) on groundwaters and fracture coatings concluded that part of this uranium has been mobile during the last 1 Ma. Mobilisation, as well as redeposition, of uranium in the upper part of the bedrock (150 m) is indicated. This is ascribed to the transition from near-surface oxidising conditions to more stable reducing conditions at depth. However, some of the deeper samples show similar behaviour which may be explained by the presence of an easily dissolvable and partly oxidised uranium-phase (possibly altered pitchblende). Mobilisation and redeposition of this phase does not mean that oxygenated water has penetrated to this depth. Instead, it suggests that mildly reducing groundwaters with sufficient HCO3 (> 30 mg/L) are capable of keeping U(VI) mobile, resulting in variable accumulations occurring within the fracture zones to maximum depths of around 600 m /Laaksoharju et al. 2008/.
- Any potential build up of reducing capacity in the fracture minerals during recent periods of reducing groundwater conditions is difficult to estimate. Processes that may contribute to an increase in the redox capacity include the production of Fe^{2+} and Mn^{2+} that may either precipitate (e.g. coprecipitation in calcite) or be sorbed on mineral surfaces due to ion exchange. In addtition, iron sulphides may be formed due to bacterial activity of sulphate reducers. However, it can be concluded that the amounts of recent (Quaternary) minerals formed is very small.

10 Summary

Mapping of fractures and fracture minerals has been carried out on all drill cores from Forsmark as part of the site investigation programme. The obtained data set has served as a basis for further and more detailed fracture mineralogical studies, which have been carried out during the past 4 years and are reported in eight P-reports (cf Table 1-1). The main results and conclusions achieved are compiled in the present report.

Chlorite (usually associated with corrensite) together with calcite are by far the most common fracture minerals. The relative abundance of additional fracture minerals is as follows; laumontite > quartz, adularia, albite, clay minerals > prehnite, epidote > hematite and pyrite. Some minerals may be more common in specific intervals or at shallow depths (e.g. asphaltite, analcime and goethite). Other identified minerals (e.g. apophyllite, fluorite, galena) have only been found as minor occurrences. The most common clay minerals are corrensite > illite > mixed layer clays > smectite > kaolinite, vermiculite and other swelling clays. No carbonates other than calcite have been identified and no sulphate-minerals have been detected except for barite which only occurs in very small amounts (e.g. as inclusions in galena). Pyrite makes up more than 99% of the identified sulphides, but galena, chalcopyrite and sphalerite have also been identified. The confidence is high that all major fracture mineral phases within the Forsmark site have been identified.

A relative sequence of fracture mineralisations has been distinguished providing input to the conceptual geological evolution in the area. Radiometric dating (especially the $^{40}Ar/^{39}Ar$ method) provide geochronological constraints on the sequence of mineralisation. Four generations of fracture mineralisation have been distinguished and are presented below with decreasing age:

Generation 1 consists of epidote, quartz and chlorite; brittle-ductile cataclasite is sealed with these minerals (T > 200°C). They are conspicuous in subhorizontal and gently dipping fractures or in steep, WNW-ESE to NW-SE fractures. However, they are also present along fractures in other steeply dipping sets. Generation 1 formed between 1.8 and 1.1 Ga and is possibly related to the late Svecokarelian and/or Gothian tectonothermal events.

Generation 2 consists of a sequence of hydrothermal fracture minerals (T ~ 150–280°C) dominated by adularia, albite, prehnite, laumontite, calcite, chlorite and hematite. Generation 2 minerals are particularly common along steep, ENE-WSW to NNE-SSW and NNW-SSE fractures. $^{40}Ar/^{39}Ar$ ages from adularia indicate that this mineral probably formed, or the isotope system was reset, in connection with early Sveconorwegian tectonothermal activity 1.1 to 1.0 Ga ago. Both reactivation of older fractures and formation of new fractures and breccias are inferred during this period.

Associated with generation 1 and 2 fracture minerals is a red-staining (oxidising) of the wall rock rock due to hydrothermal alteration. Only minor changes in whole rock geochemistry and degree of oxidation have occurred in the altered rock; mainly enrichment of Na_2O and LOI (Loss On Ignition) and depletion of CaO, SiO_2 and FeO. However, on the micro-scale, elemental redistribution is much more extensive, especially among the trace elements, with both *intra-grain* and *inter-grain* migration of elements including Ca, K, Na, Al, Si, Fe, Ba, Cs, Rb, Sr, Ti and REEs. The main mineral reactions associated with the elemental redistribution are an almost complete saussuritisation of plagioclase accompanied by total chloritisation of biotite. Magnetite has been partly replaced by hematite whereas quartz and K-feldspar were relatively unaffected during the hydrothermal alteration. The degree of oxidation is somewhat higher in the altered rock but most Fe is still present as Fe^{2+}.

Dissolution of fracture minerals occurred before the formation of generation 3 minerals.

Generation 3 consists of minerals precipitated under low to moderate temperature conditions (60–190°C). Precipitaton occurred at several events intermittently during the Palaeozoic. The most abundant minerals are calcite, quartz, pyrite, corrensite and asphaltite. Stable isotopes in calcite and the presence of asphaltite indicate that the formation fluid was influenced by organic material, which probably emanated from an overlying sedimentary cover. The orientation of fractures characterised by generation 3 minerals suggests reactivation of older fractures (with generation 1 and 2 minerals). However, formation of new fractures is also indicated by the presence generation 3 minerals in fractures without the wall rock alteration (red-staining) associated with generation 1 and 2 minerals.

Generation 4 is dominated by chlorite/clay minerals and thin precipitates of calcite in predominantly hydraulically conductive fractures and fracture zones. These minerals are prominent along sub-horizontal and gently dipping fractures, but also in different sets of steeply dipping fractures. It is important to keep in mind that the differentiation of generation 3 and generation 4 minerals can be difficult since many fractures carry minerals from both generations. It is inferred that the hydraulically conductive fractures are ancient structures (Proterozoic to Palaeozoic) and that precipitation of generation 4 minerals most likely occurred during a long period of time (after the Palaeozoic). However, some of the near-surface, sub-horizontal to gently dipping fractures, which include sheet joints formed in connection with stress release, may be Quaternary in age. Fractures without any visible minerals (mapped as "no mineral" during the drill core mapping) are also interpreted to belong to generation 4, although the origin of these fractures are unclear. Generation 4 is not as well constrained in time as generation 2 and 3 because it has not been possible to date any suitable mineral phase from this generation. The amount of precipitation of fracture minerals at present is low and mostly concentrated to the upper 200 m.

The observations that many fractures are reactivated and that most of the transmissive fractures have been water conductive during a very long period of time and during several groundwater regimes indicates that a high degree of stability exist in the fracture systems at Forsmark, i.e. newly formed transmissive fractures are rare. However, the existence of transmissive fractures without mineral coatings (which are potentially young) needs to be further studied.

The long time gap between precipitation of generation 2 and 3 minerals (> 500 Ma) may be explained by the fact that during this period, exhumation and peneplanation prevailed in the region. The present surface was exhumated during the late Neoproterozoic and thus low temperature conditions similar to the present prevailed and therefore, the amount of fracture mineral precipitation is expected to have been similarly low as at the present.

The isotopic and chemical composition of calcite has been given special attention due to the potential use of this mineral in providing information related to the palaeohydrogeological evolution of the Forsmark region. All fracture mineral generations except for generation 1 contain calcite. Three different types associated with generation 2, 3 and 4 respectively have been distinguished: a) hydrothermal calcite (generation 2), b) warm-brine type calcite precipitated from a fluid influenced by organic material (generation 3), and c) low temperature calcite precipitated from different groundwaters (meteoric and marine and brackish marine) at temperatures close to present ambient conditions (generation 4). Calcites of the last type occur only in small amounts and mostly in the upper 200 m of the bedrock.

SEM (Scanning Electron Microscope) studies of calcite have not shown any signs of recent dissolution (below 100 m) in agreement with mass balance calculations showing that the groundwaters are generally saturated in respect of calcite /Laaksoharju et al. 2008/. The calcites contain small amounts of FeO, MgO and MnO (< 1 wt%), the Sr content is below 300 ppm and both U and Th occur in concentrations below 0.2 ppm. Given the $^{87}Sr/^{86}Sr$ differences between most of the analysed calcites and the groundwater it is evident that only very small amounts of the fracture calcite are recent (i.e. Quaternary).

Chemical analyses have been carried out on fracture mineral samples using both SEM and ICP-MS/AES analyses. The ICP analyses largely confirm the mineralogy determined from the

drillcore mapping, XRD and microscopy, but have also provided useful information on the behaviour of trace elements (e.g. Cs and U), both of which show enrichment in the fracture coatings compared with the host rock.

For modelling purposes, the Forsmark area has been divided into different fracture domains, defined as parts of a rock mass that exhibits similar fracture patterns and intensity /Olofsson et al. 2007/. With the exception of asphaltite and goethite, which almost exclusively are found in open fractures within fracture domain FFM02 (and probably FFM03), the same fracture mineralogy is found in fracture domains FFM01, FFM02, FFM03 and FFM06, although the proportion of the different minerals may vary. Minerals such as chlorite show little to no variation with depth. Clay minerals are found more abundantly in fractures in the upper part of the bedrock but also at greater depths. The calcite ± quartz ± pyrite assemblage is most common in the upper 350 m of the bedrock, but occurs also abundantly at greater depths. The dominant fracture mineral assemblages in hydraulically conductive fractures are chlorite + calcite (± other minor phases) and calcite ± quartz ± pyrite. These fractures are predominantly sub-horizontal to gently dipping.

No distinct redox front has been identified in the bedrock at Forsmark, for example, no signs of pyrite dissolution have been detected in the upper 100 m of the bedrock. However, the presence of goethite in hydraulically conductive fracture zones suggests channelled flows of oxygenated water. The absence of an obvious redox front in the bedrock is partly due to: a) The present redox front is located in the Quaternary cover, and b) any earlier developed redox front may now have been overprinted by later reducing conditions. Furthermore, the uppermost hundred metres of the bedrock at Forsmark is characterised by sub-horizontal to gently dipping highly transmissive fracture zones which create a strong horizontal component in the groundwater flow, and therefore the downward propagation of a typical vertical redox front is not likely under present conditions. However, if an individual gently dipping fracture zone could be sufficiently sampled, a redox front could probably be detected. During certain periods, for example, with a thin or absent Quaternary cover, oxidising groundwaters may have penetrated via the highly transmissive channels in the gently dipping to sub-horizontal deformation zones to at least a depth of 200 m. The preservation of generation 3 pyrite and asphaltite (organic matter) in the fracture system indicate stable reducing conditions although locally, oxidising conditions can have prevailed.

The majority of the hematite present in the fracture systems is Proterozoic (mostly generation 2) and this hematite has survived long periods of reducing conditions as exemplified by e.g. occurrences of Palaeozoic pyrite precipitated on older hematite coatings.

No significant decrease in the frequency of calcite coated fractures in the uppermost part of the bedrock can be seen in the Boremap data indicating that major penetration events of groundwater unsaturated with respect to calcite (e.g. very diluted waters with low pH) have not occurred. However, Boremap data are lacking from the uppermost five metres.

Uranium-rich phases are present in some of the fracture coatings although to date only one small grain of pitchblende has been identified. It has not been possible to relate these coatings with any fracture mineral generation. The origin of these phases is largely unknown but it can be concluded that uranium has been circulating throughout the geological history of the site. For example, some of the pegmatites show slightly enriched uranium values (A maximum value of 62 ppm is indicated by gamma spectrometric data /Stephens et al. 2007/). Even more importantly, there is evidence of redistribution and deposition of uranium irregularly along permeable structures during the Proterozoic /cf Welin 1964/. Moreover, during the Palaeozoic, potentially U-rich alum shales covered the area and these may have made a contribution of uranium to the system. Uranium mobility during the last 1 Ma is documented by the use of uranium-series isotope analyses on fracture coatings and groundwaters. These analyses indicate mobilisation as well as redeposition of uranium in the upper part of the bedrock (150 m), which is ascribed to the transition from near-surface oxidising conditions to more stable reducing conditions at depth. However, at Forsmark, some of the deeper samples show also mobilisation/redeposition of uranium. This may be explained by the interaction with a dissolvable and partly oxidised uranium phase that is present in parts of the fracture system.

Acknowledgements

We would like to thank Michael Stephens (SGU), Assen Simeonov (SKB) and Ann-Chatrin Nilsson (Geosigma AB) for support and constructive discussions during the work with the detailed fracture mineralogy in Forsmark. The drill core mapping geologists at the Forsmark site Jesper Petersson, Anders Wängnerud, Göran Skogsmo, Johan Berglund (Vattenfall Power Consultant AB), Christin Döse and Eva Samuelsson (Geosigma AB), are thanked for their important input and assistance during sampling. Johan Öhman and Ola Forssberg (Golder Associates) are thanked for producing the stereographic projections and Martin Stigsson (SKB) for help with the figures of fracture mineral vs. depth. Seppo Gehör (University of Oulu) is thanked for his assistance during the fluid inclusion studies. Owe Gustavsson (University of Gothenburg) is acknowledged for carrying out stable C and O isotopes analyses on calcite. Sven Åke Larson (University of Gothenburg) is thanked for comments on the manuscript and Henrik Drake (University of Gothenburg) for fruitful discussions regarding the fracture mineralogy at the Laxemar/Simpevarp areas. Review comments by Russel Alexander (Bedrock Geosciences), Zell E. Peterman (USGS) and Michael Stephens (SGU) greatly improved the report.

References

Andersson P S, Wasserburg G J, Chen J H, Papanastassiou D A, Ingri J, 1995. ^{238}U–^{234}U and ^{232}Th–^{230}Th in the Baltic Sea and in river water. Earth and Planetary Science Letters 130, 217–234.

Bergelin A, Lindqvist A, Nilsson K, Wacker P, Nilsson A-C, 2007. Forsmark site investigation. Hydrochemical characterisation in borehole KFM08D. Results from two investigated borehole sections at 669.7–676.8 m and 828.4–835.5 m. SKB P-07-190. Svensk Kärnbränslehantering AB.

Bingen B, Skår O, Marker M, Sigmond E M O, Nordgulen O, Ragnhildstveit J, Mansfeld J, Tucker R D, Liégeois J-P, 2005. Timing of continental building in the Sveconorwegian orogen, SW Scandinavia. Norwegian Journal of Geology 85, 87–116.

Bird D K, Spieler A R, 2004. Epidote in geothermal systems. Reviews in Mineralogy and Geochemistry 56, 235–300.

Bird D K, Schiffman P, Elders W A, Williams A E, McDowell S D, 1984. Calc-silicate mineralisation in active geothermal systems. Economic Geology 79, 671–695.

Blyth A, Frape S, Blomqvist R, Nissinen P, 2000. Assessing the past thermal and chemical history of fluids in crystalline rock by combining fluid inclusion and isotopic investigations of fracture calcite. Applied Geochemistry 15, 1417–1437.

Budai J M, Martini A M, Walter L M, Ku T C W, 2002. Fracture-fill calcite as a record of microbial methanogenesis and fluid migration; a case study from the Devonian Antrim Shale, Michigan Basin. Geofluids 2, 163–183.

Byegård J, Selnert E, Tullborg E-L, 2008. Site descriptive modelling of transport properties. Retardation model Forsmark 2.3. SKB R-08-XX. Svensk Kärnbränslehantering AB.

Chacko T, Cole D R, Horita J, 2001. Equilibrium oxygen, hydrogen and carbon isotope fractionation factors applicable to geological systems. Reviews in Mineralogy and Geochemistry 43, 1–81.

Curti E, 1999. Coprecipitation of radionuclides with calcite; estimation of partition coefficients based on a review of laboratory investigations and geochemical data. Applied Geochemistry 14, 433–445.

de Albuquerque C A R, 1975. Partition of trace elements in co-existing biotite, muscovite and potassium feldspar of granitic rocks, northern Portugal. Chemical Geology 16, 89–108.

Deer W A, Howie R A, Zussman J, 1992. An introduction to the rock forming minerals. 2nd ed. Pearson Education Limited, Harlow, England.

Drake H, Tullborg E-L, 2004. Oskarshamn site investigation. Fracture mineralogy and wall rock alteration, results from drill core KSH01A+B. SKB P-04-250. Svensk Kärnbränslehantering AB, Stockholm, Sweden.

Drever J I, 1997. The geochemistry of natural waters: surface and groundwater environments. Prentice Hall. Upper Saddle River, N.J. 436 pp.

Evansen N M, Hamilton P J, O'Nions R K, 1978. Rare Earth Abundances in Chondritic Meteorites. Geochimica et Cosmochimica Acta 42, 1199–1212.

Faure G, Mensing T M, 2004. Isotopes: Principles and Applications. 3rd edition. John Wiley and Sons. Hoboken, New Jersey.

Follin S, Levén J, Hartley L, Jackson P, Joyce S, Roberts D, Swift B, 2007. Hydrogeological characterisation and modelling of deformation zones and fracture domains, Forsmark modelling stage 2.2. SKB R-07-48. Svensk Kärnbränslehantering AB.

Forsman I, Zetterlund M, Rhén I, 2004. Correlation of Posiva Flow Log anomalies to core mapped features in Forsmark (KFM01A to KFM05A). SKB R-04-77. Svensk Kärnbränslehantering AB.

Fox A, La Pointe P, Hermanson J, Öhman J, 2007. Statistical geological discrete fracture network model. Forsmark modelling stage 2.2. SKB R-07-46. Svensk Kärnbränslehantering AB.

Frey M, De Capitani C, Liou J G, 1991. A new petrogenetic grid for low-grade metabasites. Journal of Metamorphic Geology 9, 497–509.

Gimeno M J, Auqué L F, Gómez J B, Acero P, 2008. Water-rock interaction modelling and uncertainties of mixing modelling. SKB R-08-86. Svensk Kärnbränslehantering AB.

Gleeson S A, Yardley, B W D, Munz I A, Boyce A J, 2003. Infiltration of basinal fluids into high-grade basement, south Norway: Sources and behaviour of waters and brines. Geofluids 3, 33–48.

Graffner O, 2000. Mapping of fractures in crystalline rock using BIPS and borehole radar. In: G Knutsson (ed). Hardrock hydrogeology of the Fennoscandian Shield. Proc. of the Workshop on Hardrock Hydrogeology, Äspö, Sweden, May 26–27, 1998, NHP Report No. 45, 2000, pp. 13–20, KTH, Stockholm, Sweden.

Hallbeck L, Pedersen K, 2008. Explorative analysis of microbes, colloids and gases. SKB R-08-85. Svensk Kärnbränslehantering AB.

Hermansson T, Stephens M B, Corfu F, Andersson J, Page L, 2007. Penetrative ductile deformation and amphibolite-facies metamorphism prior to 1851 in the western part of the Svecofennian orogen, Fennoscandian Shield. Precambrian Research 153, 29–45.

Hermansson J, Stephens M B, Corfu F, Page L, Andersson J, 2008. Migratory tectonic switching, western Svecofennian orogen, central Sweden – Constraints from U/Pb zircon and titanite geochronology. Precambrian Research 161, 250–278.

Hoefs J, 2004. Stable isotope geochemistry. Springer-Verlag. Berlin. 244 pp.

Hunt J M, 1990. Generation and migration of petroleum from abnormally pressured fluid compartments. AAPG Bulletin 74, 1–12.

Kelley S, 2002. Excess argon in K-Ar and Ar-Ar geochronology. Chemical Geology 188, 1–22.

King R J, 2001. Analcime. Geology Today 17, 236–239.

Johnsson A, Arlinger J, Pedersen K, Ödegaard-Jensen A, Albinsson Y, 2006. Solid-Aqueous Phase Partitioning of Radionuclides by Complexing Compounds Excreted by Subsurface Bacteria. Geomicrobiology Journal 23, 621–630.

Laaksoharju M, Smellie J, Tullborg E-L, Gimeno M, Hallbeck L, Molinero J, Waber N, 2008. Bedrock hydrogeochemistry Forsmark. Site descriptive modelling. SDM-Site Forsmark. SKB R-08-47. Svensk Kärnbränslehantering AB.

Landström O, Tullborg E-L, 1995. Interaction of trace elements with fracture filling minerals from the Äspö Hard Rock Laboratory. SKB TR 95-13. Svensk Kärnbränslehantering AB.

Larson S Å, Tullborg E L, Cederbom C, Stiberg J P, 1999. Sveconorwegian and Caledonian foreland basins in the Baltic Shield revealed by fission-track thermochronology. Terra Nova 11, 210–215.

Liou J G, 1971. Analcime equilibria. Lithos 4, 389–402.

Liou J G, Kim H S, Maruyama S, 1983. Prehnite – epidote equilibria and their petrologic applications. Journal of Petrology 24, 321–342.

Liou J G, Maruyama S, Cho M, 1985. Phase equilibria and mineral paragenesis of metabasites in low-grade metamorphism. Mineralogical Magazine 49, 321–333.

Milodowski A E, Fortey N J, Gillespie M R, Pearce J M, Hyslop E K, 2002. Synthesis report on the mineralogical characteristics of fractures from the Nirex boreholes in the Sellafield area. British Geological Survey, Technical Report WG/98/8.

Milodowski A E, Tullborg, E-L, Buil B, Gômez P, Turrero M-J, Haszeldine S, England G, Gillespie M R, Torres T, Ortiz J E, Zacharias J, Silar J, Chvátal M, Strnad L, Šebek O, Bouch J E, Chenery S R, Chenery C, Shepherd T J, McKervey J A, 2005. Application of mineralogical petrological and geochemical tools for evaluating the palaeohydrogeological evolution of the PADAMOT Study sites. PADAMOT PROJECT Technical Report WP2. EU FP5 Contract nr FIKW-CT2001-20129.

Morse J W, Bender M L, 1990. Partition coefficients in calcite; examination of factors influencing the validity of experimental results and their application to natural systems. Chemical Geology 82, 265–277.

Möller P, Morteani G, 1983. On the geochemical fractionation of rare earth elements during the formation of Ca-minerals and its application to the problems of the genesis of ore deposits. In S S Augustithis (ed). The significance of trace elements in solving petrogenic problems and controversies. Theophrastus Publications S.A. Athens. 747–791.

Möller C, Snäll S, Stephens M B, 2003. Forsmark site investigation. Dissolution of quartz, vug formation and new grain growth associated with post-metamorphic hydrothermal alteration in KFM02A. SKB P-03-77. Svensk Kärnbränslehantering AB.

Nilsson K, Bergelin A, Lindquist A, Nilsson A-C, 2006. Forsmark site investigation. Hydrochemical characterisation in borehole KFM01D. Results from seven investigated borehole sections: 194.0–195.0 m, 263.8–264.8 m, 314.5–319.5 m, 354.9–355.9 m, 369.0–370.0 m, 428.5–435.6 m, 568.0–575.1 m. SKB P-06-227. Svensk Kärnbränslehantering AB.

Olofsson I, Simeonov A, Stephens M, Follin S, Nilsson,A-C, Röshoff K, Lindberg U, Lanaro, F, Fredriksson A, Persson L, 2007. Site descriptive modelling Forsmark, stage 2.2. A fracture domain concept as a basis for the statistical modelling of fractures and minor deformation zones, and interdisciplinary coordination. SKB R-07-15.
Svensk Kärnbränslehantering AB.

O'Neil J R,Clayton R N,Mayeda T K, 1969. Oxygen isotope fractionation in divalent metal carbonates. Journal of Chemistry and Physics 51, 5547–5558

Pedersen K, Ekendahl S, Tullborg E-L, Furnes H, Thorseth I, Tumyr O, 1997. Evidence of ancient life at 207 m depth in a granitic aquifer. Geology 25, 827–830.

Peterman Z E, Wallin, B, 1999. Synopsis of strontium isotope variations in groundwater at Äspö, southern Sweden. Applied Geochemistry 14. 939–952.

Petersson J, Tullborg E-L, Mattsson H, Thunehed H, Isaksson H, Berglund J, Lindroos H, Danielsson P, Wängnerud A, 2004. Forsmark site investigation. Petrography, geochemistry, petrophysics and fracture mineralogy of boreholes KFM01A, KFM02A and KFM03A+B. SKB P-04-103 Svensk Kärnbränslehantering AB.

Pitkänen P, Luukonen A, Ruotsalainen P, Leino-Forsmarn H, Vuorinen U, 1999. Geochemical modelling of groundwater evolution and residence time at the Olkiluoto site. POSIVA Report 98-10, POSIVA OY Finland.

Sandström B, Tullborg E-L, 2005. Forsmark site investigation. Fracture mineralogy. Results from fracture minerals and wall rock alteration in KFM01B, KFM04A, KFM05A and KFM06A. SKB P-05-197. Svensk Kärnbränslehantering AB.

Sandström B, Tullborg E-L, 2006a. Forsmark site investigation. Fracture mineralogy. Results from KFM06B, KFM06C, KFM07A, KFM08A and KFM08B. SKB P-06-226. Svensk Kärnbränslehantering AB.

Sandström B, Tullborg E-L, 2006b. Forsmark site investigation. Mineralogy, geochemistry, porosity and redox capacity of altered rock adjacent to fractures. SKB P-06-209. Svensk Kärnbränslehantering AB.

Sandström B, Tullborg E-L, 2007. Paleohydrogeological events in Forsmark, central Sweden, recorded by stable isotopes in calcite and pyrite. In Bullen and Wang (Eds), Water-Rock Interaction. Proceedings of the 12th international symposium on water-rock interaction. WRI-12, Kunming, China, 31 July-5 August 2007. Taylor & Francis Group, London. 773-776.

Sandström B, Tullborg E-L, in prep. Events of fluid migration in the Fennoscandian Shield recorded by stable isotopes, rare earth elements and fluid inclusions in fracture minerals at Forsmark, Sweden.

Sandström B, Savolainen M, Tullborg E-L, 2004. Forsmark site investigation. Fracture Mineralogy. Results from fracture minerals and wall rock alteration in boreholes KFM01A, KFM02A, KFM03A and KFM03B. SKB P-04-149. Svensk Kärnbränslehantering AB.

Sandström B, Page L, Tullborg E-L, 2006a. Forsmark site investigation. $^{40}Ar/^{39}Ar$ (adualaria) and Rb-Sr (adularia, prehnite, calcite) ages of fracture minerals. SKB P-06-213. Svensk Kärnbränslehantering AB.

Sandström B, Tullborg E-L, De Torres T, Ortiz J E, 2006b. The occurrence and potential origin of asphaltite in bedrock fractures, Forsmark, central Sweden. GFF 128, 233-242.

Sandström B, Page L, Tullborg E-L, 2008. Forsmark site investigation. Fracture mineralogy and $^{40}Ar/^{39}Ar$ ages of fracture filling adularia. Data from drill cores KFM01C, KFM01D, KFM02B, KFM08C, KFM08D, KFM09A, KFM09B, KFM10A and KFM11A. SKB P-08-014. Svensk Kärnbränslehantering AB.

Sandström B, Annersten H, Tullborg, E-L, in press. Fracture-related hydrothermal alteration of metagranitic rock and associated changes in mineralogy, geochemistry and degree of oxidation: a case study from Formark, central Sweden. Submitted to International Journal of Earth Sciences. doi: 10.1007/s00531-008-0369-1.

Seal R R, 2006. Sulphur isotope geochemistry of sulphide minerals. Reviews in Mineralogy and Geochemistry 61, 633–677.

Sircar A, 2004. Hydrocarbon production from fractured basement formations. Current Science 87, 147–151.

SKB, 2005. Preliminary site description. Forsmark area – version 1.2. SKB R-05-18. Svensk Kärnbränslehantering AB.

SKB, 2007. Hydrogeochemical evaluation of the Forsmark site, modelling stage 2.1 – issue report, SKB R-06-69. Svensk Kärnbränslehantering AB.

Smellie J, Tullborg E-L, Nilsson A-C, Gimeno M, Sandström B, Waber N, Gascoyne M, 2008. Explorative analysis and expert judgement of major components and isotopes. SKB R-08-84. Svensk Kärnbränslehantering AB.

Stephens M B, Fox A, La Pointe P, Isaksson H, Simeonov A, Hermansson J, Öhman J, 2007. Geology Forsmark. Site descriptive modelling. Forsmark stage 2.2. SKB R-07-45. Svensk Kärnbränslehantering AB.

Strauss H, 1997. The isotopic composition of sedimentary sulphur through time. Palaeogeography, Palaeoclimatology, Palaeoecology 132, 97-118.

Stuckless J S, Peterman Z E, Muhs D R, 1991. U and Sr isotopes in ground water and calcite, Yucca Mountain, Nevada: Evidence against upwelling Water. Science 254, 551–554.

Suksi J, Salminen S, 2007. Study of U oxidation states in groundwater with high U concentrations. SKB P-07-54. Svensk Kärnbränslehantering AB.

Sundvoll B, Neumann E-R, Larsen B T, Tuen E, 1990. Age relations among Oslo Rift magmatic rocks: implications for tectonic and magmatic modelling. Tectonophysics 178, 67–87.

Söderlund P, Hermansson T, Page L M, Stephens M B, submitted. Biotite and muscouite ^{40}AR-^{39}AR geochronological constraints on the post-Svecofennian tectonothermal evolution, Forsmark site, central Sweden. International Journal of Earth Sciences.
doi: 10.1007/s00531-008-0346-8.

Thiel K, Vorwerk R, Saager R, Stupp H D, 1983. ^{235}U fission tracks and ^{238}U-series disequilibria as a means to study recent mobilisation of uranium in Archaean pyritic conglomerates. Earth and Planetary Science Letters 65, 249–262.

Tröjbom M, Söderbäck B, Johansson P-O, 2007. Site descriptive modelling SDM-site Forsmark. Hydrochemistry in surface water and shallow groundwater. SKB R-07-55. Svensk Kärnsbränslehantering AB.

Tullborg E-L, 1989. The influence of recharge water on fissure-filling minerals – A study from Klipperås, southern Sweden. Chemical Geology 76, 309–320.

Tullborg E-L, Larson S Å, 1982. Fissure fillings from Finnsjön and Studsvik, Sweden. Identification, chemistry and dating. SKB Technical Report 82-20.
Svensk Kärnbränslehantering AB.

Tullborg E-L, Landström O, Wallin B, 1999. Low-temperature trace element mobility influenced by microbial activity; indications from fracture calcite and pyrite in crystalline basement. Chemical Geology 157, 199–218.

Tullborg E-L, Smellie J A T, MacKenzie AB, 2003. The use of natural uranium decay series studies in support of understanding redox conditions at potential radioactive waste disposal sites. MRS vol 807, Scientific basis for Nuclear Waste Management XXVII. 571–576.

Tullborg E-L, Drake H, Sandström B, 2008. Palaeohydrogeology: A methodology based on fracture mineral studies. Applied Geochemistry 23, 1881–1897.

Wallin B, Peterman Z E, 1999. Calcite fracture fillings as indicators of paleohydrology at Laxemar at the Äspo Hard Rock Laboratory, southern Sweden. Applied Geochemistry 14, 953–962.

Welin E, 1964. Uranium disseminations and vein fillings in iron ores of northern Uppland, central Sweden. Geologiska Föreningens i Stockholm Förhandlingar 86, 51–82.

Welin E, 1966. The occurrence of asphaltite and thucholite in the Precambrian bedrock of Sweden. Geologiska Föreningens i Stockholm Förhandlingar 87, 509–526.

Wiman E, 1927. Über mineralbildungen längs der spalten. Bulletin of the Geological Institutions of Upsala 2. 38–40.

Wiman E, 1930. Studies of some Archaean rocks in the neighbourhood of Upsala, Sweden, and their geological position. Bulletin of the Geological Institutions of Upsala 23.

Wiman E, 1941. Bidrag till kännedomen till Mälardepressionens sprickbildning och morfologi. Geologiska Föreningens i Stockholm Förhandlingar 63, 84–86.